

การผลิตไฮโดรเจนด้วยวิธีการรีฟอร์มมิงแก๊สมีเทนด้วยไอน้ำที่ส่งเสริมด้วยการดูดซับโดยใช้ตัวดูดซับที่  
มีการเร่งปฏิกิริยาแบบลูกผสม



นางสาวปียา เพชรอำพร

จุฬาลงกรณ์มหาวิทยาลัย  
CHULALONGKORN UNIVERSITY

บทคัดย่อและแฟ้มข้อมูลฉบับเต็มของวิทยานิพนธ์ตั้งแต่ปีการศึกษา 2554 ที่ให้บริการในคลังปัญญาจุฬาฯ (CUIR)  
เป็นแฟ้มข้อมูลของนิสิตเจ้าของวิทยานิพนธ์ ที่ส่งผ่านทางบัณฑิตวิทยาลัย

The abstract and full text of theses from the academic year 2011 in Chulalongkorn University Intellectual Repository (CUIR)  
are the thesis authors' files submitted through the University Graduate School.

วิทยานิพนธ์นี้เป็นส่วนหนึ่งของการศึกษาตามหลักสูตรปริญญาวิศวกรรมศาสตรมหาบัณฑิต

สาขาวิชาวิศวกรรมเคมี ภาควิชาวิศวกรรมเคมี

คณะวิศวกรรมศาสตร์ จุฬาลงกรณ์มหาวิทยาลัย

ปีการศึกษา 2558

ลิขสิทธิ์ของจุฬาลงกรณ์มหาวิทยาลัย

HYDROGEN PRODUCTION VIA SORPTION-  
ENHANCED STEAM METHANE REFORMING USING HYBRID CATALYTIC ADSORBENT

Miss Piya Pecharaumporn



A Thesis Submitted in Partial Fulfillment of the Requirements  
for the Degree of Master of Engineering Program in Chemical Engineering  
Department of Chemical Engineering  
Faculty of Engineering  
Chulalongkorn University  
Academic Year 2015  
Copyright of Chulalongkorn University

Thesis Title HYDROGEN PRODUCTION VIA SORPTION-  
ENHANCED STEAM METHANE REFORMING USING  
HYBRID CATALYTIC ADSORBENT

By Miss Piya Pecharaumporn

Field of Study Chemical Engineering

Thesis Advisor Professor Suttichai Assabumrungrat, Ph.D.

Thesis Co-Advisor Assistant Professor Suwimol Wongsakulphasatch,  
Ph.D.

---

Accepted by the Faculty of Engineering, Chulalongkorn University in Partial  
Fulfillment of the Requirements for the Master's Degree

.....Dean of the Faculty of Engineering  
(Professor Bundhit Eua-arporn, Ph.D.)

THESIS COMMITTEE

.....Chairman  
(Associate Professor Artiwan Shotipruk, Ph.D.)

.....Thesis Advisor  
(Professor Suttichai Assabumrungrat, Ph.D.)

.....Thesis Co-Advisor  
(Assistant Professor Suwimol Wongsakulphasatch, Ph.D.)

.....Examiner  
(Chutimon Satirapipathkul, Ph.D.)

.....External Examiner  
(Professor Navadol Laosiripojana, Ph.D.)

ปิยา เพชรอำพร : การผลิตไฮโดรเจนด้วยวิธีการรีฟอร์มมิงแก๊สมีเทนด้วยไอน้ำที่ส่งเสริมด้วยการดูดซับโดยใช้ตัวดูดซับที่มีการเร่งปฏิกิริยาแบบลูกผสม (HYDROGEN PRODUCTION VIA SORPTION-ENHANCED STEAM METHANE REFORMING USING HYBRID CATALYTIC ADSORBENT) อ.ที่ปรึกษาวิทยานิพนธ์หลัก: ศ. ดร. สุทธิชัย อัสสะบำรุงรัตน์, อ.ที่ปรึกษาวิทยานิพนธ์ร่วม: ผศ. ดร. สุวิมล วงศ์สกุลเกสัช, 100 หน้า.

ตัวเร่งปฏิกิริยาที่มีแคลเซียมอะลูมินาเป็นตัวดูดซับแบบลูกผสมได้ทำการสังเคราะห์และนำไปประยุกต์ใช้เป็นตัวเร่งปฏิกิริยาและตัวดูดซับในกระบวนการการผลิตไฮโดรเจนผ่านปฏิกิริยารีฟอร์มมิงแก๊สมีเทนด้วยไอน้ำที่ส่งเสริมด้วยการดูดซับ (SESMR) แคลเซียมดี-กลูโคินิกแอซิด ( $C_{12}H_{22}CaO_{14}$ ) และแคลเซียมไนเตรท ( $Ca(NO_3)_2 \cdot 4H_2O$ ) ถูกเลือกศึกษาผลของสารตั้งต้นบนคุณสมบัติของแคลเซียมออกไซด์ ตัวดูดซับที่มีแคลเซียมเป็นฐานที่ได้มาจากแคลเซียมดี-กลูโคินิกแอซิดแสดงค่าความจุแก๊สคาร์บอนไดออกไซด์ (0.387 กรัมของแก๊สคาร์บอนไดออกไซด์ต่อกรัมของตัวดูดซับ) มากกว่า ตัวดูดซับที่มีแคลเซียมเป็นฐานที่ได้มาจากแคลเซียมไนเตรท (0.172 กรัมของแก๊สคาร์บอนไดออกไซด์ต่อกรัมของตัวดูดซับ) ที่อุณหภูมิ 600 องศาเซลเซียส และความดันบรรยากาศ ร้อยละ 15 โดยปริมาตรของแก๊สคาร์บอนไดออกไซด์ การเติมสารลดแรงตึงผิวถูกประยุกต์ต่อการปรับปรุงค่าความจุของตัวดูดซับ จากผลแสดง 3 มิลลิโมลาร์ของเฮกซะเดซิลไตรเมทิลแอมโมเนียมโบรไมด์ (CTAB) สามารถปรับปรุงค่าความจุการดูดซับแก๊สคาร์บอนไดออกไซด์ของ CG-AN ซึ่งค่าความจุการดูดซับแก๊สคาร์บอนไดออกไซด์สามารถปรับปรุงถึง 0.45 กรัมคาร์บอนไดออกไซด์ต่อกรัมตัวดูดซับ ในทางตรงข้ามการเพิ่มสารลดแรงตึงผิวไม่สามารถปรับปรุงค่าความจุการดูดซับแก๊สคาร์บอนไดออกไซด์ของ CN-AN ได้ นอกจากนี้ความเสถียรของตัวดูดซับถูกทดสอบ 10 รอบ และผลแสดง CG-AN-CTAB 3mM ให้ค่าความจุการดูดซับแก๊สคาร์บอนไดออกไซด์สูงกว่า CN-AN-CTAB 3mM ที่ทุกรอบ ค่าความจุการดูดซับของ CG-AN-CTAB 3mM ถูกลดลงร้อยละ 36.8 จากรอบที่ 1 ถึงรอบที่ 10 และค่าความจุการดูดซับของ CN-AN-CTAB 3mM ถูกลดลงร้อยละ 30.9 จากรอบที่ 1 ถึงรอบที่ 10 เมื่อตัวดูดซับที่มีแคลเซียมเป็นฐานที่ดัดแปลงถูกใช้ในกระบวนการ SESMR ที่อุณหภูมิ 600 องศาเซลเซียส ไอน้ำต่อแก๊สมีเทนเท่ากับ 3 และความดันบรรยากาศ ในกรณีนี้ 12.5%Ni-CG-AN-CTAB 3mM ถูกเตรียมด้วยวิธีการผสมแบบเปียกแสดงร้อยละ 91.2 ของความบริสุทธิ์แก๊สไฮโดรเจนสำหรับ 45 นาทีและ ร้อยละ 83 ของค่าการแปลงแก๊สมีเทน ซึ่งสูงกว่า 12.5%Ni-CG-AN โดยปราศจาก CTAB ของ ร้อยละ 88.7 ของความบริสุทธิ์แก๊สไฮโดรเจนสำหรับ 45 นาทีและ ร้อยละ 79.4 ของค่าการแปลงแก๊สมีเทน นอกจากนี้จากการสังเกตจากการศึกษาของเราวิธีการสังเคราะห์ตัวดูดซับที่มีการเร่งปฏิกิริยาแบบลูกผสมส่งผลต่อการผลิตไฮโดรเจน โดยการเตรียม 12.5%Ni-CG-AN โดยใช้การผสมแบบโซลสามารถปรับปรุงแสดงร้อยละ 82.3 ของค่าการแปลงแก๊สมีเทนและร้อยละ 94 ของแก๊สไฮโดรเจนสำหรับ 45 นาที

ภาควิชา วิศวกรรมเคมี

ลายมือชื่อนิสิต .....

สาขาวิชา วิศวกรรมเคมี

ลายมือชื่อ อ.ที่ปรึกษาหลัก .....

ปีการศึกษา 2558

ลายมือชื่อ อ.ที่ปรึกษาร่วม .....

# # 5570552421 : MAJOR CHEMICAL ENGINEERING

KEYWORDS: H<sub>2</sub> PRODUCTION, SORPTION-ENHANCED STEAM METHANE REFORMING, CAO, CO<sub>2</sub> CAPACITY, STABILITY, HYBRID CATALYTIC SORBENT

PIYA PECHARAUMPORN: HYDROGEN PRODUCTION VIA SORPTION-ENHANCED STEAM METHANE REFORMING USING HYBRID CATALYTIC ADSORBENT. ADVISOR: PROF. SUTTICHAJ ASSABUMRUNGRAT, Ph.D., CO-ADVISOR: ASST. PROF. SUWIMOL WONGSAKULPHASATCH, Ph.D., 100 pp.

Synthesis of hybrid catalytic CaO-based alumina sorbent has been investigated to use for H<sub>2</sub> production via sorption enhanced steam methane reforming. Calcium D-gluconic acid, (C<sub>12</sub>H<sub>22</sub>CaO<sub>14</sub>) and Calcium nitrate tetrahydrate (Ca(NO<sub>3</sub>)<sub>2</sub>·4H<sub>2</sub>O) were selected to study the effect of calcium precursor on CaO properties. Calcium-based sorbent derived from calcium d-gluconic acid (CG-AN) shows higher CO<sub>2</sub> sorption capacity (0.387g CO<sub>2</sub>/g sorbent) than calcium-based sorbent derived from calcium nitrate (0.172g CO<sub>2</sub>/g sorbent) at 600°C and atmospheric pressure under 15%v/v CO<sub>2</sub>. Adding surfactant was further applied to improve capacity of sorbent. The results show 3 mM of Hexadecyltrimethylammonium bromide (CTAB) can improve CO<sub>2</sub> sorption capacity of CG-AN as CO<sub>2</sub> sorption capacity can be improved to 0.45 g CO<sub>2</sub>/g sorbent whereas addition of surfactant cannot improve CO<sub>2</sub> sorption capacity for CN-AN. In addition, stability of both sorbents were tested for 10 cycles and the results show that CG-AN-CTAB 3 mM provides higher CO<sub>2</sub> sorption capacity than CN-AN-CTAB 3mM at all cycles; sorption capacity of CG-AN-CTAB 3 mM is reduced 36.8% from the 1<sup>st</sup> cycle to the 10<sup>th</sup> cycle and that of CN-AN-CTAB 3 mM is reduced 30.9% from the 1<sup>st</sup> cycle to the 10<sup>th</sup> cycle. When modified calcium-based sorbent was used in SESMR process at 600°C, S/C=3 and atmospheric pressure, 12.5%Ni-CG-AN-CTAB 3mM prepared by wet mixing shows 91.2% H<sub>2</sub> purity for 45 minutes and 83%CH<sub>4</sub> conversion, which was higher than those of 12.5%Ni-CG-AN without CTAB of 88.7% H<sub>2</sub> purity for 45 minutes and 79.4% CH<sub>4</sub>. In addition, it was observed from our studies that method to synthesize hybrid catalytic sorbent has an effect on H<sub>2</sub> production. By preparing 12.5%Ni-CG-AN using sol-mixing can improved CH<sub>4</sub> conversion to 82.3% and H<sub>2</sub> purity to 94% for 30 minutes.

Department: Chemical Engineering

Student's Signature .....

Field of Study: Chemical Engineering

Advisor's Signature .....

Academic Year: 2015

Co-Advisor's Signature .....

## ACKNOWLEDGEMENTS

I would like firstly to express my sincere gratitude and appreciation to my advisor, Professor Suttichai Assabamrungrat, for his valuable advice and suggestions for the successful in Master study, research, and life. The suggestions made me to have positive thinking, strength, and happiness throughout my study here in Chulalongkorn University.

Secondly, my gratitude and appreciation would like to go to my co-advisor, Assistant Professor Suwimol Wongsakulphasatch, for her suggestions, stimulation and useful discussion throughout this research and devotion to revise this thesis. Also I would like to thank Assistant Professor Worapon Kiatkittipong, for his discussion on the research relevant to this thesis.

Appreciation would further go to Associate Professor Artiwan Shotipruk, Chutimon Satirapipathkul, and Professor Navadol Laosiripojana, the chair and members of the thesis committee for the kind comments and suggestions.

I acknowledge my colleagues Mr. Janewit Phromprasit for his assistance, advice, and support in the laboratory. Mr. Panupong Jamrunroj, Ms. Chanita Wattanasomboon, and Ms. Mintra Aupahad are also acknowledged for their support.

Finally, I would like to thank my parents, my sister and my brother, Mr. Nutchapon Chotigkrai, for their encouragements and support.

## CONTENTS

	Page
THAI ABSTRACT .....	iv
ENGLISH ABSTRACT .....	v
ACKNOWLEDGEMENTS .....	vi
CONTENTS .....	vii
LIST OF TABLES .....	x
LIST OF FIGURES .....	xii
CHAPTER I INTRODUCTION .....	1
1.1 Rationale .....	1
1.2 Objective .....	2
1.3 Scope of work .....	3
CHAPTER II THEORY .....	4
2.1 Definition of reactants, products and sorbents. ....	4
2.1.1 Methane (CH <sub>4</sub> ).....	4
2.1.2 Hydrogen (H <sub>2</sub> ).....	5
2.1.3 Carbon dioxide (CO <sub>2</sub> ).....	6
2.1.4 Calcium oxide (CaO).....	7
2.1.5 Calcium aluminate cements (Ca <sub>12</sub> Al <sub>14</sub> O <sub>33</sub> ) or mayenite.....	8
2.2 Surfactants .....	11
2.3 CO <sub>2</sub> capture and hydrogen production process .....	14
2.3.1 Steam methane reforming (SMR) .....	14
2.3.2 Sorption-enhanced steam methane reforming (SESMR).....	16
2.3.3 Fixed bed adsorption .....	17

	Page
2.3.4 Breakthrough curve .....	17
CHAPTER III LITERATURE REVIEWS.....	19
CHAPTER IV EXPERIMENTAL .....	31
4.1 Materials.....	31
4.2 Catalytic sorbent preparation .....	32
4.2.1. Synthesis of Ca-based sorbent without surfactant .....	32
4.2.2 Synthesis of Ca-based sorbent modified by surfactant .....	32
4.2.3 Incipient wetness impregnation method .....	33
4.3 Catalytic sorbent characterization .....	33
4.3.1 X-ray diffraction (XRD).....	33
4.3.2 N <sub>2</sub> adsorption desorption .....	34
4.3.3 Scanning electron microscope (SEM).....	35
4.3.4 H <sub>2</sub> Chemisorption.....	35
4.3.5 Thermogravimetric analysis (TGA) (For Characterization) .....	35
4.3.6 Temperature-programmed reduction (TPR) .....	36
4.3.7 Thermogravimetric analysis (TGA) (Set up experiment).....	36
4.4 Adsorption performance test using fixed-bed system .....	37
4.5 Catalytic performance test (Sorption enhance steam methane reforming, SESMR).....	37
CHAPTER V RESULTS AND DISCUSSION .....	40
5.1 CO <sub>2</sub> Sorption.....	40
5.1.1 Comparison of technique to measure CO <sub>2</sub> sorption capacity.....	40
5.1.2 Effect of CO <sub>2</sub> sorption temperature.....	41



	Page
5.1.3. Effect of Calcium precursors on CO <sub>2</sub> sorption capacity.....	43
5.1.4 Effect of adding surfactant on CO <sub>2</sub> sorption .....	47
5.1.5 Effect of CTAB concentration on CO <sub>2</sub> sorption.....	51
5.1.6 Stability of modified sorbents.....	62
5.2 Sorption enhanced steam methane reforming (SESMR).....	65
5.2.1 The use of CaO-based alumina as sorbent material.....	65
5.2.2 The use of surfactant-modified CaO-based alumina as sorbent material.....	70
5.2.3 The effect of synthesis method for catalytic sorbent material .....	73
CHAPTER VI CONCLUSION AND RECOMMENDATION .....	80
6.1 Conclusion .....	80
6.2 Recommendation.....	81
REFERENCES .....	82
APPENDIX.....	89
VITA.....	100

## LIST OF TABLES

<b>Table 2. 1:</b> Structure and properties of methane.....	4
<b>Table 2.2 :</b> Structure and properties of hydrogen molecule. ....	5
<b>Table 2.3:</b> Structure and properties of carbon dioxide molecule .....	6
<b>Table 2.4 :</b> Structure and properties of calcium oxide molecule.....	7
<b>Table 3.1:</b> Summary of the use of different Ni-based catalysts and supports and conditions for steam methane reforming reaction.....	22
<b>Table 3.2 :</b> summarized the summarized the use of multifunctional catalysts for sorption enhanced steam methane reforming process. ....	29
<b>Table 4.1:</b> Operating conditions for Gas chromatography .....	39
<b>Table 5.1 :</b> BET surface area, pore volume and pore diameter of calcium-based sorbent at different calcium precursors including calcium nitrate (CN) and calcium d-gluconic acid (CG) .....	45
<b>Table 5.2:</b> BET surface area, pore volume and pore diameter of CG-AN calcium-based sorbent at different surfactants including cetyltrimethyl ammonium bromide (CTAB) and sodium dodecyl sulfate (SDS).....	50
<b>Table 5.3:</b> BET surface area, pore volume and pore diameter of modified CG-AN calcium-based sorbent.....	56
<b>Table5.4:</b> BET surface area, pore volume and pore diameter of modified CN-AN calcium-based sorbent at different concentration (1, 3, 5, 7 and 10 mM of CTAB).....	58
<b>Table5.5:</b> CaO and $\text{Ca}_{12}\text{Al}_{14}\text{O}_{33}$ inert support content (%) on modified calcium-based sorbent by TGA.....	62
<b>Table 5.6:</b> Summary textural properties results of sorbents and hybrid multifunctional catalysts when Nickel was impregnated on sorbents.....	78

<b>Table 5.7:</b> Summary results of all hybrid multifunctional catalysts for sorption-enhanced steam methane reforming (SESMR). Condition: 2 g. of catalyst at atmospheric pressure, reaction temperature of 600°C, S/C of 3 and total flow rate 60ml/min.....	79
<b>Table A.1:</b> BET surface area, pore volume and pore diameter of CaO and Ni/Al <sub>2</sub> O <sub>3</sub> .....	91



## LIST OF FIGURES

<b>Figure 2.1:</b> (a) Cage of $\text{Ca}_{12}\text{Al}_{14}\text{O}_{33}$ (b) Unit cell of $\text{Ca}_{12}\text{Al}_{14}\text{O}_{33}$ containing 12 cages [25].....	9
<b>Figure 2.2:</b> Scheme of the mechanism of temperature calcination of $\text{Ca}_{12}\text{Al}_{14}\text{O}_{33}$ . [26].....	9
<b>Figure 2.3:</b> Phase diagram of calcium aluminate presented in the anhydrous calcium aluminate cement before hydration. ( <a href="http://en.wikipedia.org/wiki/">http://en.wikipedia.org/wiki/</a> ). .....	10
<b>Figure 2.4:</b> Anionic Surfactants.....	11
<b>Figure 2.5:</b> Cationic Surfactant .....	11
<b>Figure 2.6:</b> Nonionic Surfactants .....	12
<b>Figure 2.7:</b> Amphoteric or Zwitterionic.....	12
<b>Figure 2.8:</b> Examples of I-anionic (SDS), II-cationic (CTAB), III- nonionic ( $\text{C}_{12}\text{E}_4$ ) and VI-zwitterionic ( $\text{C}_8$ -lecithin) surfactants.....	13
<b>Figure 2.9:</b> (a) Schematic illustration of the reversible monomer-micelle thermodynamic equilibrium. The blue and red circles represent the surfactant heads and the black curved lines represent the surfactant tails [27] (b) Typical plot of the surface tension against logarithm of surfactant concentration ( <a href="http://www.attension.com">http://www.attension.com</a> ). .....	13
<b>Figure 2.10:</b> Flow sheet of a conventional SMR process [29]. .....	15
<b>Figure 2.11:</b> Schematic diagram of sorption-enhanced steam reforming using $\text{CaO}$ as $\text{CO}_2$ adsorbent [31].....	16
<b>Figure 2.12:</b> Basic types of catalytic fixed-bed reactors a) adiabatic fixed-bed reactor; b) multitubular fixed-bed reactor. ....	17
<b>Figure 2.13:</b> Breakthrough curve of sorption process.....	18
<b>Figure 3.1:</b> Flow diagram of a conventional SMR process [29]. .....	25

<b>Figure 3.2:</b> Simplified block-scheme of the sorption-enhanced steam reforming process (SER) [47].....	25
<b>Figure 4.1:</b> principle of XRD .....	33
<b>Figure 4.2:</b> N <sub>2</sub> adsorption/desorption analyzer.....	34
<b>Figure 4.3:</b> Schematic of TGA equipment [59].....	37
<b>Figure 4.4:</b> Experimental set up for hydrogen production via sorption enhance steam methane reforming. ....	38
<b>Figure 5.1:</b> Comparison CO <sub>2</sub> sorption capacity between fixed-bed and thermogravimetric analyzer (TGA), condition: atmospheric pressure, 600 °C, total flow 60 ml/min, and using 15% CO <sub>2</sub> in N <sub>2</sub> as feed composition.....	41
<b>Figure 5.2:</b> CO <sub>2</sub> sorption capacity by commercial CaO at different temperatures ranging from 500-800 °C, atmospheric pressure, and 15%v/v CO <sub>2</sub> (balanced N <sub>2</sub> ). .	43
<b>Figure 5.3:</b> Weight loss of CaCO <sub>3</sub> determined by TGA analysis.....	43
<b>Figure 5.4:</b> XRD pattern of different calcium precursors (CG-AN and CN-AN sorbent).....	44
<b>Figure 5.5:</b> Breakthrough curves of CO <sub>2</sub> sorption by 1g of calcium-based sorbent synthesized from calcium nitrate (CN) and calcium d-gluconic acid (CG). Operating conditions: atmospheric pressure, 600°C, and 15%v/v CO <sub>2</sub> (balanced N <sub>2</sub> )......	45
<b>Figure 5.6:</b> CO <sub>2</sub> sorption capacity of calcium-based sorbent synthesized from calcium nitrate (CN) and calcium d-gluconic acid (CG). Operating conditions: atmospheric pressure, 600°C, and 15%v/v CO <sub>2</sub> (balanced N <sub>2</sub> )......	46
<b>Figure 5.7:</b> SEM photos of Ca-based sorbents a) CN-AN sorbent and b) CG-AN.....	47
<b>Figure 5.8:</b> XRD pattern of different surfactants modified CG-AN sorbent (CG-AN modified with CTAB and CG-AN modified with SDS).....	48
<b>Figure 5.9:</b> Breakthrough curves of CO <sub>2</sub> sorption by 1 g of CaO-based alumina modified by cetyltrimethyl ammonium bromide (CTAB) and sodium dodecyl	

sulfate (SDS). Operating condition: atmospheric pressure, 600°C, and 15%v/v CO<sub>2</sub> (balanced N<sub>2</sub>). .....49

**Figure 5.10:** CO<sub>2</sub> sorption capacity of CaO-based alumina modified by cetyltrimethyl ammonium bromide (CTAB) and sodium dodecyl sulfate (SDS). Operating condition: atmospheric pressure, 600°C, and 15%v/v CO<sub>2</sub> (balanced N<sub>2</sub>). .....49

**Figure 5.11:** Morphology of modified Ca-based sorbents a) CG-AN-CTAB 1mM and b) CG-AN-SDS 9mM.....50

**Figure 5.12:** XRD pattern of modified CG-AN sorbent by different concentration of CTAB .....52

**Figure 5.13:** Morphology of modified Ca-based alumina sorbents at different CTAB concentrations a) CG-AN without CTAB and b) CG-AN-CTAB 1mM c) CG-AN-CTAB 3mM d) CG-AN-CTAB 5mM e) CG-AN-CTAB 7mM and f) CG-AN-CTAB 10mM. ....53

**Figure 5.14:** Breakthrough curves of CO<sub>2</sub> sorption by 1g of CG-AN calcium-based sorbent at different concentration of CTAB at 1,3,5,7 and 10mM, Operating condition: atmospheric pressure, 600°C, and 15%v/v CO<sub>2</sub> (balanced N<sub>2</sub>).....54

**Figure 5.15:** Comparison CO<sub>2</sub> sorption capacity by 1g of CG-AN calcium-based sorbent at different concentration of CTAB at 1,3,5,7 and 10mM. Operating condition: atmospheric pressure, 600°C, and 15%v/v CO<sub>2</sub> (balanced N<sub>2</sub>).....55

**Figure 5.16:** XRD pattern of different concentration of CTAB at 1,3,5,7 and 10mM modified CN-AN sorbent. ....57

**Figure 5.17:** Breakthrough curves of CO<sub>2</sub> sorption by 1g of CN-AN calcium-based sorbent at different concentration of CTAB at 1,3,5,7 and 10mM. Operating condition: atmospheric pressure, 600°C, and 15%v/v CO<sub>2</sub> (balanced N<sub>2</sub>).....59

**Figure 5.18:** Comparison CO<sub>2</sub> sorption capacity by 1g of CN-AN calcium-based sorbent at different concentration of CTAB at 1,3,5,7 and 10mM. Operating condition: atmospheric pressure, 600°C, and 15%v/v CO<sub>2</sub> (balanced N<sub>2</sub>).....59

- Figure 5.19:** Morphology of modified Ca-based sorbents at different CTAB concentrations a) CN-AN without CTAB and b) CN-AN-CTAB 1mM c) CN-AN-CTAB 3mM d) CN-AN-CTAB 5mM e) CN-AN-CTAB 7mM and f) CN-AN-CTAB 10mM. ....60
- Figure 5.20:** Stability of CG-AN-CTAB 3mM and CN-AN-CTAB 3mM modified sorbents. Condition: atmospheric pressure, 600°C of adsorption and 850°C of regeneration, using 15% CO<sub>2</sub> in N<sub>2</sub> as feed composition. ....63
- Figure 5.21:** Morphology of modified sorbent particles. a) fresh CN-AN-CTAB 3mM b) after 10 cycles of CN-AN-CTAB 3mM c) fresh CG-AN-CTAB 3mM d) after 10 cycles of CG-AN-CTAB 3mM. ....64
- Figure 5.22:** XRD of fourth hybrid multifunctional catalyst. (a) fresh and (b) after test of SESMR (12.5%Ni-CN-AN, 12.5%Ni-CG-AN, 12.5%Ni-CN-AN-CTAB 3mM and 12.5%Ni-CG-AN-CTAB 3mM).....66
- Figure 5.23:** Gas product composition (dry basis) of 12.5%Ni-CG-AN (a) and 12.5%Ni-CN-AN (b) for sorption enhanced steam methane reforming Condition: at atmospheric pressure, reaction temperature of 600°C, S/C of 3 and total flow rate 60ml/min.....67
- Figure 5.24:** CH<sub>4</sub> conversion of 12.5%Ni-CG-AN and 12.5%Ni-CN-AN for sorption enhanced steam methane reforming Condition: at atmospheric pressure, reaction temperature of 600°C, S/C of 3 and total flow rate 60ml/min.....68
- Figure 5.25:** Morphology of 12.5%Ni-CG-AN and 12.5%Ni-CN-AN for sorption enhanced steam methane reforming Condition: at atmospheric pressure, reaction temperature of 600°C, S/C of 3 and total flow rate 60ml/min. a) fresh of 12.5%Ni-CG-AN b) 12.5%Ni-CG-AN after test of SESMR c) fresh of 12.5%Ni-CN-AN d) 12.5%Ni-CN-AN after test of SESMR. ....69
- Figure 5.26:** Gas product composition (dry basis) of (a) 12.5%Ni-CG-AN-CTAB 3mM and (b) 12.5%Ni-CN-AN-CTAB 3mM for sorption enhanced steam methane reforming Condition: at atmospheric pressure, reaction temperature of 600°C, S/C of 3 and total flow rate 60ml/min.....70

<b>Figure 5.27:</b> CH <sub>4</sub> conversion of 12.5%Ni-CG-AN-CTAB 3mM and 12.5%Ni-CN-AN-CTAB 3mM for sorption enhanced steam methane reforming Condition: at atmospheric pressure, reaction temperature of 600°C, S/C of 3 and total flow rate 60ml/min.....	71
<b>Figure 5.28:</b> Morphology of 12.5%Ni-CN-AN-CTAB 3mM for sorption enhanced steam methane reforming Condition: at atmospheric pressure, reaction temperature of 600°C, S/C of 3 and total flow rate 60ml/min. a) fresh of 12.5%Ni-CG-AN-CTAB 3mM b) 12.5%Ni-CG-AN-CTAB 3m after test of SESMR c) fresh of 12.5%Ni-CN-AN-CTAB 3mM d) 12.5%Ni-CN-AN-CTAB 3m after test of SESMR.....	72
<b>Figure 5.29:</b> XRD of fourth hybrid multifunctional catalyst fresh (a) and after SESMR test (b). (12.5%Ni-12.5%Ni-CG-AN-wet mixing and 12.5%Ni-CG-AN-sol mixing).....	74
<b>Figure 5.30:</b> Gas product composition (dry basis) of 12.5%Ni-CG-AN at different synthesis method including wet mixing (a) and sol mixing (b) for sorption enhanced .....	75
<b>Figure 5.31:</b> CH <sub>4</sub> conversion of 12.5%Ni-CG-AN wet mixing and 12.5%Ni-CG-AN sol mixing for sorption enhanced steam methane reforming Condition: at atmospheric pressure, reaction temperature of 600°C, S/C of 3 and total flow rate 60ml/min.....	76
<b>Figure 5.32:</b> morphology of 12.5%Ni-CG-AN wet mixing and 12.5%Ni-CG-AN sol mixing for sorption enhanced steam methane reforming Condition: at atmospheric pressure, reaction temperature of 600°C, S/C of 3 and total flow rate 60ml/min. a) fresh of 12.5%Ni-CG-AN wet mixing b) 12.5%Ni-CG-AN wet mixing after test of SESMR c) fresh of 12.5%Ni-CG-AN sol-mixing d) 12.5%Ni-CG-AN sol mixing after test of SESMR.....	77
<b>Figure A.1:</b> XRD pattern of commercial calcium oxide.....	90
<b>Figure A.2:</b> XRD of 12.5%Ni/Al <sub>2</sub> O <sub>3</sub> conventional catalyst.....	90
<b>Figure A.3:</b> Morphology of Calcium oxide .....	91



<b>Figure A.4:</b> Morphology of 12.5%Ni/Al <sub>2</sub> O <sub>3</sub> .....	91
<b>Figure A.5:</b> H <sub>2</sub> -TPR of fourth hybrid multifunctional catalyst. (12.5%Ni-CN-AN, 12.5%Ni-CG-AN, 12.5%Ni-CN-AN-CTAB 3mM and 12.5%Ni-CG-AN-CTAB 3mM) Condition: 10%v/v of H <sub>2</sub> in N <sub>2</sub> , total flow rate 50ml/min. ....	92
<b>Figure A.6:</b> Gas product composition (dry basis) of 2 g. of 12.5%Ni/Al <sub>2</sub> O <sub>3</sub> Condition: atmospheric pressure at 600°C, S/C =3 and total flow 60 ml/min. ....	93
<b>Figure A.7:</b> CH <sub>4</sub> conversion of 2 g. of 12.5%Ni/Al <sub>2</sub> O <sub>3</sub> Condition: atmospheric pressure at 600°C, S/C =3 and total flow 60 ml/min. ....	93
<b>Figure B.1:</b> Breakthrough curves of CO <sub>2</sub> sorption by 1g of Calcium Oxide Operating conditions: atmospheric pressure, 600°C, and 15%v/v CO <sub>2</sub> (balanced N <sub>2</sub> ). ....	94
<b>Figure C.1:</b> Calibration curve of H <sub>2</sub> .....	97
<b>Figure C.2:</b> Calibration curve of CH <sub>4</sub> .....	97
<b>Figure C.3:</b> Calibration curve of CO .....	98
<b>Figure C.4:</b> Calibration curve of CO <sub>2</sub> .....	98
<b>Figure C.5:</b> Calibration curve of N <sub>2</sub> .....	99

## CHAPTER I

### INTRODUCTION

#### 1.1 Rationale

The demand of energy has increased significantly as it is essential for many industries. Moreover, current energy sources derived from fossil fuels, such as coal, natural gas, or crude oil, etc. However, such current energy sources are now limited and are the main cause of global warming due to greenhouse gas emissions. As such, searching for new or alternative energy to replace fossil fuels is therefore an interesting issue.

Hydrogen is considered to be an ideal energy carrier and plays an important role in the clean energy system [1] due to a very high energy density [2] and does not cause pollution, especially when applied to fuel cells for power generation. Hydrogen can be produced from a variety of reactants and processes, for example, hydrogen production from water (electrolysis) [3]. This technique has advantage of which high hydrogen purity can be obtained but large amount of energy is also required. Reforming process has been applied for hydrogen production in industrial [3] because this process has high efficiency [2]. Reforming process can be divided into several categories, depending upon the substances used, for example, steam reforming, carbon dioxide reforming, partial oxidation or autothermal reforming [4]. In these processes, many reactants can be used to produce hydrogen i.e. methane [5-12], methanol [13-15], ethanol [16-18], or biomass [19-21]. However, the obtained hydrogen from biomass is uncertain due to the complex and diverse structure of biomass. At present, methane is widely used to produce hydrogen, because it is cheap and common in nature [22]. Steam methane reforming is a conventional process that is widely used for hydrogen production in industry because this process has high efficiency and low cost than other methods but this process still have some disadvantages such as catalyst deactivation due to carbon formation and it requires a

CO<sub>2</sub> separation unit for H<sub>2</sub> purification causing large amount of energy consumption [3]. To minimize the above disadvantages, different techniques have been applied [23]. One of those is the combine of CO<sub>2</sub> capture process with reforming process, which is known as sorption enhanced steam reforming (SESR). Sorption enhance steam methane reforming process has been developed for H<sub>2</sub> production. This process has many advantages such as increasing conversion of CH<sub>4</sub>, decreasing operating temperature, lower energy consumption as well as lower capital and operating cost, and simplified process [22].

One improvement of SESR process is the development of one-body catalytic sorbent material, named as multi-functional catalyst. Multi-functional catalyst is a combination of catalyst and sorbent. Several studies have suggested that using a single catalyst has advantage of which an amount of catalyst use is less than that of the separated adsorbent-catalyst; however, its efficiency is still not satisfy. As a consequence, the development of one-body multifunctional catalyst is a challenging task for SESMR process. In SESMR process, nickel is mostly used as catalyst due to its high thermal stability and it is cheaper than precious metals whereas calcium oxide has been applied as CO<sub>2</sub> adsorbent to shift equilibrium toward high purity of hydrogen production as it is cheap and readily available in nature, good kinetic, high capacity and has ability to regenerate. However, its disadvantages are that the requirement of high temperature for regeneration causes sorbent deactivation, poor stability for a long period of time (capacity loss upon multiple cycles use) [24]. This study is focused on the synthesis of hybrid sorbent multifunctional catalyst for sorption enhanced methane steam reforming for hydrogen production with the emphasis on improvement of calcium oxide properties to possess high CO<sub>2</sub> sorption capacity and high thermal stability.

## 1.2 Objective

To develop hybrid catalytic adsorbent for hydrogen production via sorption enhanced steam methane reforming.

### 1.3 Scope of work

- Investigate the effect of calcium precursors on properties of the synthesized CaO-based sorbent and on the ability to adsorb CO<sub>2</sub>. CaO-based sorbents are synthesized via wet-mixing technique with different calcium precursors and the addition of additive surfactants.
  - Two different calcium precursors are investigated: calcium nitrate tetrahydrate and calcium d-gluconic acid.
  - Two types of surfactants are used: Cetyltrimethylammonium bromide (CTAB) and Sodium dodecyl sulfate (SDS)
  - Five concentrations of surfactant are used : 1,3,5,7,10 mM of CTAB and 9 mM of SDS (at CMC of surfactant)
- Investigate the effect of sorption temperature on CO<sub>2</sub> sorption capacity. The sorption temperature is varied in the range of 600-800°C.
- Investigate thermal stability of the adsorbent upon multiple-cycle use.
- Investigate the catalytic performance of hybrid catalyst sorbent material for sorption enhanced steam methane reforming process.

## CHAPTER II

### THEORY

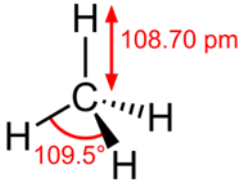
In this chapter, the necessary information for hydrogen production via sorption enhance steam methane reforming such as definition of reactants, products, sorbents (methane, hydrogen, carbon dioxide, calcium oxide and mayenite), surfactants and processes relating to this research (steam methane reformation, sorption enhanced steam methane reforming and fixed bed adsorption) are provided.

#### 2.1 Definition of reactants, products and sorbents.

##### 2.1.1 Methane (CH<sub>4</sub>)

Methane (CH<sub>4</sub>) is a very simple molecule having chemical formula CH<sub>4</sub>. State of methane is gas phase at room temperature and atmospheric pressure. Methane molecule is tetrahedral in structure, where carbon is a central atom and four H-atoms are surrounding in three-dimensions. Methane is a colorless, odorless gas and non-poisonous gas. Methane is created predominantly by bacteria that feed on organic material. (<http://www.giss.nasa.gov>) Some properties of methane are summarized in Table 2.1.

**Table 2. 1:** Structure and properties of methane

Molecular formula	CH <sub>4</sub>
Structure	

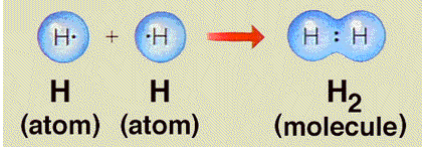
Molar mass	16.04 kg kmol <sup>-1</sup>
Appearance	Colorless gas
Density	0.717 kg/m <sup>3</sup> (gas, 0°C) 416 kg/m <sup>3</sup> (liquid)
Melting point	-182.5°C, 90.7 K, -296.5°F
Boiling point	-161.6°C, 111.6 K, -258.9°F
Solubility in water	35 mg/L (17°C)
Heating value (www.eoearth.org)	21511 BTU/lb, 909 BTU/ft <sup>3</sup>
Viscosity	0.0001027 Poise (at 1.013 bar and 0°C)
Thermal conductivity	32.81 mW/(m.K) (at 1.013 bar and 0°C)

(<http://encyclopedia.airliquide.com>)

### 2.1.2 Hydrogen (H<sub>2</sub>)

Hydrogen gas is a substance. At standard temperature and pressure, hydrogen is an odorless, colorless, non-toxic and non-flavored wireless flammable gas atom. The molecular formula is H<sub>2</sub>. Hydrogen gas is lighter than air. Some properties of hydrogen are shown in Table 2.2 (<http://en.wikipedia.org>).

**Table 2.2** : Structure and properties of hydrogen molecule.

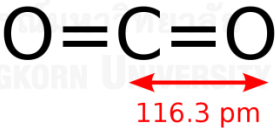
Molecular formula	H <sub>2</sub>
Structure	
Molar mass	2.016 kg kmol <sup>-1</sup>
Appearance	Colorless gas
Density (1.013 bar at boiling point)	1.312 kg/m <sup>3</sup> (gas) 70.973 kg/m <sup>3</sup> (liquid)
Melting point	-259°C, 14.15 K, -227°F

Boiling point	-252.8°C, 20.35 K, -423.2°F
Solubility in water	1.92 mg/L (0°C)
Heating value	51596 BTU/lb, 274 BTU/ft <sup>3</sup>
Viscosity	0.0000865 Poise (at 1.013 bar and 15°C)
Thermal conductivity	168.35 mW/(m.K) (at 1.013 bar and 0°C)

### 2.1.3 Carbon dioxide (CO<sub>2</sub>)

Carbon dioxide is a gas in the atmosphere composing of one carbon atom and two oxygen atoms per molecule. Carbon dioxide is a colorless gas, non-flammable and non-reactive. Carbon dioxide is considered as a main greenhouse gas. Some properties of carbon dioxide are shown in Table 2.3.

**Table 2.3:** Structure and properties of carbon dioxide molecule

Molecular formula	CO <sub>2</sub>
Structure	
Molar mass	44.01 kg kmol <sup>-1</sup>
Appearance	Colorless gas
Odor	Odorless
Density	1562 kg/m <sup>3</sup> (solid at 1 atm, -78.5°C) 0.717 kg/m <sup>3</sup> (liquid at 56 atm, 20°C) 416 kg/m <sup>3</sup> (gas at 1 atm, 0°C)
Melting point	-78°C, 194.7 K, -109°F
Boiling point	-57°C, 216.6 K, -70°F (at 5.185 bar)
Solubility in water	1.45 g/L (at 25°C, 100kPa)
Acidity (pK <sub>a</sub> )	6.35, 10.33

Refractive index ( $n_D$ )	1.1120
Viscosity	0.0001372 Poise (at 1.013 bar and 0°C)
Thermal conductivity	14.65 mW/(m.K) (at 1.013 bar and 0°C)
Dipole moment	zero

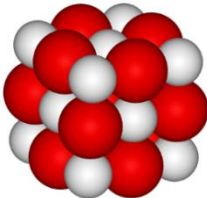
#### 2.1.4 Calcium oxide (CaO)

Calcium oxide (CaO) is a white crystalline solid. It is manufactured by heating limestone, which are mainly  $\text{CaCO}_3$ , to drive off carbon dioxide.



This reaction is reversible of which calcium oxide can react with carbon dioxide to form calcium carbonate.

**Table 2.4** : Structure and properties of calcium oxide molecule

Molecular formula	CaO
Structure	 <p>3-D structural of calcium oxide</p>
Molar mass	56.0774 kg kmol <sup>-1</sup>
Appearance	White to pale yellow/brown powder
Odor	Odorless
Density	3.35 g/cm <sup>3</sup>

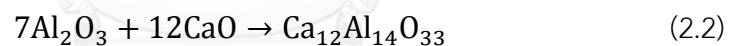


Melting point	2899°C, 3172 K, 5250°F
Boiling point	3621°C, 3894 K, 6550°F
Solubility in water	1.19 g/L (25 °C), 0.57 g/L (100 °C), exothermic reaction
Solubility in acid	soluble (also in glycerol, sugar solution)
Solubility in methanol	insoluble (also in diethyl ether, n-octanol)
Acidity (pKa)	12.8

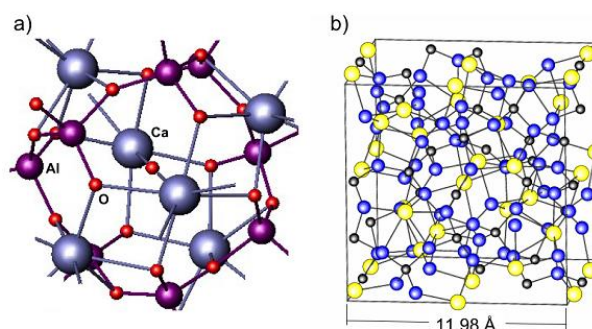
(<http://en.wikipedia.org>)

### 2.1.5 Calcium aluminate cements ( $\text{Ca}_{12}\text{Al}_{14}\text{O}_{33}$ ) or mayenite

Calcium aluminate cements is chemical compound of cubic symmetry.  $\text{Al}_2\text{O}_3$  reacts with  $\text{CaO}$  through an exothermic reaction, the reaction starts at 800°C and forming a transient phase,  $\text{Ca}_{12}\text{Al}_{14}\text{O}_{33}$ . The first formation of  $\text{Ca}_{12}\text{Al}_{14}\text{O}_{33}$  occurs between small aggregates of  $\text{CaO}$  and amorphous alumina particles. The reaction is shown in the following equation

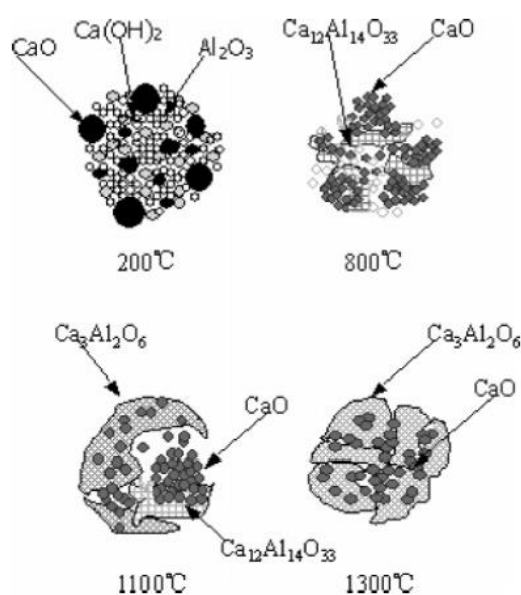


The structure of calcium aluminate cement is a body centered cubic crystal that belongs to the space group  $I-43d$  with a lattice parameter equal to 11.989 Å. The unit cell composes of 118 atoms and contains two molecules of  $\text{Ca}_{12}\text{Al}_{14}\text{O}_{33}$ . It is a cage-like structure with 12 cages per unit cell as shown in Figure 2.1 (<http://en.wikipedia.org/wiki/Mayenite>)



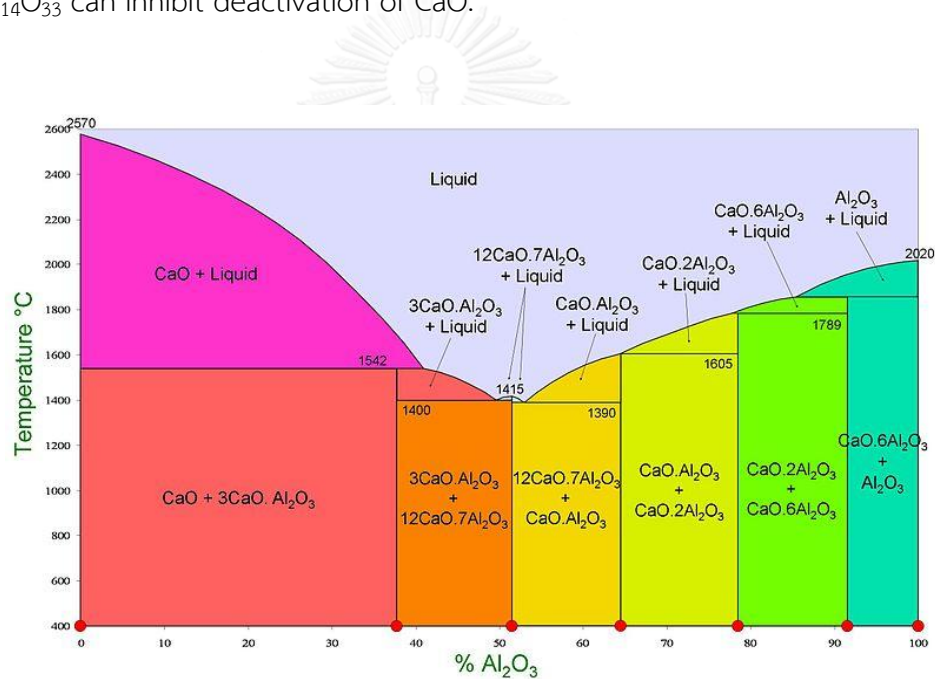
**Figure 2.1:** (a) Cage of  $\text{Ca}_{12}\text{Al}_{14}\text{O}_{33}$  (b) Unit cell of  $\text{Ca}_{12}\text{Al}_{14}\text{O}_{33}$  containing 12 cages [25]

Figure 2.2 shows schematic of the effect of calcination temperature on  $\text{Ca}_{12}\text{Al}_{14}\text{O}_{33}$ . When sample is calcined at higher temperature than  $1000^\circ\text{C}$ , CaO and  $\text{Al}_2\text{O}_3$  inside the particle react to generate a new kind of material of  $\text{Ca}_{12}\text{Al}_{14}\text{O}_{33}$ ,  $\text{Ca}_3\text{Al}_2\text{O}_6$  or  $\text{Ca}_9\text{Al}_{16}\text{O}_{18}$ .



**Figure 2.2:** Scheme of the mechanism of temperature calcination of  $\text{Ca}_{12}\text{Al}_{14}\text{O}_{33}$ . [26].

Temperature of calcination is an important for formation of calcium-alumina compound due to calcium-alumina formation was changed according to temperature and ratio of CaO and  $\text{Al}_2\text{O}_3$ . Figure 2.3 shows ration of  $\text{Al}_2\text{O}_3$  and CaO for calcium-alumina formation. Data observed in phase diagram of calcium aluminates presented in the anhydrous calcium aluminate cement before hydration (see Figure 2.3).  $\text{Ca}_{12}\text{Al}_{14}\text{O}_{33}$  contains elements of alumina approximately 51-65%, it is a solid phase at 400-1390°C and liquid phase at temperature higher than 1390°C. In carbonation reaction, the  $\text{Ca}_{12}\text{Al}_{14}\text{O}_{33}$  acts as an inert support due to it does not react with  $\text{CO}_2$  in the reaction but its role is to prevent sintering of CaO during calcination. Consequently,  $\text{Ca}_{12}\text{Al}_{14}\text{O}_{33}$  can inhibit deactivation of CaO.



**Figure 2.3:** Phase diagram of calcium aluminate presented in the anhydrous calcium aluminate cement before hydration. (<http://en.wikipedia.org/wiki/>).

## 2.2 Surfactants

Surfactants are compounds that consists of hydrophilic group (head) and hydrophobic group (tail). Because the distinct properties of surfactants, surfactants can lower the surface tension of the liquid, allows for better distribution of liquid and reduces the surface tension between two liquids or between a liquid and a solid. Surfactants can be classified into four different types according to the properties of its head including anionic surfactants, cationic surfactants, Zwitterionic surfactants.

- **Anionic surfactants**

When the hydrophilic part of the surfactant consists of a negatively charged group like a sulphonate, sulphate or carboxylate the surfactant is called anionic. Basic soaps are anionic surfactants.

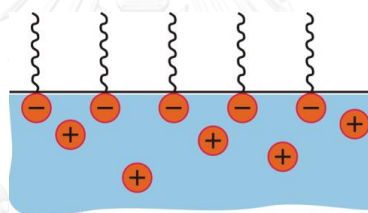


Figure 2.4: Anionic Surfactants

- **Cationic surfactants**

Cationic surfactants are dissociated in water into an amphiphilic cation. A very large proportion of this class corresponds to nitrogen compounds as amine. Cationic surfactants are not cheap; they are used in two cases, (1) as bactericide and (2) as positively charged substance which are able to adsorb on negatively charged substrates. They have an application to produce antistatic and corrosion inhibition.

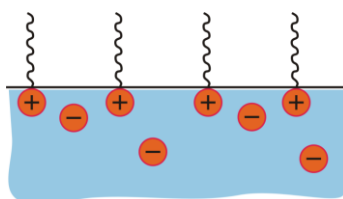
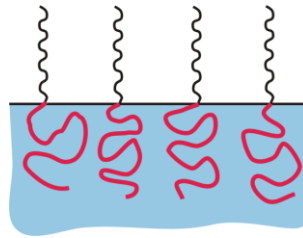


Figure 2.5: Cationic Surfactant

- **Nonionic surfactants**

Surfactants with non-charged hydrophilic part, e.g. ethoxylate, are considered as non-ionic. These substances are well suited for cleaning purposes and are not sensitive to water hardness. They have a wide applications within cleaning detergents.



**Figure 2.6:** Nonionic Surfactants

- **Amphoteric or Zwitterionic surfactants**

Amphoteric or Zwitterionic is a single surfactant molecule contains both anionic and cationic. For the amphoteric surfactants the charge of the hydrophilic part is controlled by the pH of the solution. This means that they can act as anionic surfactant in an alkali solution or as cationic surfactant in an acidic solution.

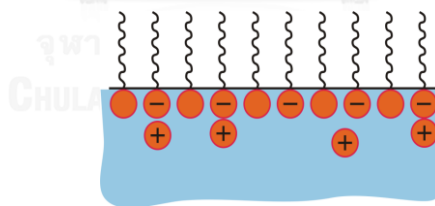


**Figure 2.7:** Amphoteric or Zwitterionic

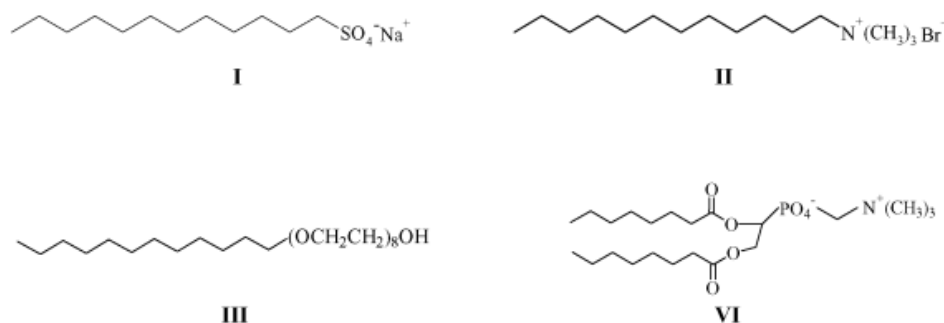


**Figure 2.8:** Examples of I-anionic (SDS), II-cationic (CTAB), III- nonionic ( $\text{C}_{12}\text{E}_4$ ) and VI-zwitterionic ( $\text{C}_8$ -lecithin) surfactants.

### Micellization

Micelles are formed at the *critical micelle concentration* (CMC), which is detected as an inflection point when physicochemical properties such as surface tension are plotted as a function of concentration (Figure 2.9).

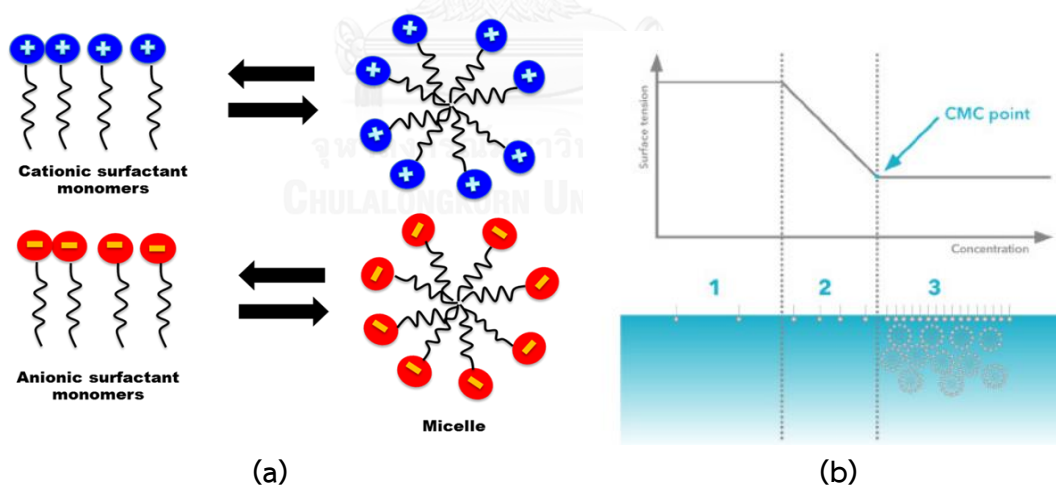


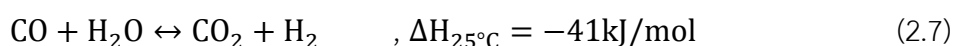
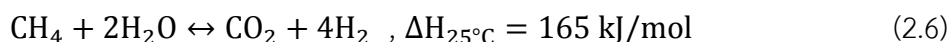
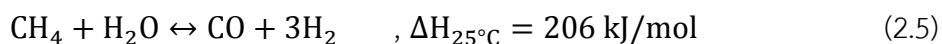
**Figure 2.9:** (a) Schematic illustration of the reversible monomer-micelle thermodynamic equilibrium. The blue and red circles represent the surfactant heads and the black curved lines represent the surfactant tails [27] (b) Typical plot of the surface tension against logarithm of surfactant concentration (<http://www.attension.com>).

As seen in Figure 2.9 (b), at low surfactant concentration, the surfactant molecules dissociate on the surface as a monomer (1). When more surfactants are added the surface tension of the solution starts to rapidly decrease (2). When the surface becomes saturated (3), the addition of the surfactant molecules will lead to the formation of micelles. This concentration point is called critical micelle concentration (CMC). The CMC of surfactant depends on temperature of solution and also the shape of micelle depend on concentration of surfactant solution. Consequently, particle size and shape of micelle depends on temperature and concentration of surfactant [28].

## 2.3 CO<sub>2</sub> capture and hydrogen production process

### 2.3.1 Steam methane reforming (SMR)

Steam methane reforming (SMR) is conventional process for large scale manufacture of hydrogen. In this process, natural gas or other light hydrocarbons react with steam produces a mixture of hydrogen, carbon monoxide, carbon dioxide and water. SMR is found to compose of three main reactions, two reactions for steam methane reforming (Eq. 2.5-2.6) and one reaction for water gas shift (Eq. 2.7), which is a reversible and strongly endothermic reaction [29] all reactions as shown in Equations (2.5-2.7).



Flowsheet of a conventional SMR process is shown in Figure 2.10. Three main units of SMR process are reforming unit, water-gas shift reactor, and CO<sub>2</sub> removal unit. In the reformer, catalytic reaction between methane and steam is taken place resulting in the production of hydrogen and carbon monoxide in an endothermic reaction. Operating temperature of this reaction is 800–1000 °C and a pressure is 14–20 atm with mostly use of a nickel as a catalyst. After the reaction, the obtained products from the reforming unit is further fed into a WGS reactor to reduce CO content. In this unit, CO is reacted with H<sub>2</sub>O producing H<sub>2</sub> and CO<sub>2</sub> (Eq. 2.7). This reaction is moderately exothermic and is favored by low temperatures (300-400 °C). Then, the mixture of H<sub>2</sub> and CO<sub>2</sub> is fed to CO<sub>2</sub> removal unit to improve high purity of H<sub>2</sub> to the desired value (up to 99%). Normally, pressure swing adsorption (PSA) or amine scrubbing is used to remove CO<sub>2</sub>.

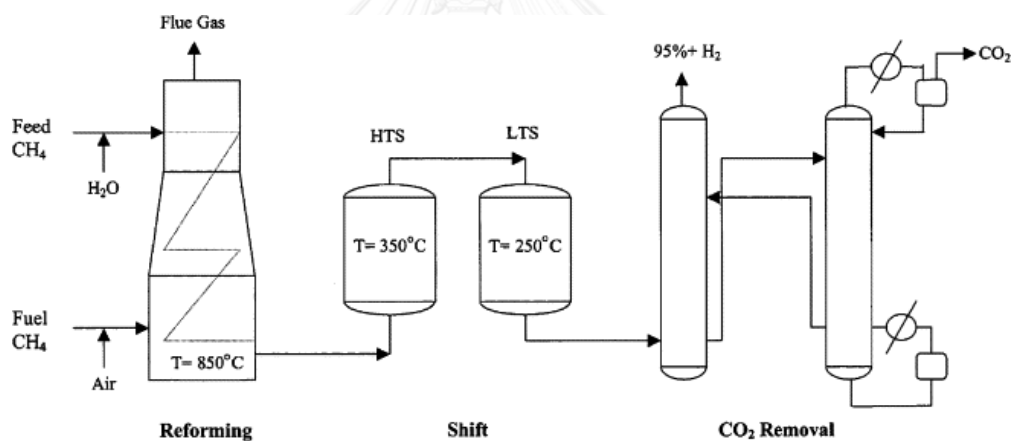


Figure 2.10: Flow sheet of a conventional SMR process [29].



### 2.3.2 Sorption-enhanced steam methane reforming (SESMR)

Sorption enhanced steam methane reforming (SESMR) is a process that combines steam methane reforming process with CO<sub>2</sub> sorption process in one unit operation. The sorption enhanced reaction process (SERP) is the addition of a sorbent into the reaction for selectively uptaking CO<sub>2</sub> products. It can shift the equilibrium of the reversible reaction followed by the Le Chatelier's principle. Carbonation-calcination of CO<sub>2</sub> capture is presented in Equation 2.8 [30].



In Figure 2.11 shows mechanism of SESMR using CaO as CO<sub>2</sub> adsorbent. The advantages of SESMR.

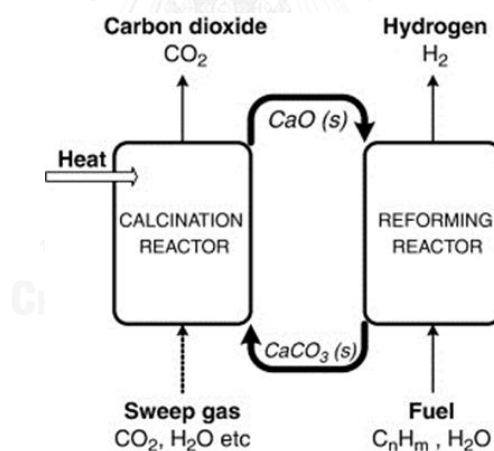


**Figure 2.11:** Schematic diagram of sorption-enhanced steam reforming using CaO as CO<sub>2</sub> adsorbent [31].

### 2.3.3 Fixed bed adsorption

Fixed-bed is mostly operating in the large scale operation because it is easier to operate continuously and scale up for industrial use. Fixed-bed reactors is mostly used with heterogeneous catalyst for catalytic process. However, disadvantage of the fixed-bed reactor is hot-spot in the reactor occurs due to non-uniform distribution of the flow in the catalyst packing and pressure drop when particle size of catalyst is small. (GERHART EIGENBERGER, Institut für Chemische Verfahrenstechnik, Universität Stuttgart, Stuttgart, Federal Republic of Germany vol. B4)

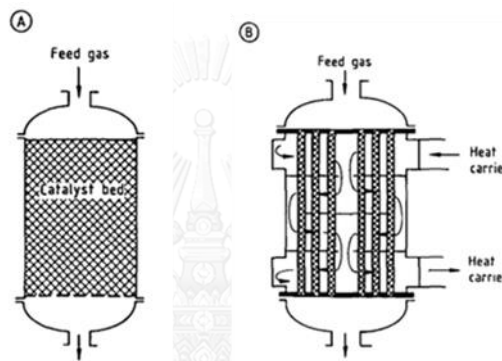


**Figure 2.12:** Basic types of catalytic fixed-bed reactors a) adiabatic fixed-bed reactor; b) multitubular fixed-bed reactor.

### 2.3.4 Breakthrough curve

Breakthrough is a plot between outlet concentrations of reactant to inlet concentration of reactant ( $C_{out}/C_F$ ) versus time. Breakthrough can be divided into three periods: at  $0 < t < t_b$ , the outlet concentration is less than  $C_{out}/C_F = 0.05$ , this range is called prebreakthrough, at  $t_b < t < t_e$ , the outlet concentration is increased rapidly, this range is called breakthrough, and at  $t > t_e$ , this range is called postbreakthrough where equilibrium adsorption is reached. Prebreakthrough represents time of adsorption of materials and breakthrough represents kinetic of adsorption of material. (J. D. Seader, Ernest J. Henley. Separation Process Principles. 2<sup>nd</sup> ed. New York: John Wiley & Sons Inc; 2005).

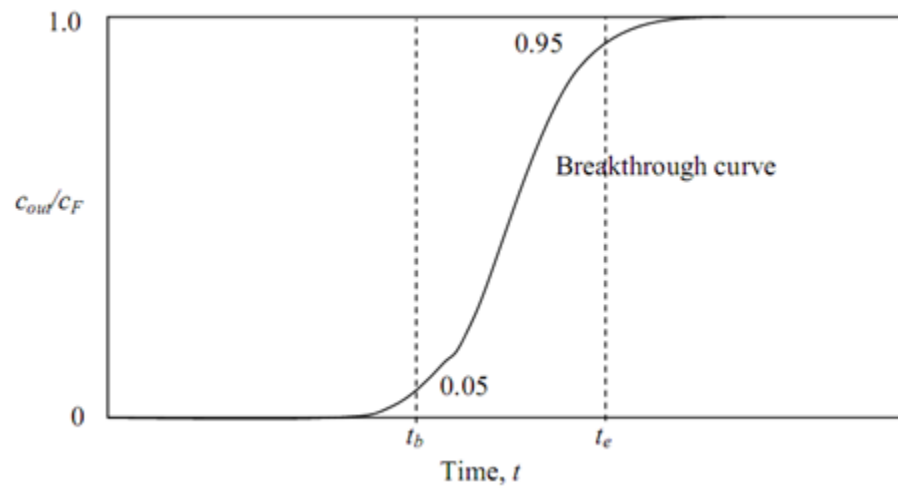


Figure 2.13: Breakthrough curve of sorption process



## CHAPTER III

### LITERATURE REVIEWS

In this chapter, the development of calcium oxide sorbent for carbon dioxide capture and process development concerning hydrogen production are reviewed. Topics include high-temperature CO<sub>2</sub> sorption, steam methane reforming, and sorption enhance steam methane reforming. Each topic is presented in details below.

Hydrogen can be produced from a variety of processes such as thermo-chemical process, electro chemical process and bio-chemical process [32]. At present, reforming process has been developed to use in industrial scale such as steam reforming, carbon dioxide reforming, partial oxidation or autothermal reforming [33]. For carbon dioxide reforming, although reducing the release of carbon dioxide is the advantage of this process as it is partly used as reactants; however the disadvantages of this process are lower proportion of hydrogen when compared to SR process and faster catalyst deactivation. Partial oxidation is a process in which hydrocarbons is mixed with a limited amount of oxygen in an exothermic process [2]. The main advantage of this process is no external energy is required. However, the limitations of this process are high cost of purified oxygen and feeding amount of oxygen must be carefully controlled. Autothermal reforming is another process that is used to produce hydrogen. This process relies on the combination of steam reforming process and partial oxidation process. By using this process, larger amount of hydrogen can be obtained when compared to partial oxidation process; however it requires larger downstream purification system. Steam reforming (SR) process is a process that is nowadays widely used for hydrogen production in industry because SR provides higher hydrogen concentration than other reformings such as dry reforming (DR), autothermal reforming (ATR), and partial oxidation (POX) [9].

Current commercial process for the production of hydrogen has been derived from a variety of sources. Several reactants can be used in steam reforming such as

methane [5-12], methanol [13, 14] and ethanol [16-18], etc. However, the common raw material is methane because it is cheap and easily found in nature [22]. Steam methane reforming has been developed from several researchers in different points of view such as process modification, catalysts, new designed reactors, etc. [2, 21]. Extensive studies have been focused on process and catalyst development because it is easy to develop and can reduce energy and cost during operation. In the development of catalysts, most precious metals, which possess high thermal stability, are used as catalyst, for example platinum [34-36], palladium [37, 38], rhodium [37, 39-41], etc. However, the precious metals are relatively expensive. Nickel-based catalyst is widely used for steam methane reforming (SMR) due to its high thermal stability and cheaper than precious metals although, it has been found that  $\text{CH}_4$  conversion obtained from the use of precious metals is slightly higher than nickel [39]. For SMR process, using appropriate support is also essential. The support may be inert or participate in the catalytic reactions. Typical supports for SMR process are, for example, various kinds of carbon, alumina and silica because they possess high surface area, high thermal stability and high reactivity.  $\text{NiO}/\text{Al}_2\text{O}_3$  catalyst with Mo oxide promoter was used in catalytic reaction of SMR process as reported in ref. [5]. Effect of feed of steam to carbon ratio (S/C), amount of Mo on metal area and specific activity were studied in this research. High stability was observed with S/C=4 for reaction time of 1500 minutes. At S/C=4,  $\text{CH}_4$  conversion and hydrogen yield of the catalyst with 0.05% Mo was 85 and 55%, respectively. However, at S/C=2, only the catalyst with 1.0% Mo remained stable for 400 minutes. At S/C=2,  $\text{CH}_4$  conversion and hydrogen yield of the catalyst with 1.0% Mo was 70 and 47%. From these results, it could be concluded that an increase of S/C ratio can lead to an increase of  $\text{CH}_4$  and  $\text{H}_2$  yield. Alumina supported nano-NiO-SiO<sub>2</sub> catalyst was studied in SMR process by Barnali Bej et al. [12]. In this work, the catalyst was prepared by sol-gel method and controlled crystallize size by calcination temperature. It was observed that 10% Ni loading in the catalyst with the use of calcination temperature of 400°C was an optimum Ni containing on catalyst for steam reforming reaction with the highest methane conversion: at optimum condition of 700°C and S/C=3.5, the conversion of methane was 95.7% and the yield of hydrogen was 3.8 moles of hydrogen per mole of methane

reacted. Hyo-Won Kim et al. [6] investigated the use of various metal oxide-supported nickel catalysts with core/shell structures such as Ni/Al<sub>2</sub>O<sub>3</sub>, Ni/MgAl<sub>4</sub>, Ni/CeO<sub>2</sub> and Ni/Ce<sub>0.4</sub>Zr<sub>0.6</sub>O<sub>2</sub> for SMR process. Ten percent of Ni loading on supports was tested at 750°C, S/C=2. Ni/Al<sub>2</sub>O<sub>3</sub> showed 97% CH<sub>4</sub> conversion and 73.5% composition whereas Ni/MgAl<sub>2</sub>O<sub>4</sub> provided 97.2% CH<sub>4</sub> conversion and 71.5% H<sub>2</sub> composition. Ni/CeO<sub>2</sub> and Ni/Ce<sub>0.4</sub>Zr<sub>0.6</sub>O<sub>2</sub> showed CH<sub>4</sub> conversion and H<sub>2</sub> composition lower than Ni/Al<sub>2</sub>O<sub>3</sub>. From these results, Ni/Al<sub>2</sub>O<sub>3</sub>, Ni/MgO–Al<sub>2</sub>O<sub>3</sub> showed the best performance on steam reforming of methane. Izquierdo et al. [11] investigated Ni-based over MgO and Al<sub>2</sub>O<sub>3</sub> and Pd and Pt-based over Al<sub>2</sub>O<sub>3</sub> catalysts for SMR. In the case of the Ni/Al<sub>2</sub>O<sub>3</sub> catalyst, 60.52% methane and natural gas conversions were obtained but it showed fast deactivation. In contrast, Ni/MgO catalyst did not show apparent deactivation and it presented the highest hydrogen production (methane conversion approximately 62.5%) at 800°C and S/C of 1.5 for SMR reaction. For Pt/Al<sub>2</sub>O<sub>3</sub> and Pd/Al<sub>2</sub>O<sub>3</sub> catalysts, low catalytic activity of less than 5% methane conversion was obtained, which might be due to bad impregnation and the carbon formation.

The stabilities of catalysts (catalyst deactivation) were important for industrial operations in production of hydrogen from steam methane reforming. The main cause of catalyst deactivation in steam methane reforming is coke and carbon formation. Many researches have been focused on the improvement of catalysts to overcome this problem. Zhai et al. [42] studied Ni/ZrO<sub>2</sub>/Al<sub>2</sub>O<sub>3</sub>, Ni/La–Ca/Al<sub>2</sub>O<sub>3</sub> and Ni<sub>0.5</sub>Mg<sub>2.5</sub>AlO<sub>9</sub> catalysts for steam methane reforming (SMR) at high space velocities. It was found that Ni/ZrO<sub>2</sub>/Al<sub>2</sub>O<sub>3</sub> and Ni/La–Ca/Al<sub>2</sub>O<sub>3</sub> catalysts showed a poor performance, while Ni<sub>0.5</sub>Mg<sub>2.5</sub>AlO<sub>9</sub> exhibited excellent activity and stability, of which approximately 100% methane conversion was obtained for 150 h at a lower GHSV of 1.8x10<sup>5</sup>h<sup>-1</sup> for SMR at a short residence time of 20 ms. Abreu et al. [43] studied the use of Ni-catalysts on a mixed oxide support for increases the oxygen vacancies of the support for removal carbon deposit from active site. It was found that methane conversion of NiCeO<sub>2</sub>, NiAl<sub>2</sub>O<sub>3</sub> and NiZrO<sub>2</sub> were more than 75%, 50-75% and 50-65%, respectively. The supports, with various ratios of Ce to Zr (xCeO<sub>2</sub>:(1-x)ZrO<sub>2</sub>; where x=0.2, 0.4, 0.6, 0.8), were investigated at S/C=2:1 at 700°C. The results showed Ni<sub>(0.8</sub>Ce<sub>0.2</sub>Zr)Al and Ni<sub>(0.6</sub>Ce<sub>0.4</sub>Zr) provided high conversion of methane and low deactivation; however,

$\text{Ni}_{(0.8}\text{Ce}_{0.2}\text{Zr)}\text{Al}$  suffered lower carbon deposition, possibly due to the smaller Ni crystallites. Roh et al. [44] investigated Ni-based catalyst for SMR process. Ni/Ce-ZrO<sub>2</sub>/ $\theta$ -Al<sub>2</sub>O<sub>3</sub>, Ni/ $\theta$ -Al<sub>2</sub>O<sub>3</sub> and Ni/ $\gamma$ -Al<sub>2</sub>O<sub>3</sub> were tested in this research. Ni/Ce-ZrO<sub>2</sub>/ $\theta$ -Al<sub>2</sub>O<sub>3</sub> showed high methane conversion for reforming reaction, Ni/Ce-ZrO/ $\theta$ -Al<sub>2</sub>O<sub>3</sub>, with various %Ni loading of 3,6,9,12,15, were tested for their performances at 750°C, S/C=1.0 and GHSV=72,000 ml/g<sub>cat</sub>h. The experiments showed that 12% Ni catalyst, which is found to be an optimum Ni loading, provided 83% CH<sub>4</sub> conversion, 85% H<sub>2</sub> yield, 78% CO yield and a H/CO ratio of 3.0. Comparison stability between Ni/Ce-ZrO<sub>2</sub>/ $\theta$ -Al<sub>2</sub>O<sub>3</sub> and Ni/MgAl<sub>2</sub>O<sub>4</sub> commercial catalyst revealed that Ni/MgAl<sub>2</sub>O<sub>4</sub> deactivated with time on stream, which is most likely due to the carbon formation, while 12% Ni/Ce-ZrO<sub>2</sub>/ $\theta$ -Al<sub>2</sub>O<sub>3</sub> catalyst maintained its stability. Salhi et al. [45] investigated the effect of %wt NiO with mixed oxides (NiAl<sub>2</sub>O<sub>4</sub>, 5 wt% NiO/NiAl<sub>2</sub>O<sub>4</sub>, 10 wt% NiO/NiAl<sub>2</sub>O<sub>4</sub> and 15 wt% NiO/NiAl<sub>2</sub>O<sub>4</sub>) for steam methane reforming process. NiAl<sub>2</sub>O<sub>4</sub> showed the best performance catalyst at 800°C, S/C=3 (CH<sub>4</sub> conversion≈99%, CO yield≈80%, CO<sub>2</sub> yield 0% and H<sub>2</sub>/CO=3). Over 5 wt% of NiO excess, the CH<sub>4</sub> conversion, CO and H<sub>2</sub> selectivities were found to reduce. From these results, it could be concluded that when %Ni loading was increased, methane conversion and CO yield were decreased due to large Ni particle formation after rapid sintering. Table 3.1 summarizes the use of different Ni-based catalysts for steam methane reforming reaction.

**Table 3.1:** Summary of the use of different Ni-based catalysts and supports and conditions for steam methane reforming reaction.

Catalyst	Condition		CH <sub>4</sub> conversion (%)	H <sub>2</sub> concentration (%)	Ref.
	T(°C)	S/C			
NiO/Al <sub>2</sub> O <sub>3</sub>	700°C	4:1	77%	55%	[5]
0.05%Mo-NiO/Al <sub>2</sub> O <sub>3</sub>	700°C	4:1	85%	58%	
0.5%-Mo-NiO/Al <sub>2</sub> O <sub>3</sub>	700°C	4:1	73%	57%	
1.0%Mo-NiO/Al <sub>2</sub> O <sub>3</sub>	700°C	4:1	60%	39%	
2.0%Mo-NiO/Al <sub>2</sub> O <sub>3</sub>	700°C	4:1	80%	53%	

10%Ni/Al <sub>2</sub> O <sub>3</sub> ,	750°C	2.0	97%	73.5%	[6]	
10%Ni/MgO–Al <sub>2</sub> O <sub>3</sub> ,	750°C	2.0	97%	71.5%		
10%Ni/CeO <sub>2</sub>	750°C	2.0	89%	70.5%		
10%Ni/Ce <sub>0.4</sub> Zr <sub>0.6</sub> O <sub>2</sub>	750°C	2.0	91%	70.3%		
20%Ni-MgO	800°C	1.0	55%	30%	[11]	
20%Ni-MgO	800°C	1.5	60.52%	50%		
20%Ni-MgO	800°C	2.0	54%	55%		
18%Ni-Al <sub>2</sub> O <sub>3</sub>	800°C	1.0	72.9%	10%		
18%Ni-Al <sub>2</sub> O <sub>3</sub>	800°C	1.5	62.5%	-		
18%Ni-Al <sub>2</sub> O <sub>3</sub>	800°C	2.0	62.5%	15%		
Alumina supported- 5.0%NiO–SiO <sub>2</sub>	600°C	3:5	31%	-	[12]	
Alumina supported- 7.0%NiO–SiO <sub>2</sub>	600°C	3:5	66%	-		
Alumina supported- 10.0%NiO–SiO <sub>2</sub>	600°C	3:5	75%	-		
Alumina supported- 12.5%NiO–SiO <sub>2</sub>	600°C	3:5	68%	-		
Alumina supported- 15.0%NiO–SiO <sub>2</sub>	600°C	3:5	59%	-		
Alumina supported- 10.0%NiO–SiO <sub>2</sub>	700°C	3:5	95%	75% (yield=4)		
19.9%Ni/ZrO <sub>2</sub> /Al <sub>2</sub> O <sub>3</sub> ,	N/A	3.0	<5%	-		[42]
21.6%Ni/La–Ca/Al <sub>2</sub> O <sub>3</sub>	N/A	3.0	95%	-		
11.3%Ni <sub>0.5</sub> Mg <sub>2.5</sub> AlO <sub>9</sub>	N/A	3.0	100%	-		
5%NiAl <sub>2</sub> O <sub>3</sub> <sup>a</sup>	700°C	2:1	50%	2.4*	[43]	
5%NiCeO <sub>2</sub> <sup>a</sup>	700°C	2:1	75%	2.9*		
5%NiZrO <sub>2</sub> <sup>a</sup>	700°C	2:1	47%	2.2*		
5%Ni <sub>(0.2</sub> Ce <sub>0.8</sub> Zr)Al <sup>a</sup>	700°C	2:1	30%	3.2*		



5%Ni <sub>(0.4Ce<sub>0.6</sub>Zr)</sub> Al <sup>a</sup>	700°C	2:1	40%	3.6*	
5%Ni <sub>(0.6Ce<sub>0.4</sub>Zr)</sub> Al <sup>a</sup>	700°C	2:1	62.5%	3.3*	
5%Ni <sub>(0.8Ce<sub>0.2</sub>Zr)</sub> Al <sup>a</sup>	700°C	2:1	61%	3.4*	
3%Ni/ $\theta$ -Al <sub>2</sub> O <sub>3</sub>	750°C	2:2	-	-	[44]
3%Ni/Ce-ZrO <sub>2</sub> / $\theta$ Al <sub>2</sub> O <sub>3</sub>	750°C	2:2	71%	74%	
6%Ni/Ce-ZrO <sub>2</sub> / $\theta$ Al <sub>2</sub> O <sub>3</sub>	750°C	1	75%	77%	
9%Ni/Ce-ZrO <sub>2</sub> / $\theta$ Al <sub>2</sub> O <sub>3</sub>	750°C	1	79%	83%	
12%Ni/Ce-ZrO <sub>2</sub> / $\theta$ Al <sub>2</sub> O <sub>3</sub>	750°C	1	82%	85%	
15%Ni/Ce-ZrO <sub>2</sub> / $\theta$ Al <sub>2</sub> O <sub>3</sub>	750°C	1	77%	76%	
NiAl <sub>2</sub> O <sub>4</sub> ,	800°C	3	99%	2.8**	[45]
5 wt% NiO/NiAl <sub>2</sub> O <sub>4</sub> ,	800°C	3	98%	5**	
10 wt% NiO/NiAl <sub>2</sub> O <sub>4</sub>	800°C	3	78%	4.2**	
15 wt% NiO/NiAl <sub>2</sub> O <sub>4</sub>	800°C	3	85%	4.8**	

<sup>a</sup> time on steam at 300 minutes; \* H<sub>2</sub>/CH<sub>4</sub> ratio; \*\* H<sub>2</sub>/CO ratio

As seen from the above review, although high methane conversion and high H<sub>2</sub> yield can be obtained with the use of different amount of catalysts and supports; however, some disadvantages of conventional SMR process are still encountered such as catalyst deactivation due to carbon formation or additional separation unit is required for purification of H<sub>2</sub> [23]. Recently, the so-called multi-functional process has been developed in order to reduce separation unit for H<sub>2</sub> purification, simplified operation of process and reduce energy consumption as well as lower capital and operating cost. One of such is the combination of reforming process and CO<sub>2</sub> capture unit, which is known as sorption-enhanced steam reforming (SESR) [46].

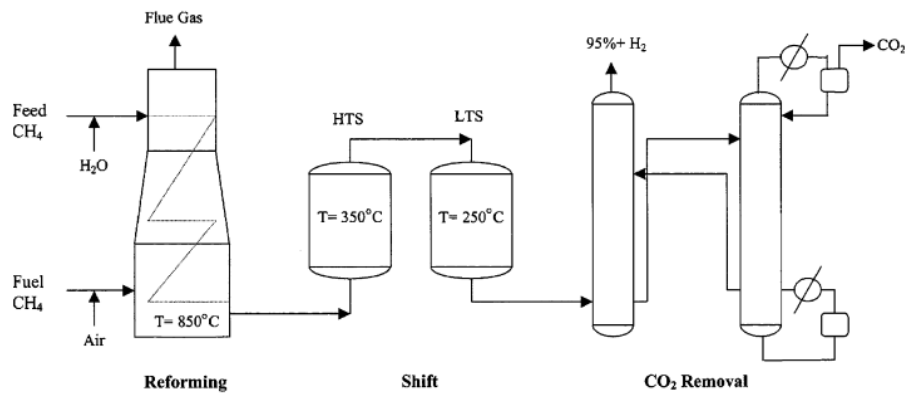


Figure 3.1: Flow diagram of a conventional SMR process [29].

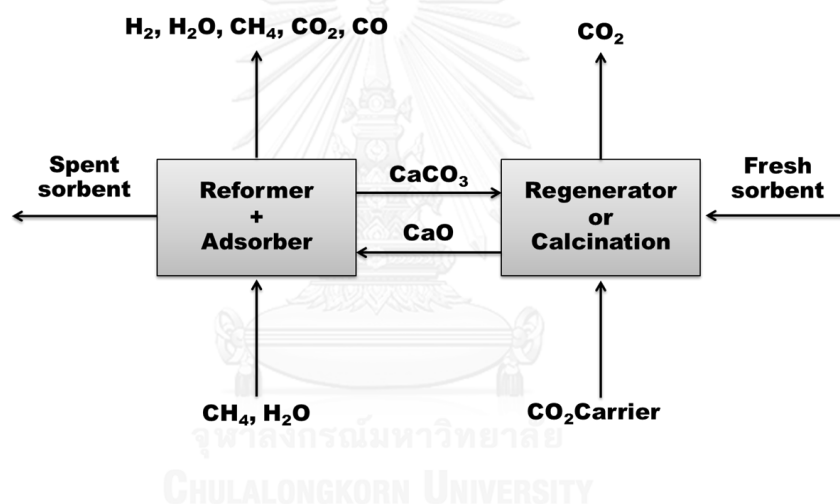


Figure 3.2: Simplified block-scheme of the sorption-enhanced steam reforming process (SER) [47].

The concept of sorption enhanced steam reforming (SESR) is based on Le Chatelier's principle that the conversion of reactants to products and the rate of forward reaction in an equilibrium controlled reaction can be increased by selectively removing some of the reaction products from the reaction zone. Advantages of the combined process are that the conversion of  $\text{CH}_4$  can be improved as well as high purity of hydrogen. Moreover, less severe operating condition can be used, which leads to minimization of energy and cost [29]. In sorption-enhanced steam reforming process, adsorbent is combined with catalyst to selective separation of substances from

reaction mixture. Calcium oxide (CaO) is widely used in SESR process because it is cheap and readily available in nature, good kinetic, high capacity and it can be regenerated. However, the drawback of this material is it requires high temperature for regeneration causes sorbent deactivation, poor stability for a long period of time. As such, many researches have been conducted to improve both capacity and stability of CaO to use in SESR process such as the addition of other high thermal stability materials, increase surface area and improve distribution of active site on catalyst, etc. The following part of this review will be focused on the development of CaO adsorbent to use as sorbent to capture CO<sub>2</sub> at high temperature in the range that could be applied for SESR system. Witton [48] used waste eggshell as raw material for calcium oxide-based sorbent production. The results showed that the carbonation conversion of the calcined eggshell was higher than that of the calcined commercial calcium carbonate after several cycles at the same reaction conditions. The authors claimed that this behavior is due to its smaller CaO particle size which provides a higher exposed surface reaction for CO<sub>2</sub> capture. Li et al. [49] compared CO<sub>2</sub> capture performances of rice husk ash/CaO and original CaO. The carbonation conversions and surface area of rice husk ash/CaO were found to be higher than those of original CaO (conversion = 50% and 20%, respectively) during the 50 carbonation/calcination cycles for carbonation temperature of 700 °C and for calcination temperature of 850°C. Rice husk ash/CaO were also found to have better anti-sintering performance than the original CaO at high temperature, especially above 950°C. Quincoces et al. [50] studied the use of CaO with Ni-Al<sub>2</sub>O<sub>3</sub> for reforming of methane. Catalytic activity was evaluated at 650°C and atmospheric pressure. Results showed that catalysts modified with CaO improve the stability of Ni-Al<sub>2</sub>O<sub>3</sub> as the rate of catalyst deactivation is lower than the nickel-based catalysts without CaO due to CaO modified the behaviour of the active sites cause formation of carbon decreased. Adding surfactant is another technique that is used to improve properties and reactivity of adsorbents. Calcium lignosulfonate (CLS) is anionic polymer surfactant that is used to improve properties of CaO. Adding 0.5% CLS into CaO can improve properties and reactivity of sorbent such as specific surface area, pore volume, and pore size diameter, leading to an improvement of CO<sub>2</sub> sorption capacity of 0.893 g CO<sub>2</sub>/g sorbent. It was found that particle of sorbent slightly

deactivated after 10 cycles because CLS-CaO can retard the sintering rate [51]. Akgornpeak et al. [52] used cetyltrimethyl ammonium bromide (CTAB) surfactant to modify CaO derived from calcium nitrate. Optimum ratio of calcium to CTAB was 10:3 mmol. CTAB-modified CaO can improve carbonation conversion of 54% higher than that of CaO without CTAB at pellet size less than 25 $\mu$ m and can prevent the agglomeration of CaO particles. Luo et al. [53] improved the capacity and stability of CaO during carbonation/calcination cycles by varying amount of Al<sub>2</sub>O<sub>3</sub> in synthetic CaO/Al<sub>2</sub>O<sub>3</sub> sorbents synthesized by sol-gel method. It was found that the synthetic sorbent showed higher carbonation conversions and surface area than those of the pure CaO sorbent. It showed that 20 wt% of Al<sub>2</sub>O<sub>3</sub> provided much better conversion than others (at 10 and 40 wt% Al<sub>2</sub>O<sub>3</sub>) on cyclic CO<sub>2</sub> capture. The results indicated that CaO/Al<sub>2</sub>O<sub>3</sub> = 80:20 wt% sorbent provided a competitive performance of capture capacity of 0.43 g CO<sub>2</sub>/g sorbent after 20 cycles. Huang et al. [54] developed a modified CaO-based mesoporous material with high sorption and long-term stability for CO<sub>2</sub> sorption. Mesoporous silica SBA-15 was used as inert support. Calcium acetate was used as the precursor for dispersion on silica support by using an impregnation method. Sample CaO-SBA-15 (from evaporation method) exhibited a 43 wt% increase in sorption capacity (equal to 0.44 g CO<sub>2</sub>/g- sorbent) when compared with SBA-15 during the carbonation step. Stability tests showed that the CO<sub>2</sub> adsorption capacity remained 7.84 mol/kg sorbent (80% adsorption ratio) after 40 cyclic runs at carbonation temperature of 700°C and calcination temperature of 910°C.

Liu et al. [55] investigated the effect of calcium precursors on properties of CaO and the ability to adsorb CO<sub>2</sub>. Different types of calcium precursors including calcium carbonate (CC-CaO), calcium hydroxide (CH-CaO), nanosized (<70nm) calcium carbonate (CC70 nm-CaO), nanosized (<160 nm) calcium oxide (CaO160 nm-CaO), calcium acetate hydrate (CA-CaO), calcium L-lactate hydrate (CL-CaO), calcium formate (CF-CaO), calcium citrate tetrahydrate (CCi-CaO), and calcium D-gluconate monohydrate (CG-CaO), were tested for CO<sub>2</sub> capture at high temperature. CG-CaO showed the best capacity for CO<sub>2</sub> capture (83% carbonation conversion), which was referred to as a self-reactivation phenomena. CG-CaO has more pore structure causes faster rate decomposition reaction.

Zhou et al. [56] reported the synthetic CaO-based sorbents derived from different calcium and aluminum precursors. It showed much higher capacity and stability over multi carbonation-calcination cycles.  $\text{Ca}_9\text{Al}_{16}\text{O}_{18}$  is an inert support. It was used as a stable framework inhibiting deactivation of CaO same as  $\text{Ca}_{12}\text{Al}_{14}\text{O}_{33}$  but step of synthesis more than  $\text{Ca}_{12}\text{Al}_{14}\text{O}_{33}$ . CaO-based sorbent ( $\text{CaO-Ca}_9\text{Al}_{16}\text{O}_{18}$ ) derived from calcium acetate showed high maximum carbonation conversion but after 10 cycles CaO-based sorbent ( $\text{CaO-Ca}_9\text{Al}_{16}\text{O}_{18}$ ) derived from calcium citrate exhibited the best performance for  $\text{CO}_2$  capture in terms of capacity and stability, which was shown as 0.59  $\text{g.CO}_2/\text{g.sorbent}$  in the first cycle and 0.51  $\text{g.CO}_2/\text{g.sorbent}$  in 28 cycles. The carbonation conversion reduced from 0.94 to 0.81. Consequently, CaO-based sorbent ( $\text{CaO-Ca}_9\text{Al}_{16}\text{O}_{18}$ ) derived from calcium citrate is an excellent sorbent in this research. Lemonidou et al. [47] studied the use of different Ca-Al precursors to form a complex sorbent  $\text{Ca}_{12}\text{Al}_{14}\text{O}_{33}$  and used it as a sorbent for high-temperature  $\text{CO}_2$  sorption. Calcium hydroxide ( $\text{Ca(OH)}_2$ ) and calcium acetate ( $\text{Ca(CH}_3\text{COO)}_2$ ) were selected as calcium precursors. The results showed that calcined calcium acetate provided the highest  $\text{CO}_2$  uptake ability: 50% weight increase of the sorbent at  $690^\circ\text{C}$  in the flow of 15%v/v  $\text{CO}_2$  (balanced  $\text{N}_2$ ). The improved adsorbent resulted in a higher number of carbonation-calcination over 40 cycles. Dennis et al. [57] investigated the use of Ca-based sorbent containing 85 wt % CaO and 15 wt %  $\text{Ca}_{12}\text{Al}_{14}\text{O}_{33}$  for  $\text{CO}_2$  sorption test. The behavior of the synthetic sorbent in response to increasing concentrations of  $\text{CO}_2$  because %v/v of  $\text{CO}_2$  carbonation increased from 14% to 27%,  $\text{CO}_2$  uptake increased from 0.19 to 0.42  $\text{g CO}_2/\text{g sorbent}$ . The sorbent showed a steady uptake of  $\text{CO}_2$  over a large number of cycles, 44 cycles, of both %carbonation.

Xie et al. [22] studied the use of physical mixture between  $\text{Ni}_{0.50}/\text{Mg}_{2.50}\text{Al}$  catalyst and  $\text{CaO-Ca}_9\text{Al}_{16}\text{O}_{18}$  sorbent (active phase and inert phase) for SESMR process. The results showed that at  $550^\circ\text{C}$ , 1 atm,  $S/C=4.2$  and methane inlet feed of 14.7 mL/min, 97%  $\text{H}_2$  purity (on dry basis) can be obtained whereas increasing temperature to  $600^\circ\text{C}$  at the same operating conditions resulted in a slight decrease of  $\text{H}_2$  purity (96% $\text{H}_2$ ) but for a significantly shorter period of time: from 60 minutes ( $550^\circ\text{C}$ ) to 45 minutes ( $600^\circ\text{C}$ ). Martavaltzi et al. [46] developed a hybrid material by combining sorbent with catalyst for SESMR process named  $\text{Ni-CaO-Ca}_{12}\text{Al}_{14}\text{O}_{33}$ . The results showed

that 16% of Ni on the hybrid sorbent showed higher catalytic activity (80%) and higher H<sub>2</sub> yield (90% instead of 84% in SR process) with H<sub>2</sub> concentration of 90%. Kim et al. [58] studied one-body catalytic adsorbent, which includes CaO, Ca<sub>12</sub>Al<sub>14</sub>O<sub>33</sub> and Ni-metallic. The material was tested for sorption enhanced methane reforming process at 630°C, steam to methane ratio of 3 and atmospheric pressure. Seven percent weight of Ni loading showed excellent performance in terms of H<sub>2</sub> production and CH<sub>4</sub> conversion. When comparison between physical mixing of 3 g of Ni catalyst with 9 g of CaO-Ca<sub>12</sub>Al<sub>14</sub>O<sub>33</sub> sorbent and 12 g of Ni-CaO-Ca<sub>12</sub>Al<sub>14</sub>O<sub>33</sub>, one-body catalytic adsorbent found that H<sub>2</sub> concentration of one-body catalytic adsorbent produced H<sub>2</sub> better than physical mixing. One-body catalytic adsorbent was observed to be very stable and maintained at 94-95% H<sub>2</sub> during the sorption enhanced period around 70 min. Physical mixing of catalyst-adsorbent showed 95% of H<sub>2</sub> concentration around 45 minutes for all 4 cycles.

**Table 3.2 :** summarized the summarized the use of multifunctional catalysts for sorption enhanced steam methane reforming process.

Catalyst	Condition		CH <sub>4</sub> conversion (%)	H <sub>2</sub> concentration (%)	Ref.
	T(°C)	S/C			
80%CaO–20%Ca <sub>9</sub> Al <sub>6</sub> O <sub>18</sub> + Ni <sub>0.50</sub> /MgAl <sub>2.50</sub>	600°C	4.2	90%	75%	[22]
CaO+ Ni <sub>0.50</sub> /MgAl <sub>2.50</sub>	600°C	4.2	85%	-	
12.5wt%Ni-CaO	600°C	3	86%	70%	[24]
12.5wt%Ni/Al <sub>2</sub> O <sub>3</sub> +CaO	600°C	3	89%	65%	
NiO-CaO <sup>c</sup>	580°C	2	97%	98%	[31]
16%NiO-CaO-Ca <sub>12</sub> Al <sub>14</sub> O <sub>33</sub>	650°C	3.4	70%	77%	[46]

3%Ni-CaO-Ca <sub>12</sub> Al <sub>14</sub> O <sub>33</sub> <sup>b</sup>	630°C	3	630°C	75%	[58]
7%Ni-CaO-Ca <sub>12</sub> Al <sub>14</sub> O <sub>33</sub> <sup>b</sup>	630°C	3	630°C	95%	
CaO-Ca <sub>12</sub> Al <sub>14</sub> O <sub>33</sub> +Ni	630°C	3	630°C	75%	
commercial catalyst <sup>a</sup>					

<sup>a</sup> the duration of sorption enhanced period lasted to 45 min for all 4 cycles.

<sup>b</sup> the duration of sorption enhanced period lasted to 70 min for all 4 cycles.

<sup>c</sup> NiO/CH<sub>4</sub> ratio = 1.1



## CHAPTER IV

### EXPERIMENTAL

Catalytic sorbent for sorption enhanced steam methane reforming process is a subject of investigation in this work. CaO-based sorbent was synthesized to use as sorbent for high-temperature CO<sub>2</sub> sorption and NiO was added into the sorbent to act as catalyst for the reforming reaction. In this chapter, details of sorbent and catalytic sorbent preparation are provided. Then, characterization techniques including XRD, BET, SEM, TGA H<sub>2</sub>-TPR and H<sub>2</sub> chemisorption are summarized. Finally, details of experimental investigation of high-temperature CO<sub>2</sub> and of sorption enhanced steam methane reforming are presented in the last topic.

#### 4.1 Materials

Calcium D-gluconic acid, (C<sub>12</sub>H<sub>22</sub>CaO<sub>14</sub>, Acros) and Calcium nitrate tetrahydrate (Ca(NO<sub>3</sub>)<sub>2</sub>·4H<sub>2</sub>O Sigma Aldrich) were used as CaO precursors. Aluminum nitrate enneahydrate precursor (Al(NO<sub>3</sub>)<sub>3</sub>·9H<sub>2</sub>O, Panreac) and 2-propanol (Carlo Erba) were used in the synthesis of the sorbent and nickel nitrate hexahydrate (Ni(NO<sub>3</sub>)<sub>2</sub>·6H<sub>2</sub>O, Sigma Aldrich) was used in the synthesis of the catalytic sorbent. Commercial calcium oxide (CaO, Riedel-deHaen) and commercial alumina (Al<sub>2</sub>O<sub>3</sub>, Sigma Aldrich) were used in comparison for synthesis of the sorbent with calcium and aluminum precursors. Hexadecyltrimethylammonium bromide (CTAB, Acros) and Sodium dodecyl sulfate (SDS, Carlo Erba) were used for enhancement of surface area. Nitrogen gas was used as purge gas during calcination period for stability test and as dilution gas with carbon dioxide during CO<sub>2</sub> adsorption period, hydrogen gas was used to reduce catalyst, and methane gas was used as raw material for sorption enhance reaction. All gases had a purity of 99.999%.



## 4.2 Catalytic sorbent preparation

In this work, the effect of the addition of additive on surface properties of the sorbent, CO<sub>2</sub> sorption ability are subjects of investigation. The experimental details are provided as follows.

### 4.2.1. Synthesis of Ca-based sorbent without surfactant

The preparation procedure is as follows. First, aluminum nitrate nonahydrate and calcium precursors, calcium D-gluconic acid (C<sub>12</sub>H<sub>22</sub>CaO<sub>14</sub>) or calcium nitrate tetrahydrate (Ca(NO<sub>3</sub>)<sub>2</sub>·4H<sub>2</sub>O), were added into the 190-ml de-ionized water mixed with 32.5 ml of 2-propanol solution. Then, 27.6 g of calcium nitrate and 7.11 of alumina or 21.5 g of calcium d-gluconic acid and 3 g of alumina were added in solution. The solution was continuously stirred at 75°C for 1 h and then allowed to dry at 120°C in an oven for 18 h. The powder was collected from the oven and calcined at 500°C for 3 h in air. Distilled water was added to the resulting powder to form a paste which was then dried at 120 °C for 2 h and calcined at 900 °C for 1.5 h in air.

### 4.2.2 Synthesis of Ca-based sorbent modified by surfactant

The preparation procedure is as follows. First, 190 ml of de-ionized water and 32.5 ml of 2-propanol were used as a solvent. The solvent was then heated up to 75°C under continuous stirring. A 0.584-g (9mM) sodium dodecyl sulfate (SDS), 27.6 g of calcium nitrate and 7.11 of alumina or 21.5 g of calcium d-gluconic acid and 3 g of alumina were mixed in the solution. . The solution was continuously stirred at 75°C for 1 h and then allowed to dry at 120°C in an oven for 18 h. The powder was collected from the oven and calcined at 500°C for 3 h in air. Distilled water was added into the resulting powder to form a paste which was then dried at 120 °C for 2 h and calcined at 900 °C for 1.5 h in air. Then, CaO-Ca<sub>12</sub>Al<sub>14</sub>O<sub>33</sub> sorbent was obtained. For applying CTAB, similar methodology to the case of SDS was conducted with the use of 0.082,

0.246, 0.410, 0.574 and 0.820 g (1, 3, 5, 7 and 10 mM, respectively) of cetyltrimethylammonium bromide (CTAB).

#### 4.2.3 Incipient wetness impregnation method

To synthesize catalytic sorbent material, 12.5wt% nickel nitrate hexahydrate ( $\text{Ni}(\text{NO}_3)_2 \cdot 6\text{H}_2\text{O}$ ) was dissolved in 75 ml of deionized water. After that, the synthetic CaO-based sorbent was added into nickel solution. Then, the sample was stirred for 30 min at  $100^\circ\text{C}$  and dried at  $100^\circ\text{C}$  overnight and calcined at  $900^\circ\text{C}$  for 1.5 h in air

### 4.3 Catalytic sorbent characterization

#### 4.3.1 X-ray diffraction (XRD)

X-ray diffraction analysis (XRD) is used to analyze the properties of materials such as fingerprint, crystal structure, amount of components, particle sized of particles of each unit cell and the crystallite sized of the sample. The results of the XRD can determine the relationship of compounds with Pattern diffraction of X-rays. It can find for all components in the sample.

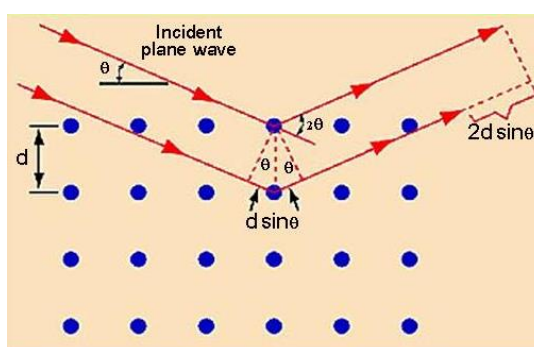


Figure 4.1: principle of XRD

From equation

$$2d \sin \theta = n\lambda \quad (4.1)$$

where

$d$  = interplanar spacing ( $1 \text{ \AA} = 10^{-10} \text{ m}$ )

$\theta$  = angle between X-ray and crystal planes (degree)

$\lambda$  = wavelength ( $\text{\AA}$ )

$n$  = an integer

Crystalline structure of the hybrid catalytic sorbent was characterized by X-ray diffraction (XRD). XRD pattern was determined by D8 Advance of Bruker AXS using  $\text{Cu K}\alpha$  radiation ( $\lambda=1.5406 \text{ \AA}$ ). The pattern was recorded in the range of  $10^\circ < 2\theta < 80^\circ$  with an increasing step of  $0.04^\circ$  and scan speed of 0.5.

#### 4.3.2 $\text{N}_2$ adsorption desorption

BET analysis is used to measure specific surface area, pore volume, and pore diameter of materials determining from nitrogen adsorption/desorption measurement as a function of relative pressure ( $P/P_0$ ) using an automatic analyzer. The principle of BET measurement is calculated based on adsorption of nitrogen molecules on the surface of the material.



**Figure 4.2:**  $\text{N}_2$  adsorption/desorption analyzer

The formula used to calculate the surface area is

$$S = 4.35V_m \quad (4.2)$$

In this work, measurements were carried out by using Micromeritics Chemisorp 2750. The nitrogen adsorption/desorption isotherm was tested at 77 K with 0.1 g of hybrid catalytic sorbent.

#### 4.3.3 Scanning electron microscope (SEM)

The morphologies of samples were observed with a JEOL JSM 6360 LV scanning electron microscope (SEM). An energy-dispersive spectrometry (EDS, Falcon, EDX) is couple to the SEM. SEM (EDS) was used to determine metal distribution on the catalytic sorbent.

#### 4.3.4 H<sub>2</sub> Chemisorption

Metals dispersion of the as-synthesized samples were determined by ChemiSorb 2750 ( Micromeritics 2750 system ).

#### 4.3.5 Thermogravimetric analysis (TGA) (For Characterization)

Weight loss and temperature adsorption-desorption of sorbent were determined by SDT Q600 TA Instrument. Percent of CaO on sorbent can be calculated from weight loss of sorbent, the equation used to calculate amount of CaO in the sorbent is

$$X = \frac{m_0 - m_1}{m_1} \frac{M_{CaO}}{M_{H_2O}} \quad (4.3)$$

where  $m_o$  is the hydrated sorbent weight (excluding physisorbed water),  $m_1$  is the sorbent weight after dehydration,  $M_{H_2O}$  is the molar weight of  $H_2O$  [56].

#### 4.3.6 Temperature-programmed reduction (TPR)

Temperature-programmed reduction (TPR) is a technique used for characterization of solid materials and is often used to find the most efficient reduction conditions. Mass spectrometry GSD 32001 OMNI<sup>Star</sup>™ was applied for  $H_2$ -TPR analysis in this work.  $H_2$ -TPR was used to determine temperature reduction to reduce NiO to Ni on hybrid catalytic sorbents.

#### 4.3.7 Thermogravimetric analysis (TGA) (Set up experiment)

TGA-50, Shimadzu, was used to test  $CO_2$  sorption capacity for comparison with fixed-bed reactor flow pattern. Schematic of the set up TGA is shown in Figure 4.3. To test the ability of CaO-based sorbent to adsorb  $CO_2$ , 10 mg of the sorbent was pretreated at 850°C in 50 mL/min flow of pure  $N_2$  for 5 min. The temperature was then decreased to 600°C and the valve was switched to 10 mL/min  $CO_2$  flow (15%  $CO_2$  with balanced  $N_2$ ). Capacity of  $CO_2$  sorption was determined by equation 4.4 as;

$$X = \frac{m_{T_{Cal}} - m_{T_{Car}}}{m_{T_{Car}}} \quad (4.4)$$

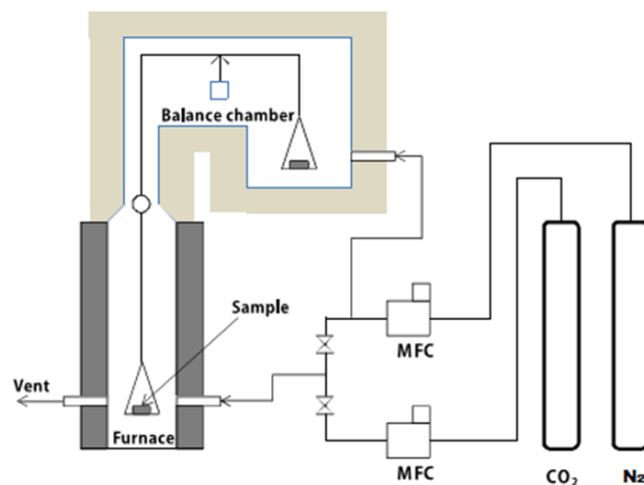


Figure 4.3: Schematic of TGA equipment [59]

#### 4.4 Adsorption performance test using fixed-bed system

A mass spectrometry was used to measure CO<sub>2</sub> adsorption capacity (carbonation and calcination experiments). To test CO<sub>2</sub> sorption capacity, 1 g of sorbent was pretreated at 850°C in 50 mL/min using pure N<sub>2</sub> for 1 hr. The temperature was then decreased to 600°C and the valve was switched to 10 mL/min CO<sub>2</sub> flow (15% v/v, balanced N<sub>2</sub>). The adsorption duration was carried out until to full capacity of sorbent, which was observed by an amount of outlet gas is equal to that of inlet gas. Multiple cycles of adsorption and desorption were repeated in order to test the ability of the material to retain its CO<sub>2</sub> sorption capacity. Desorption was conducted by purging pure N<sub>2</sub> of 50 mL/min at 850°C for 0.5 hr.

#### 4.5 Catalytic performance test (Sorption enhance steam methane reforming, SESMR)

Sorption enhanced steam methane reforming reaction was conducted in fixed-bed quartz reactor (ID of 10 mm, OD of 12 mm, and length of 500 mm). Two grams of hybrid catalytic sorbent (Ni-CaO-Ca<sub>12</sub>Al<sub>14</sub>O<sub>33</sub>) were packed in the reactor, which was supported by quartz wool. The hybrid catalytic sorbent was pretreated at 850°C for 1

h with  $N_2$  (30 mL/min) before running the reaction and then its catalyst sites were reduced in a flow of  $H_2/N_2$  (50% in  $H_2$ ) at  $850^\circ C$  for 1 hr. A 10-mL/min methane was fed into the reactor with the co-flow of nitrogen of 20 mL/min (total inlet flow of methane and nitrogen was 30 mL/min). The flow rate of inlet steam was 30 mL/min, which would yield the steam-to-methane ratio of 3. Product stream was analyzed by gas chromatography (GC-8A, shimazu). Figure 4.4 shows the experimental set up of SESMR and Table 4.1 shows details and conditions of gas chromatography.

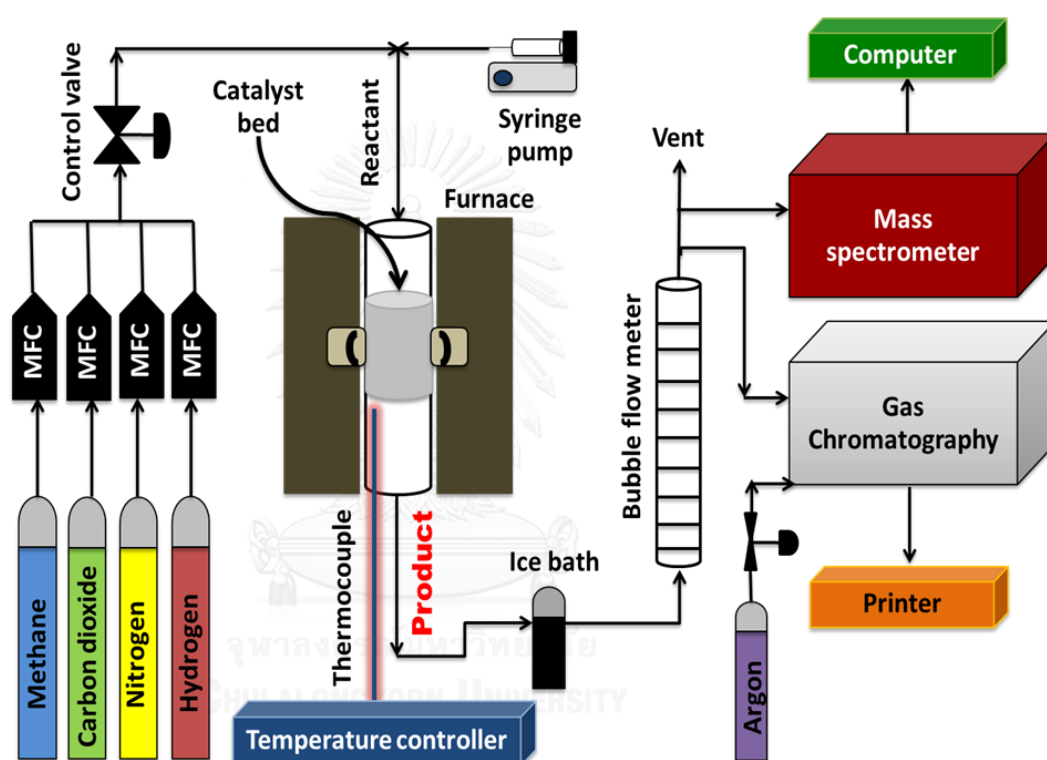


**Figure 4.4:** Experimental set up for hydrogen production via sorption enhance steam methane reforming.

Product stream was analyzed by gas chromatography (GC-8A, shimazu). Operating condition of GC is shown in Table 4.1

**Table 4.1:** Operating conditions for Gas chromatography

Gas Chromatography	Shimazu GC-8A	
Detector	TCD	
Column	Molecular sieve 5A*	Parapak-Q*
Column material	SUS	SUS
Length (m)	2	2
Outer diameter (mm)	4	4
Inner diameter (mm)	3	3
Mesh range	60/80	60/80
Maximum temperature (°C)	350	350
Carrier gas	Ar (99.999%)	Ar (99.999%)
Carrier gas flow (mL/min)	30	30
Column temperature		
Initial (°C)	50	50
Final (°C)	50	50
Injector temperature (°C)	70	70
Detector temperature (°C)	100	100
Current (mA)	70	70
Analyzed gas	N <sub>2</sub> , H <sub>2</sub> , CO, CH <sub>4</sub>	CO <sub>2</sub>



## CHAPTER V

### RESULTS AND DISCUSSION

This chapter presents the results concerning the ability of calcium-based sorbent, synthesized from two different calcium oxide precursors, on CO<sub>2</sub> capture at high temperature and on CO<sub>2</sub> sorption in sorption-enhanced methane steam reforming process.

#### 5.1 CO<sub>2</sub> Sorption

##### 5.1.1 Comparison of technique to measure CO<sub>2</sub> sorption capacity

TGA is widely used to investigate the ability of sorbent material on gas adsorption because the technique is easy to operate, the calculation of sorption capacity is simple as only weight change is required, and a small amount of sorbent is needed. However, to apply for industrial sorption enhanced steam reforming reaction using fixed-bed reactor, as a consequence, the ability of the sorbent to adsorb CO<sub>2</sub> was tested with fixed-bed reactor in this work. We firstly compared the difference of sorption capacity measured by TGA and fixed-bed systems, the results are shown in Figure 5.1. The results showed that examining CO<sub>2</sub> sorption capacity using TGA offers higher value than using fixed-bed reactor: This might be due to CO<sub>2</sub> molecules can diffuse through surface and pore of sorbent better than fixed-bed system as the gas molecules can flow in all direction around sample in pan.

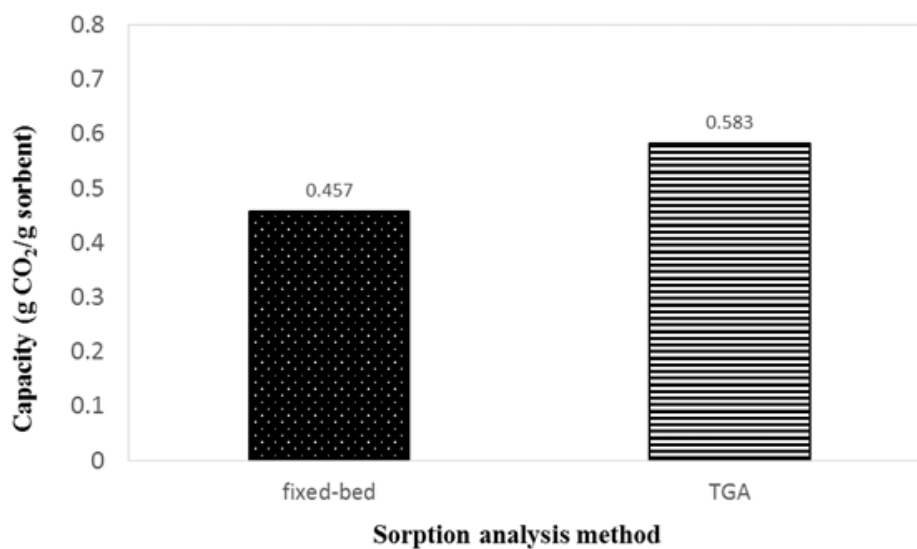


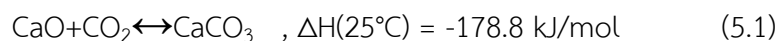
**Figure 5.1:** Comparison CO<sub>2</sub> sorption capacity between fixed-bed and thermogravimetric analyzer (TGA), condition: atmospheric pressure, 600 °C, total flow 60 ml/min, and using 15% CO<sub>2</sub> in N<sub>2</sub> as feed composition.

### 5.1.2 Effect of CO<sub>2</sub> sorption temperature.

Carbonation reaction has been shown that is usually occur at high temperature in the range of 600-800°C and this parameter is found to be a significant effect on CO<sub>2</sub> sorption capacity [60]. As a consequence, we firstly investigated the effect of carbonation temperature on CO<sub>2</sub> sorption capacity using commercial CaO (properties of commercial CaO are shown in Figs. A.1, A.3 and Table A.1 in Appendix).

Figure 5.2 demonstrates CO<sub>2</sub> sorption capacity of commercial CaO. The results show that sorption capacity at temperature between 600-700°C is comparable at approximately 0.45 g CO<sub>2</sub>/g sorbent, whereas a dramatic dropped of sorption capacity is observed at 800°C of which CO<sub>2</sub> capacity is only 0.183 g CO<sub>2</sub>/g sorbent. An increase of CO<sub>2</sub> sorption capacity with increasing temperature in the carbonation reaction is due to the overall kinetics is favored at high temperature but at 700°C capacity decreased because CaCO<sub>3</sub> was initially regenerated, the result was observed from figure 5.3 and

was confirmed in ref [24]. In contrast, low adsorption capacity observed at 800°C is due to calcination reaction is favored by thermodynamics at this temperature according to the carbonation-calcination reaction [24].



Also, the favorable of calcination reaction at 800°C is confirmed by the result of TGA analysis shown in Figure 5.3. Weight loss of CaCO<sub>3</sub> is observed at temperature where CaCO<sub>3</sub> was decomposed of 700-750°C and CO<sub>2</sub> molecules were found to completely desorbed at 850°C. This result indicates that by calcination of CaCO<sub>3</sub> at temperature higher than 850°C, pure CaO can be obtained. As a consequence, temperature of 850°C was selected to set as calcination temperature throughout this work for pre-treatment of CaO before conducting sorption experiments and for regeneration of the sorbent.

In addition, maximum CO<sub>2</sub> sorption capacity is observed at 650°C but noted that the capacity did not differ and the temperature was lower than 50°C, so the 600°C is optimum temperature to be used in the test. For this reason, the sorption ability tests of CaO-based sorbent for sorption enhanced methane reforming was carried out at this temperature.

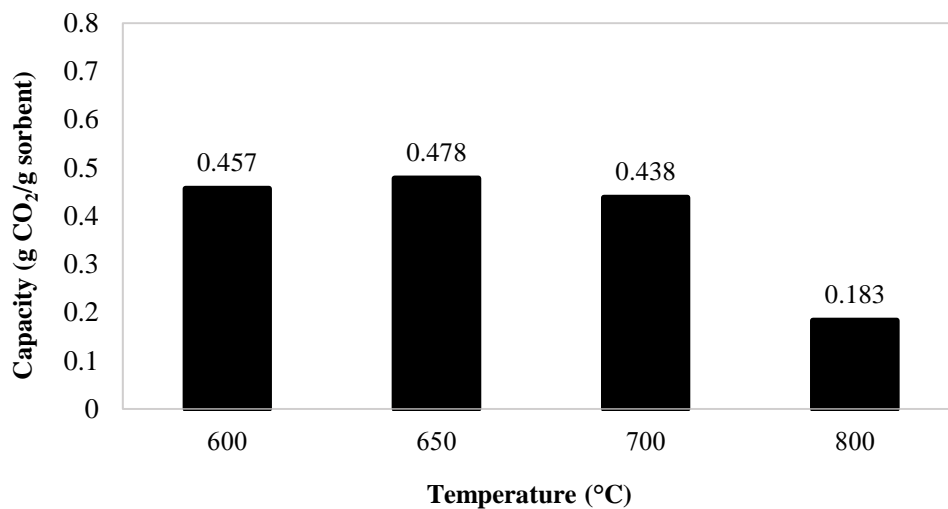


**Figure 5.2:** CO<sub>2</sub> sorption capacity by commercial CaO at different temperatures ranging from 500-800 °C, atmospheric pressure, and 15%v/v CO<sub>2</sub> (balanced N<sub>2</sub>).

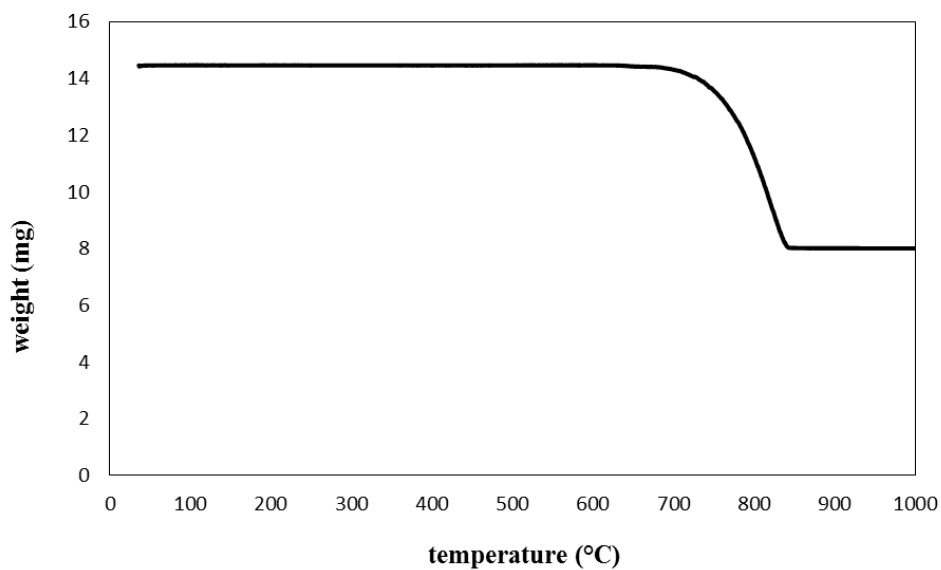
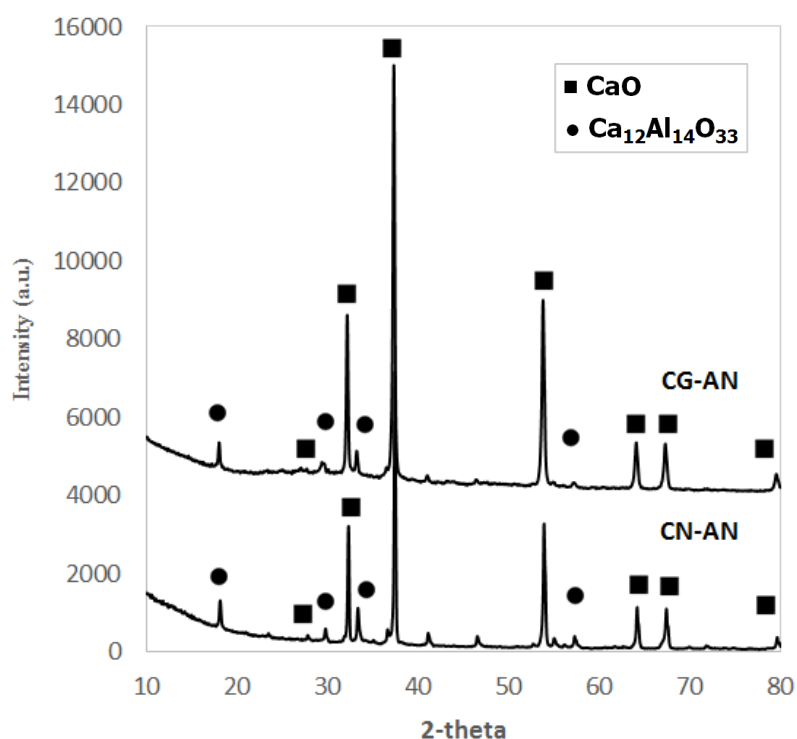


**Figure 5.3:** Weight loss of CaCO<sub>3</sub> determined by TGA analysis

### 5.1.3. Effect of Calcium precursors on CO<sub>2</sub> sorption capacity

Calcium precursor is an important factor that can also affect properties of synthetic Ca-based sorbents (CaO-Ca<sub>12</sub>Al<sub>14</sub>O<sub>33</sub>). Calcium nitrate and calcium d-gluconic

acid are of particular interested in this study and the CaO-based alumina sorbent synthesized from from calcium nitrate is designated as CN-AN and that synthesized from calcium d-gluconic acid is designated as CG-AN. Figure 5.4 shows XRD pattern of two synthetic sorbents. Both sorbents exhibit typical diffraction peak of CaO at position  $2\theta=28.2, 32.3, 37.4, 53.8, 64.3, 67.6$  and  $79.1^\circ$  and those of  $\text{Ca}_{12}\text{Al}_{14}\text{O}_{33}$  inert support at  $2\theta$  approximate 18, 30, 34 and  $57^\circ$  [60].



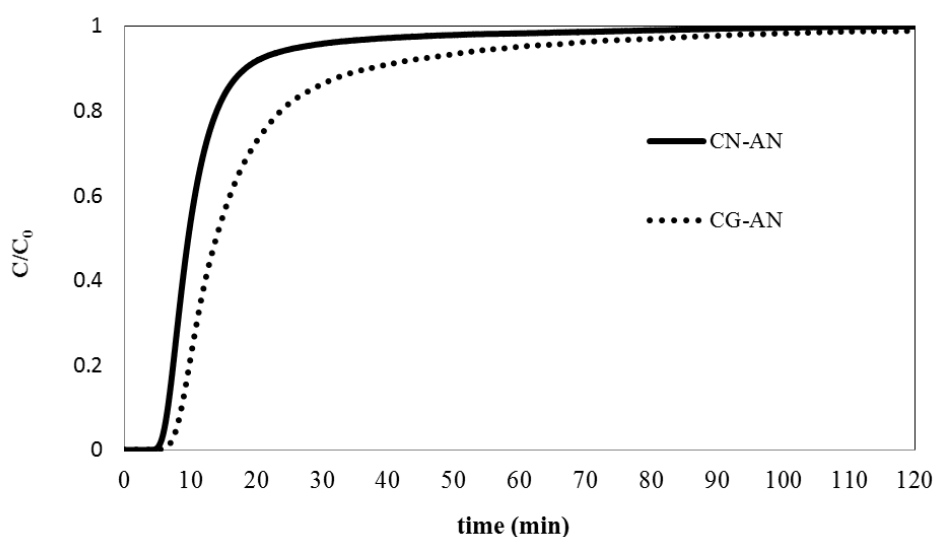
**Figure 5.4:** XRD pattern of different calcium precursors (CG-AN and CN-AN sorbent)

Figure 5.5 shows breakthrough curves of  $\text{CO}_2$  sorption by 1 gram of calcium-based sorbent prepared by calcium nitrate (CN) and calcium d-gluconic acid (CG) precursors. Pre-breakthrough of CN-AN and CG-AN is shown at 5 and 7 minute, respectively, and then rapid increase in breakthrough period until 20 and 30 minute. Finally, equilibrium of adsorption (post-breakthrough) is found at 80 and 100 minute for CN-AN and CG-AN, respectively. Longer pre-breakthrough period observed with CG-AN could be attributed to its higher surface area of  $11.27 \text{ m}^2/\text{g}$  when compared with

that of CN-AN ( $2.67 \text{ m}^2/\text{g}$ ) as shown in Table 5.1. The slope observed in breakthrough period of CN-AN is steeper than that of CG-AN, implying that diffusion of  $\text{CO}_2$  molecules through the sorbent of CN-AN is faster than CG-AN. This behavior could be due to larger pore diameter of CN-AN (Table 5.1).

**Table 5.1** : BET surface area, pore volume and pore diameter of calcium-based sorbent at different calcium precursors including calcium nitrate (CN) and calcium d-gluconic acid (CG)

Sample	Surface area ( $\text{m}^2/\text{g}$ )	Pore volume ( $\text{cm}^3/\text{g}$ )	Pore diameter (nm)
CN-AN	7.31	0.0134	8.76
CG-AN	11.27	0.0100	6.79



**Figure 5.5:** Breakthrough curves of  $\text{CO}_2$  sorption by 1g of calcium-based sorbent synthesized from calcium nitrate (CN) and calcium d-gluconic acid (CG). Operating conditions: atmospheric pressure,  $600^\circ\text{C}$ , and 15%v/v  $\text{CO}_2$  (balanced  $\text{N}_2$ ).

Figure 5.6 shows the corresponding CO<sub>2</sub> sorption capacity of the breakthrough curve depicted in Figure 5.5. The results show CO<sub>2</sub> capacity of CN-AN and CG-AN is 0.172 and 0.387 g CO<sub>2</sub>/g sorbent, respectively. Higher CO<sub>2</sub> adsorption observed with CG-AN is due to higher BET surface area and small particle size of the sorbent as depicted by SEM shown in Table 5.1 and Figure 5.7, respectively. Particle size of CN-AN is 0.5 and that of CG-AN is 0.35 μm. When compared with commercial CaO, it is revealed that our synthetic CaO can improve CO<sub>2</sub> sorption capacity of which 6% of sorption capacity is increased for the same amount of CaO. This is because the synthetic CaO possesses higher BET surface area and pore volume with small particle size.

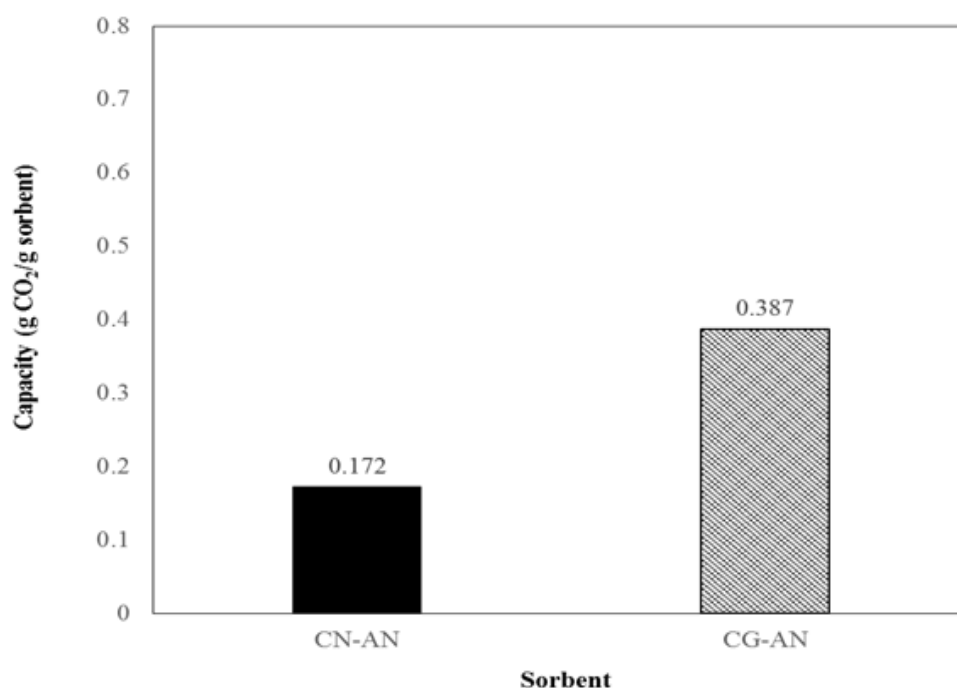


**Figure 5.6:** CO<sub>2</sub> sorption capacity of calcium-based sorbent synthesized from calcium nitrate (CN) and calcium d-gluconic acid (CG). Operating conditions: atmospheric pressure, 600°C, and 15%v/v CO<sub>2</sub> (balanced N<sub>2</sub>).

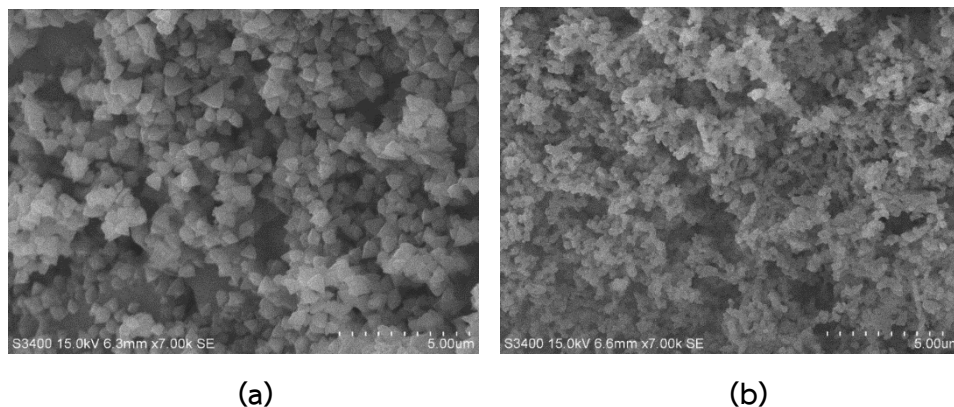


**Figure 5.7:** SEM photos of Ca-based sorbents a) CN-AN sorbent and b) CG-AN

#### 5.1.4 Effect of adding surfactant on CO<sub>2</sub> sorption

In this work, the effect of adding surfactant on CaO-based sorbent properties was studied with two different surfactant types: cetyltrimethyl ammonium bromide (CTAB) and sodium dodecyl sulfate (SDS). CG-AN sorbent was selected to study the effect of adding surfactant because it provides high CO<sub>2</sub> sorption capacity as shown in the previous section.

Figure 5.8 demonstrates XRD pattern of CG-AN sorbent modified by CTAB and SDS surfactants. The results show that there are two main peaks corresponding to CaO and Ca<sub>12</sub>Al<sub>14</sub>O<sub>33</sub> inert support similar to the unmodified by surfactant as shown in Figure 5.4. These results demonstrate that addition of surfactants does not affect phase of CaO and Ca<sub>12</sub>Al<sub>14</sub>O<sub>33</sub>. However, the intensity at  $2\theta = 18, 30$  and  $34^\circ$ , which is correspond



to  $\text{Ca}_{12}\text{Al}_{14}\text{O}_{33}$ , of CG-AN-SDS is higher than those of CG-AN-CTAB, indicating that the amount of  $\text{Ca}_{12}\text{Al}_{14}\text{O}_{33}$  of CG-AN-SDS (9 mM) is larger than that of CG-AN-CTAB (1 mM).

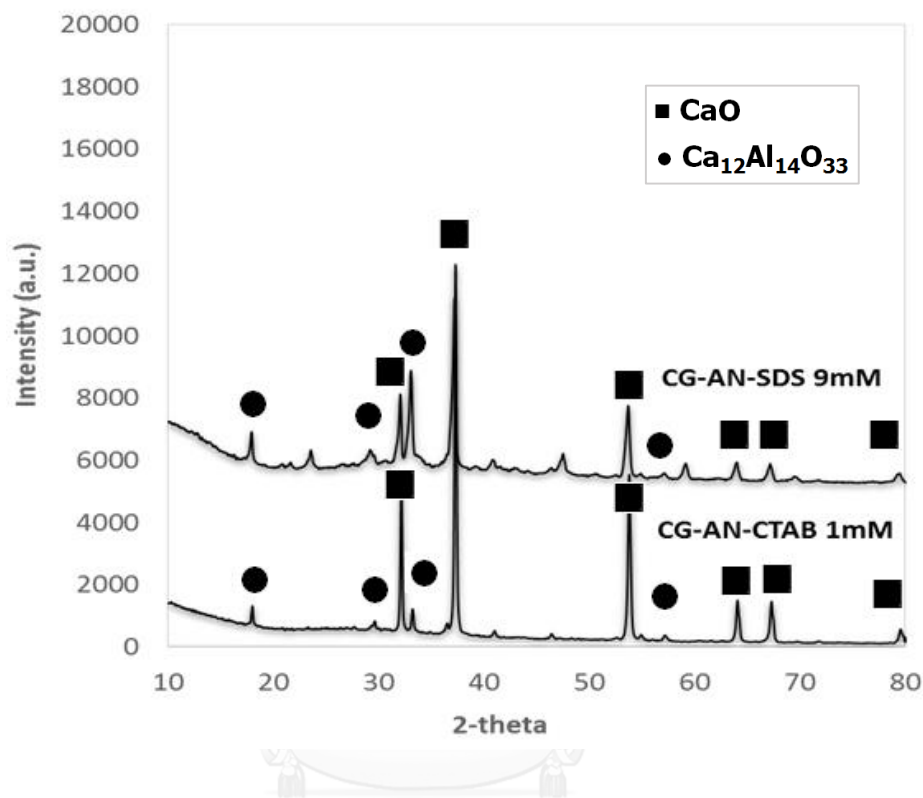


**Figure 5.8:** XRD pattern of different surfactants modified CG-AN sorbent (CG-AN modified with CTAB and CG-AN modified with SDS)

Breakthrough curve of CG-AN-CTAB (1 mM) and CG-AN-SDS (9 mM) is shown in Figure 5.9. Both sorbents show similar breakthrough pattern; pre-breakthrough is observed at approximately 8 minute and equilibrium is found at 120 minute. The resulting  $\text{CO}_2$  sorption capacity is 0.418 g  $\text{CO}_2/\text{g}$  sorbent for CG-AN-CTAB and is 0.382 g  $\text{CO}_2/\text{g}$  sorbent for CG-AN-SDS as shown in Figure 5.10. According to the XRD pattern shown in Figure 5.8, CG-AN-SDS shows phase  $\text{Ca}_{12}\text{Al}_{14}\text{O}_{33}$  more than CaO and confirm with textural properties and morphology of CG-AN-CTAB 1mM and CG-AN-SDS 9mM in table 5.2.

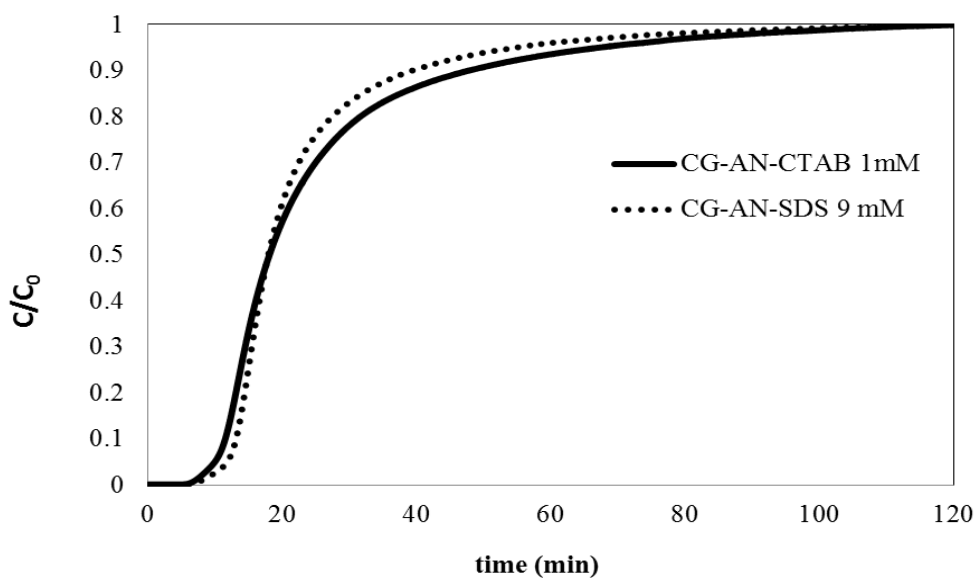


**Figure 5.9:** Breakthrough curves of CO<sub>2</sub> sorption by 1 g of CaO-based alumina modified by cetyltrimethyl ammonium bromide (CTAB) and sodium dodecyl sulfate (SDS). Operating condition: atmospheric pressure, 600°C, and 15%v/v CO<sub>2</sub> (balanced N<sub>2</sub>).

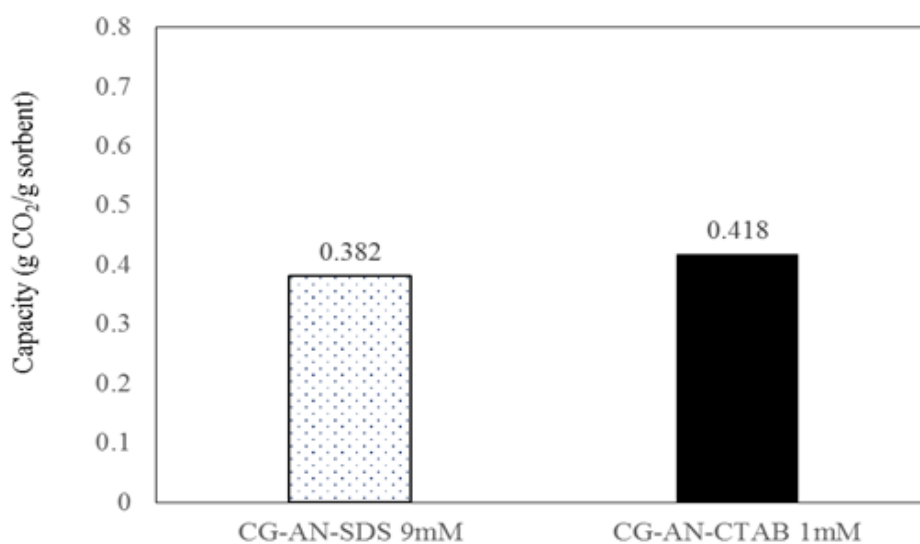


**Figure 5.10:** CO<sub>2</sub> sorption capacity of CaO-based alumina modified by cetyltrimethyl ammonium bromide (CTAB) and sodium dodecyl sulfate (SDS). Operating condition: atmospheric pressure, 600°C, and 15%v/v CO<sub>2</sub> (balanced N<sub>2</sub>).

Higher CO<sub>2</sub> sorption capacity observed with CG-AN-CTAB is due to it possesses higher BET surface area: CG-AN-CTAB 1mM = 12.40 m<sup>2</sup>/g while CG-AN-SDS 9mM has 8.61 m<sup>2</sup>/g. In addition, morphology of sorbent observed by SEM depicted in Figure 5.11 shows that particle of CG-AN-CTAB 1mM has uniform small particle size compared with CG-AN-SDS 9mM, which is due to inhibition of crystal growth by CTAB as reported by [61].

**Table 5.2:** BET surface area, pore volume and pore diameter of CG-AN calcium-based sorbent at different surfactants including cetyltrimethyl ammonium bromide (CTAB) and sodium dodecyl sulfate (SDS).

Sample	Surface area (m <sup>2</sup> /g)	Pore volume (cm <sup>3</sup> /g)	Pore diameter (nm)
CG-AN-CTAB 1mM	12.40	0.0096	4.213
CG-AN-SDS 9mM	8.61	0.005768	2.679

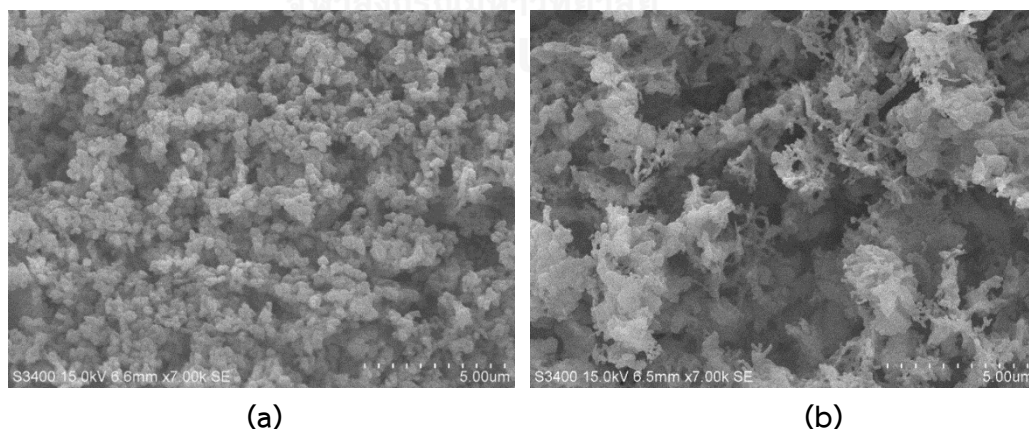


**Figure 5.11:** Morphology of modified Ca-based sorbents a) CG-AN-CTAB 1mM and b) CG-AN-SDS 9mM

### 5.1.5 Effect of CTAB concentration on CO<sub>2</sub> sorption

Concentration of surfactant is a factor that can affect CaO-based alumina since it has been known that at a certain concentration of surfactants can be in monomer form or forming into micellar structure [62]. In this thesis, the effect of concentration of surfactant was studied in the range where monomer of surfactant is presented to where micellar structure is formed. Figure 5.13 shows XRD pattern of CG-AN-CTAB at different concentrations ranging from 1 to 10mM.

Typical diffraction peaks assigned to as CaO are observed at  $2\theta = 28.2, 32.3, 37.4, 53.8, 64.3, 67.6$  and  $79.1^\circ$  and those of  $\text{Ca}_{12}\text{Al}_{14}\text{O}_{33}$  inert support is shown at  $2\theta$  of  $18, 30, 34$  and  $57^\circ$ . However, the magnitude of the peak at  $2\theta = 34$  and  $57^\circ$ , which corresponds to  $\text{Ca}_{12}\text{Al}_{14}\text{O}_{33}$  of all CG-AN-CTAB sorbents is higher than that of the unmodified one.

In this case, different intensities of XRD pattern some CaO and  $\text{Ca}_{12}\text{Al}_{14}\text{O}_{33}$  peak does not affect the composition and phase of CaO and  $\text{Ca}_{12}\text{Al}_{14}\text{O}_{33}$ , it was found approximately %composition of CaO and  $\text{Ca}_{12}\text{Al}_{14}\text{O}_{33}$  approximately 70% and 30%, respectively. The different intensity of the XRD peak indicates different crystallinity of the sorbents and crystals of  $\text{Ca}_{12}\text{Al}_{14}\text{O}_{33}$  become smaller by increased of XRD relative intensity [63]. However, the effect of CTAB addition on the formation of CaO cause CaO showed growth and agglomeration [52]. The result can observe morphology of particle, which confirmed by SEM in Figure 5.15.

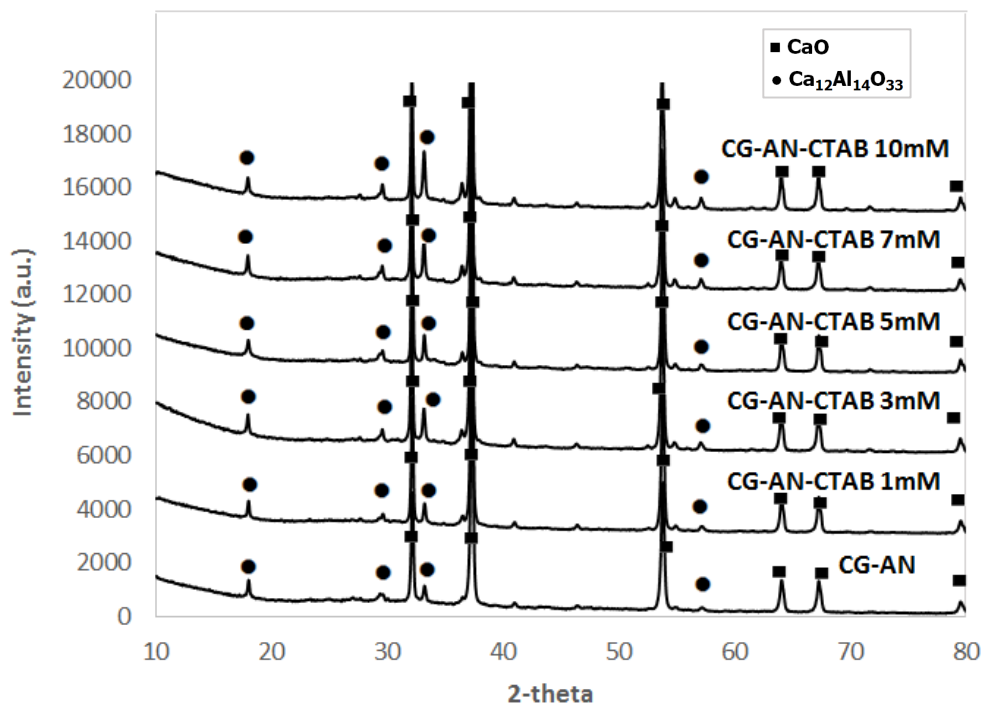


**Figure 5.12:** XRD pattern of modified CG-AN sorbent by different concentration of CTAB

Results from SEM shown in Figure 5.13 demonstrate morphology of sorbents modified by different concentrations of CTAB. Small particle size is observed with unmodified CG-AN sorbent and modified CG-AN-CTAB at 1 and 3mM whereas large aggregated particle is observed with 5, 7 and 10mM of CTAB concentration. Similar to pore size of the sorbents, the pore size becomes larger when concentration of CTAB increases due to CaO agglomerate a large number of pore could be combined into a big single pore size.

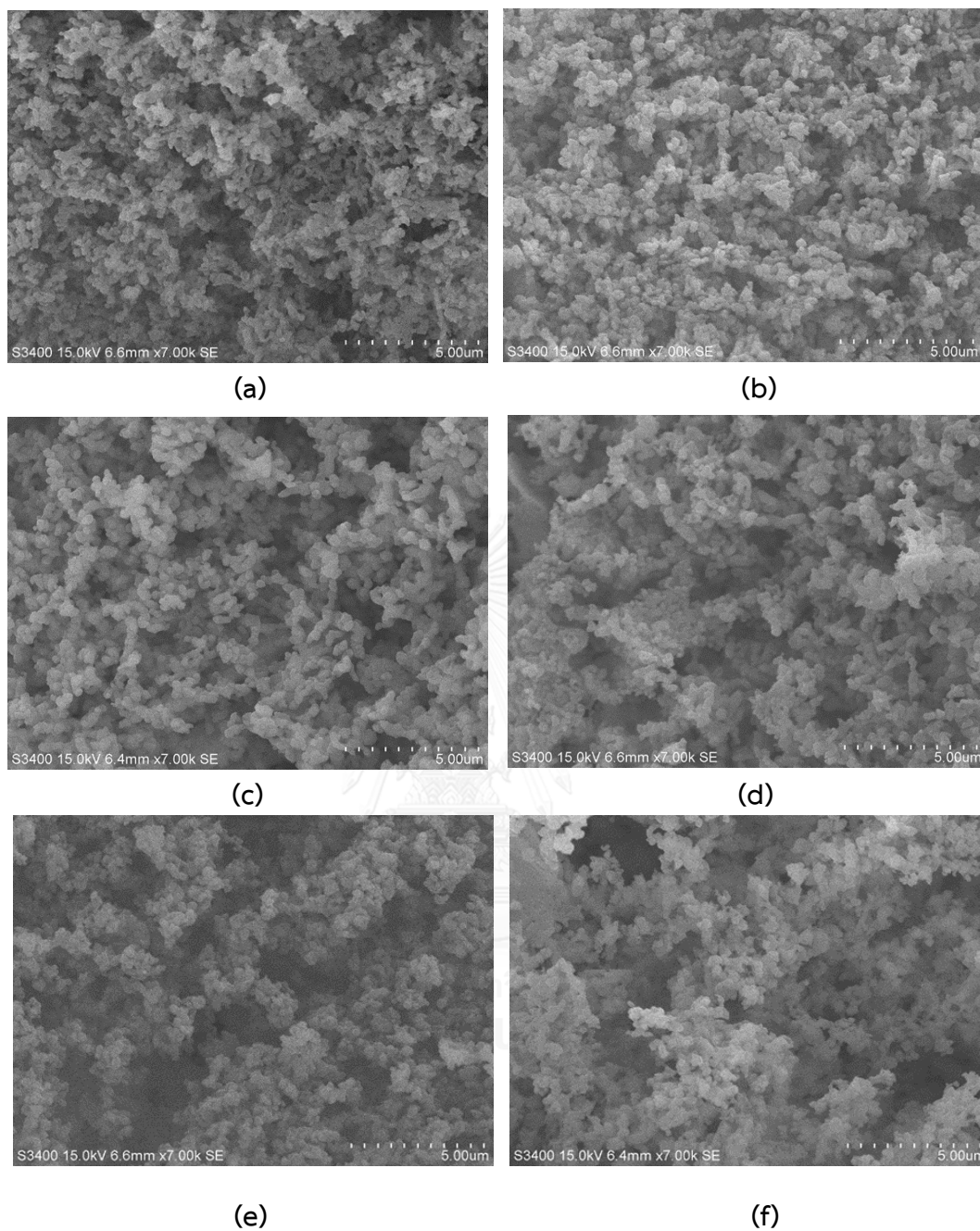


**Figure 5.13:** Morphology of modified Ca-based alumina sorbents at different CTAB concentrations a) CG-AN without CTAB and b) CG-AN-CTAB 1mM c) CG-AN-CTAB 3mM d) CG-AN-CTAB 5mM e) CG-AN-CTAB 7mM and f) CG-AN-CTAB 10mM.

Breakthrough curves of CO<sub>2</sub> sorption capacity adsorbed by modified sorbent with different concentrations of CTAB are shown in Figure 5.14. The results show that the modified and unmodified sorbents have similar breakthrough time of approximately 7-8 minutes. This is might be due to all samples have comparative BET surface area. When calculated the CO<sub>2</sub> capacity as shown in Figure 5.15, the unmodified CG-AN sorbent has lower CO<sub>2</sub> sorption capacity than the modified sorbents: CO<sub>2</sub> capacity of CG-AN is 0.387 g CO<sub>2</sub>/g sorbent and CG-AN-CTAB is 0.418, 0.45, 0.461, 0.396 and 0.381 g CO<sub>2</sub>/g sorbent for CTAB concentration of 1,3,5,7 and 10 mM, respectively. Relative high CO<sub>2</sub> sorption capacity is observed with CG-AN-CTAB 3 and 5mM and then the capacity decreases when CTAB concentration increases. This result might be due to greater increase of CTAB concentration (above its CMC value of 0.92 mM) leads to an increase of number of micelles in solution, which resulted in a large number of pore. When the sorbent is heated before or during running CO<sub>2</sub> capture test, the large number of pore could collapse into a big single pore size which could result in lower surface area and hence lower sorption capacity.

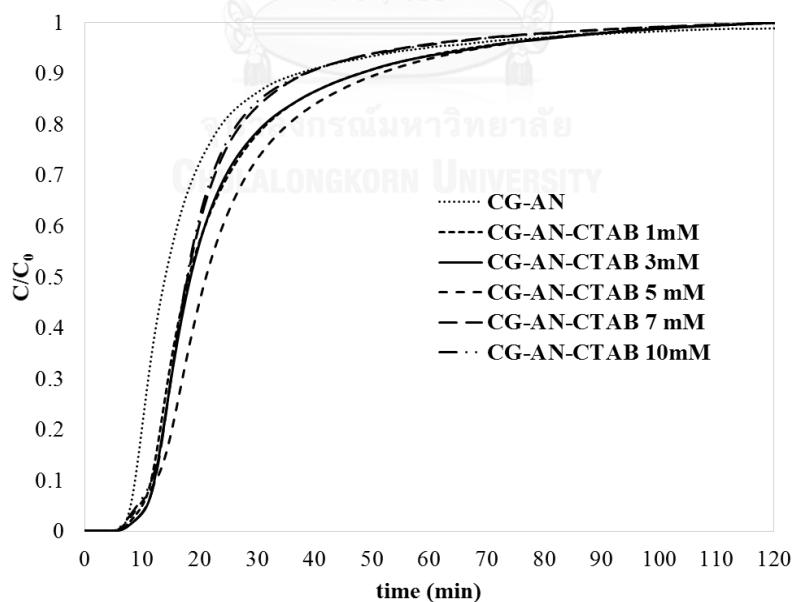


**Figure 5.14:** Breakthrough curves of CO<sub>2</sub> sorption by 1g of CG-AN calcium-based sorbent at different concentration of CTAB at 1,3,5,7 and 10mM, Operating condition: atmospheric pressure, 600°C, and 15%v/v CO<sub>2</sub> (balanced N<sub>2</sub>).

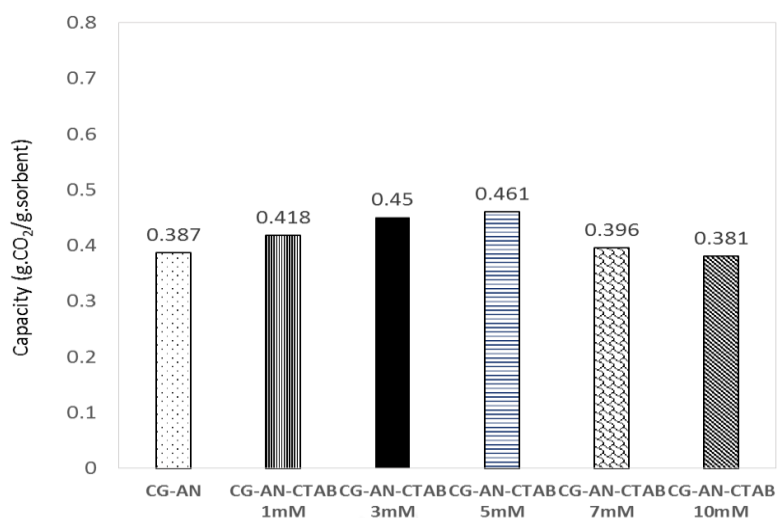


**Figure 5.15:** Comparison CO<sub>2</sub> sorption capacity by 1g of CG-AN calcium-based sorbent at different concentration of CTAB at 1,3,5,7 and 10mM. Operating condition: atmospheric pressure, 600°C, and 15%v/v CO<sub>2</sub> (balanced N<sub>2</sub>).

Textural properties of CG-AN-CTAB at with different concentrations are presented in Table 5.4. BET surface area of CG-AN-CTAB increases from that without surfactant to the one modified by 3 mM of CTAB then the surface area drops when concentration of surfactant is further increased. In contrast, pore volume and pore diameter has no relation with the concentration of surfactant added, it is could be observed based on the results of N<sub>2</sub> adsorption/desorption isotherm that increasing concentration of CTAB tends to increase pore volume and pore diameter. However, when CTAB concentration is increased further too high, which in this study is equal to 10 mM, pore volume and pore diameter become smaller. This could be due to a large number of micelles lead to a closed packing of micelles themselves, leaving less space for calcium oxide and alumina to form.



**Table 5.3:** BET surface area, pore volume and pore diameter of modified CG-AN calcium-based sorbent

Sample	Surface area (m <sup>2</sup> /g)	Pore volume (cm <sup>3</sup> /g)	Pore diameter (nm)
CG-AN	11.27	0.0100	6.79
CG-AN-CTAB 1mM	12.40	0.0096	4.213
CG-AN-CTAB 3mM	14.12	0.0162	4.587
CG-AN-CTAB 5mM	12.10	0.0198	7.847
CG-AN-CTAB 7mM	11.98	0.0229	7.206
CG-AN-CTAB 10mM	7.64	0.0126	5.526

The effect of adding CTAB on properties of sorbent was also investigated with those synthesized from calcium nitrate precursor. Figure 5.16 presents XRD pattern of CN-AN modified by different concentrations of CTAB. Typical diffraction peaks of CaO are shown at  $2\theta = 28.2, 32.3, 37.4, 53.8, 64.3, 67.6$  and  $79.1^\circ$  and the XRD pattern of  $\text{Ca}_{12}\text{Al}_{14}\text{O}_{33}$  inert support is shown at  $2\theta$  approximate 18, 30, 34 and  $57^\circ$ . All sorbents have the same phase of CaO and  $\text{Ca}_{12}\text{Al}_{14}\text{O}_{33}$  inert support as that without surfactant and similar to the case of CG-AN. However, different crystallinities of the sorbents are observed: low crystallinity is found with those synthesized with the addition of surfactant [65].

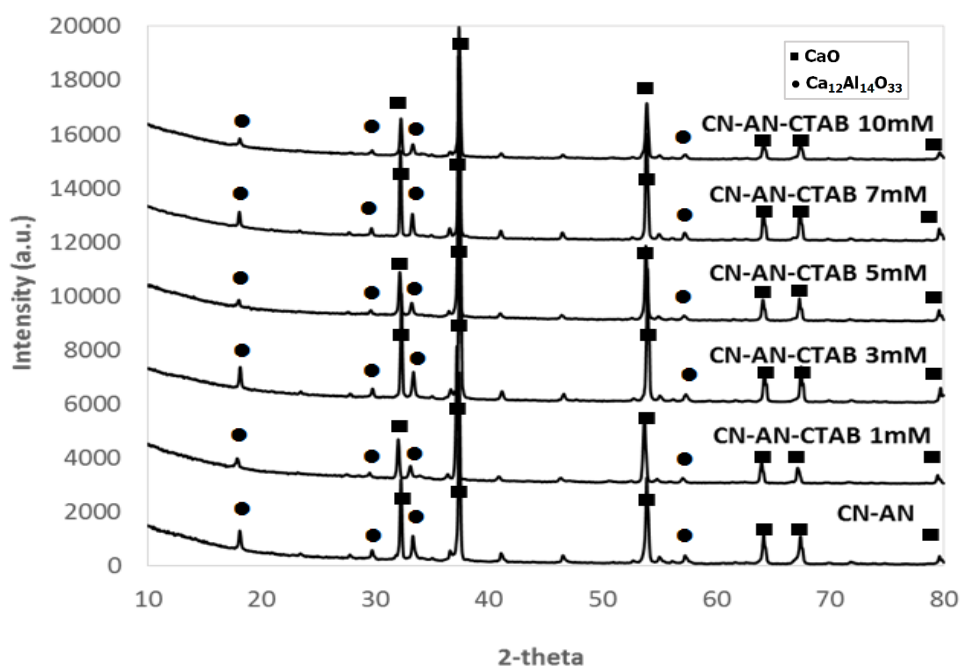


**Figure 5.16:** XRD pattern of different concentration of CTAB at 1,3,5,7 and 10mM modified CN-AN sorbent.

Textural properties of CN-AN sorbents are shown in Table 5.4. It is found that, all CTAB modified sorbents have surface area approximately 5-7 m<sup>2</sup>/g, which is lower than those of CG-AN sorbents. Morphologies of all sorbents are presented in Figure 5.19, CN-AN without CTAB shows uniform distribution of particle of octahedral structure whereas agglomerated particles are observed with CN-AN-CTAB sorbents and larger aggregated particles are found with higher CTAB concentrations.

**Table 5.4:** BET surface area, pore volume and pore diameter of modified CN-AN calcium-based sorbent at different concentration (1, 3, 5, 7 and 10 mM of CTAB)

Sample	Surface area (m <sup>2</sup> /g)	Pore volume (cm <sup>3</sup> /g)	Pore diameter (nm)
CN-AN	7.31	0.0134	8.76
CN-AN-CTAB 1mM	5.62	0.0083	9.42
CN-AN-CTAB 3mM	6.26	0.0106	10.76
CN-AN-CTAB 5mM	7.52	0.0100	15.63
CN-AN-CTAB 7mM	5.25	0.0103	9.68
CN-AN-CTAB 10mM	6.26	0.0115	10.67

Breakthrough curves of CO<sub>2</sub> sorption for different sorbents are shown in Figure 5.17. No significant difference is observed for all sorbents of studies: breakthrough time is found at 5 minute. Figure 5.18 demonstrates CO<sub>2</sub> sorption capacity corresponding to the breakthrough curve presented in Figure 5.17. As expected, comparative CO<sub>2</sub> sorption capacity is observed, which is ca. 0.2 g CO<sub>2</sub>/g sorbent. CN-AN-CTAB 3mM sorbent provides the highest CO<sub>2</sub> sorption capacity, which is 0.222 g CO<sub>2</sub>/g. As seen in Table 5.4, BET surface area of all sorbents are not significantly different as such this could be the reason for the result of the similar CO<sub>2</sub> capacity.

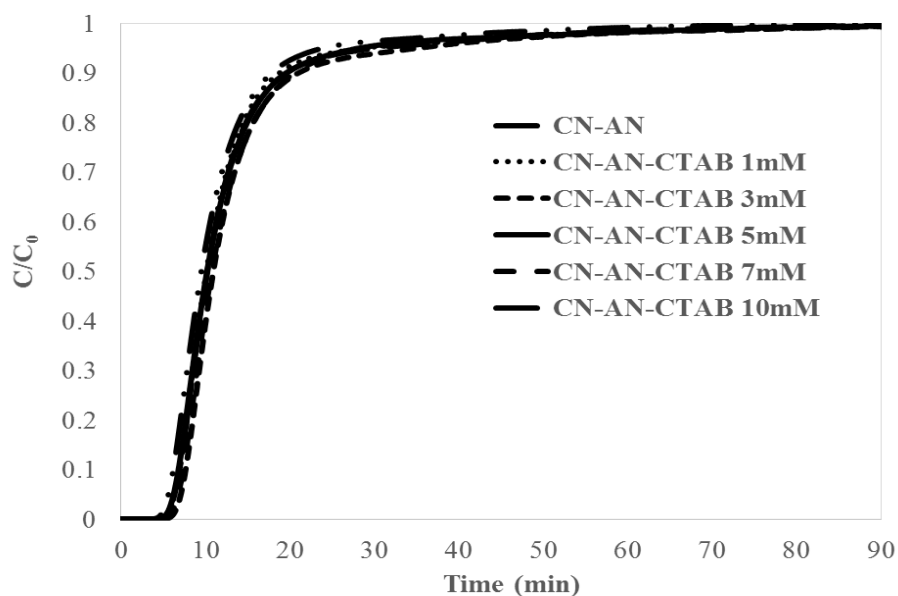


**Figure 5.17:** Breakthrough curves of  $\text{CO}_2$  sorption by 1g of CN-AN calcium-based sorbent at different concentration of CTAB at 1,3,5,7 and 10mM. Operating condition: atmospheric pressure,  $600^\circ\text{C}$ , and 15%v/v  $\text{CO}_2$  (balanced  $\text{N}_2$ ).

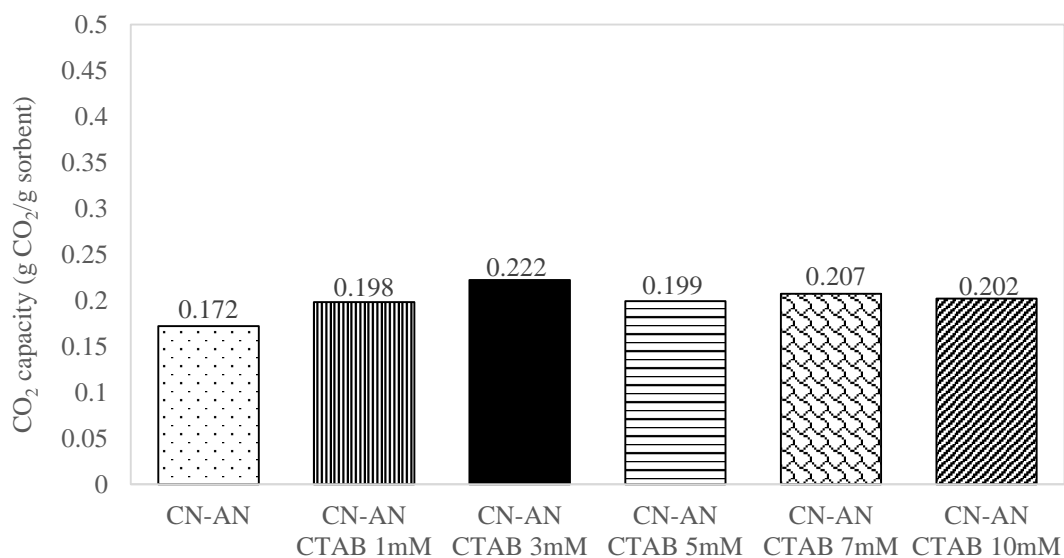


**Figure 5.18:** Comparison  $\text{CO}_2$  sorption capacity by 1g of CN-AN calcium-based sorbent at different concentration of CTAB at 1,3,5,7 and 10mM. Operating condition: atmospheric pressure,  $600^\circ\text{C}$ , and 15%v/v  $\text{CO}_2$  (balanced  $\text{N}_2$ ).

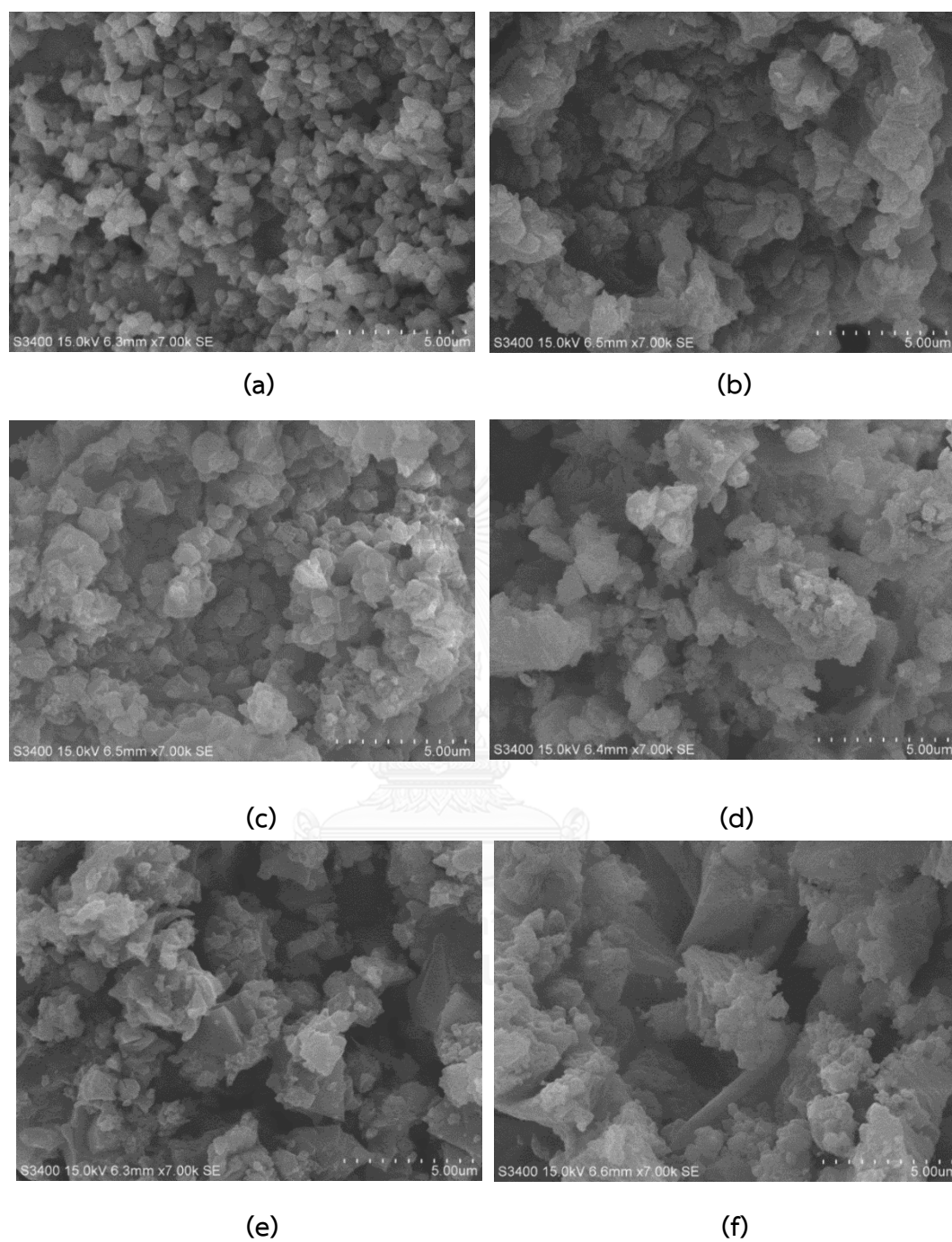


**Figure 5.19:** Morphology of modified Ca-based sorbents at different CTAB concentrations a) CN-AN without CTAB and b) CN-AN-CTAB 1mM c) CN-AN-CTAB 3mM d) CN-AN-CTAB 5mM e) CN-AN-CTAB 7mM and f) CN-AN-CTAB 10mM.

From all result of effect of CTAB concentration modified with CG-AN and CN-AN were observed, It is observed that there is a very different between CG-AN and CN-AN. CG-AN-CTAB at several concentration including 1, 3, 5, 7 and 10mM is shown differentiation of modified support because calcium d-gluconic acid presented hydrocarbon atom in a calcium precursor. From several researches reported presence of hydrocarbon in calcium precursor when comparison with non-hydrocarbon in calcium precursor. Calcium with hydrocarbon group showed high physical properties and performance of CO<sub>2</sub> sorption more than non-hydrocarbon group in calcium precursor due to low tortuosity in its pore system result decreased resistance in CO<sub>2</sub> access to the active site [46] as calcium d-gluconic acid in this case. When CTAB was added for improve physical properties of modified sorbent found that pore diameter of modified sorbent decreased due to positive charge of CTAB form to micelle, diameter is 5.7 nm [64] as a template for modified sorbent. As a result it can control pore and morphology of modified sorbent. Shape of particle effect to physical properties and performance of adsorption. Pore diameter at 1 and 3mM is reduced as diameter of CTAB micelle, so surface area increased when comparison with absence CTAB. Unlike CN-AN modified with several CTAB concentration found that using different calcium precursors result different the nature porous of sorbent. Absence CTAB on CN-AN is shown wider pore diameter (approximate 8.7 nm) when CTAB was added for improved, it cannot reduced control pore diameter of modified sorbent due to pore diameter is shown in table 5.4 larger than diameter of CTAB micelle cause surface area of modified sorbent decreased. Reason of result of CTAB modified CN-AN might be nature of pore of calcium nitrate when CN-AN was modified by CTAB, it cannot show better improvement of modified sorbent.

**Table 5.5:** CaO and  $\text{Ca}_{12}\text{Al}_{14}\text{O}_{33}$  inert support content (%) on modified calcium-based sorbent by TGA

Sorbent	% CaO	% $\text{Ca}_{12}\text{Al}_{14}\text{O}_{33}$
CG-AN-CTAB 3mM	0.73	0.27
CN-AN-CTAB 3mM	0.74	0.26
CG-AN	0.70	0.30
CN-AN	0.75	0.25

#### 5.1.6 Stability of modified sorbents

Stability of both modified sorbents: CG-AN-CTAB 3mM and CN-AN-CTAB 3mM, was tested for the re-use of sorbents. The results of  $\text{CO}_2$  sorption capacity for 10 cycles are shown in Figure 5.20. CG-AN-CTAB 3mM shows higher capacity than CN-AN-CTAB 3mM at all cycles; however, the results show that CN-AN-CTAB 3mM is more stable than CG-AN-CTAB 3mM as  $\text{CO}_2$  sorption capacity of CN-AN-CTAB 3mM decreases 30.9% from cycle 1 to 10 while  $\text{CO}_2$  sorption capacity of CG-AN-CTAB 3mM reduced 36.8% from cycle 1 to 10. This might be due to Particle of CG-AN-CTAB 3mM is aggregated after multicycle tests whereas the particles of CN-AN-CTAB seems to not being change as revealed by morphologies of each particle before and after 10 cycles of stability test shown in Figure 5.21.

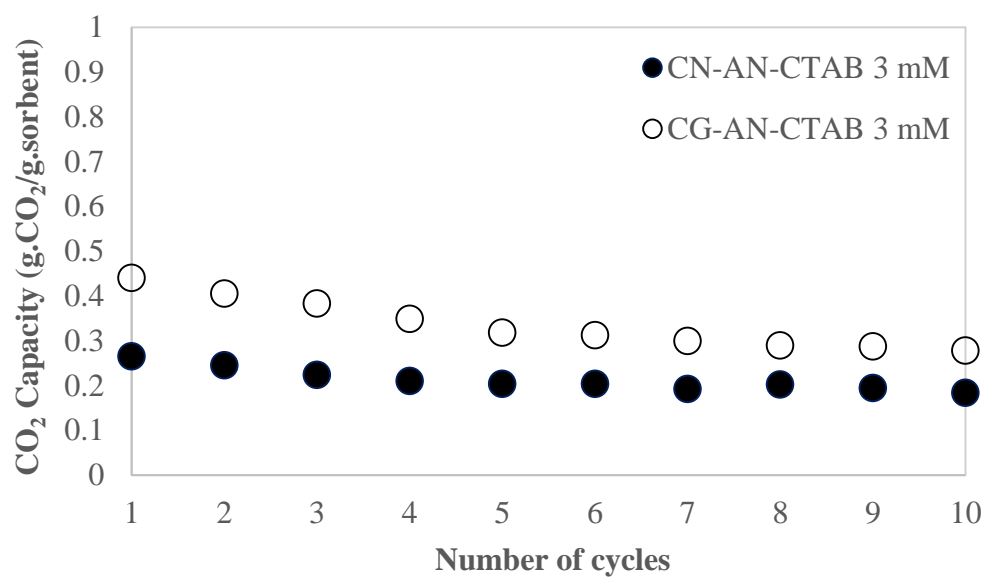


**Figure 5.20:** Stability of CG-AN-CTAB 3mM and CN-AN-CTAB 3mM modified sorbents. Condition: atmospheric pressure, 600°C of adsorption and 850°C of regeneration, using 15% CO<sub>2</sub> in N<sub>2</sub> as feed composition.





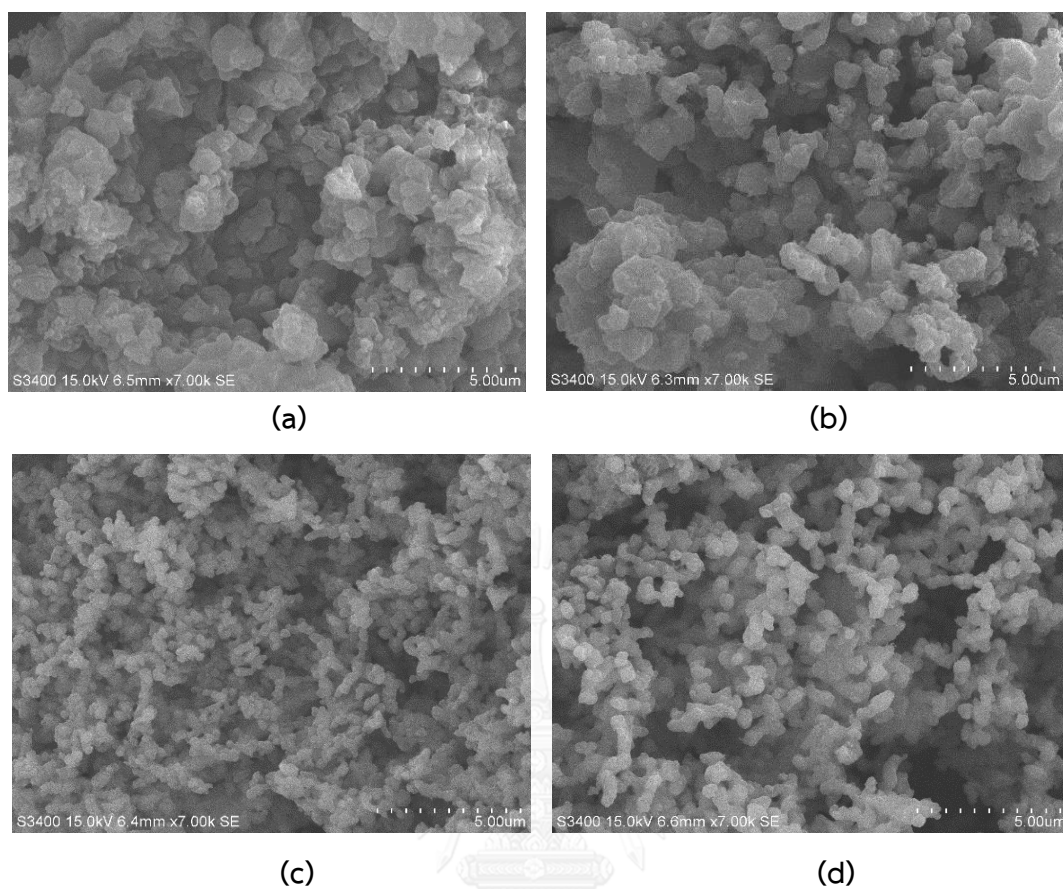


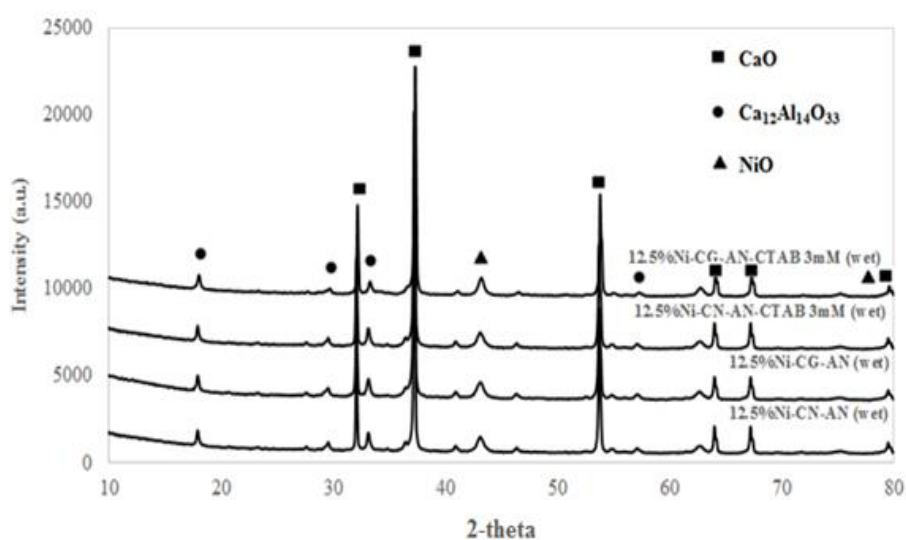
**Figure 5.21:** Morphology of modified sorbent particles. a) fresh CN-AN-CTAB 3mM b) after 10 cycles of CN-AN-CTAB 3mM c) fresh CG-AN-CTAB 3mM d) after 10 cycles of CG-AN-CTAB 3mM.

## 5.2 Sorption enhanced steam methane reforming (SESMR)

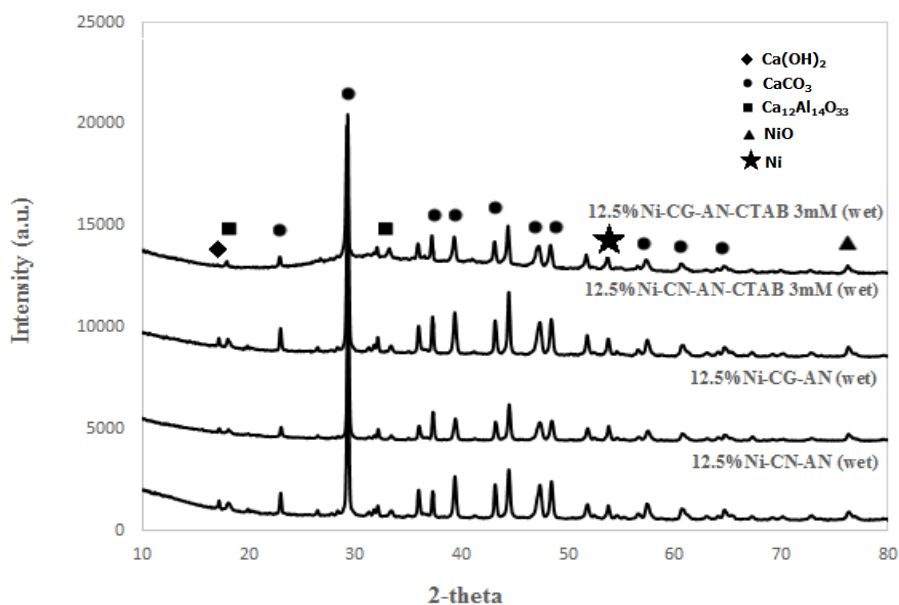
### 5.2.1 The use of CaO-based alumina as sorbent material

Normally, conventional catalyst  $\text{Ni}/\text{Al}_2\text{O}_3$  has been used as catalyst for  $\text{H}_2$  production. Amount of Ni sites have been reported from several researches that 12.5% Ni can provide reasonable  $\text{H}_2$  production performance. Chanburanasiri et al. [24] reported 82% of methane conversion and 73% of  $\text{H}_2$  product composition can be obtained when 12.5% $\text{Ni}/\text{Al}_2\text{O}_3$  catalyst was used. Kim et al. [4] reported that 83% of methane conversion was obtained with 10% $\text{Ni}/\text{Al}_2\text{O}_3$  conventional catalyst, and Roh et al. [44] reported 12%Ni on  $\text{Ce-ZrO}_2/\theta\text{-Al}_2\text{O}_3$  could provide 85%  $\text{H}_2$  production. As a consequence, 12.5% Ni loading was used in this work to test the ability of our synthetic sorbents for SESMR.

Figure 5.22a shows XRD pattern of hybrid catalytic sorbent materials. The main peaks representing  $\text{CaO-Ca}_{12}\text{Al}_{14}\text{O}_{33}$  are observed similar to those found in Figure 5.12 and 5.17. The additional peaks of NiO show at  $2\theta$  at 43 and  $79.1^\circ$  which is in consistent with [65]. XRD was used identified  $\text{CaCO}_3$ ,  $\text{Ca}(\text{OH})_2$ , Ni as increased substrate on multifunction catalyst after SESMR test in figure 5.22b.



(a)

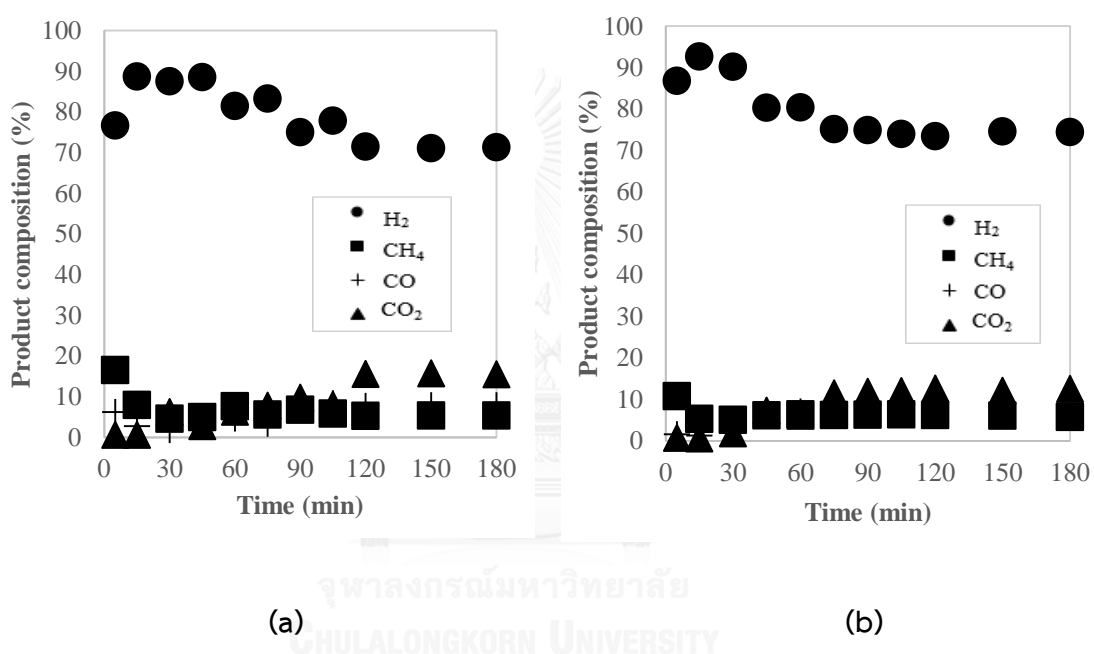


(b)

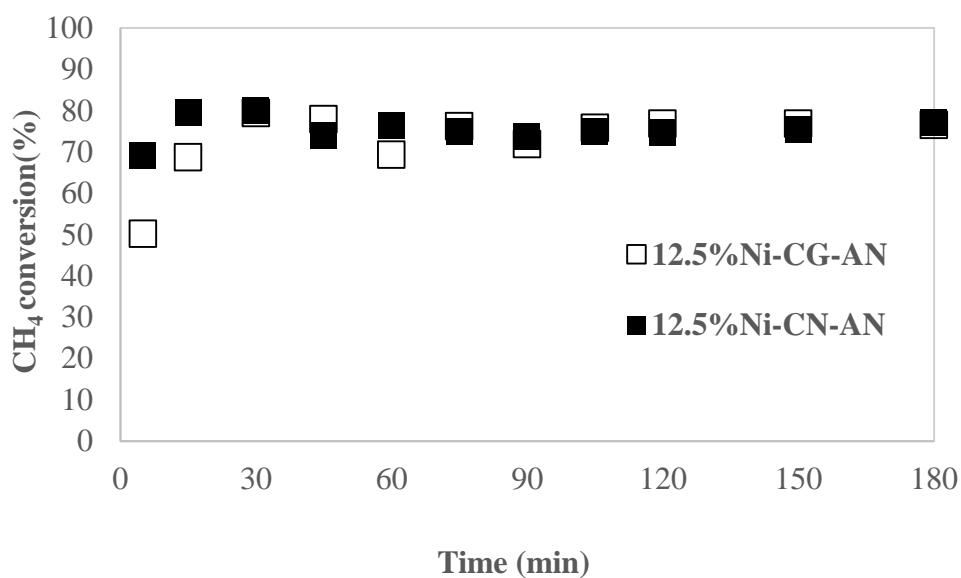
**Figure 5.22:** XRD of fourth hybrid multifunctional catalyst. (a) fresh and (b) after test of SESMR (12.5%Ni-CN-AN, 12.5%Ni-CG-AN, 12.5%Ni-CN-AN-CTAB 3mM and 12.5%Ni-CG-AN-CTAB 3mM

Figure 5.23 shows product composition obtained from SESMR using 12.5%Ni-CG-AN and 12.5%Ni-CN-AN as hybrid catalytic sorbent. The results indicate that  $\text{CO}_2$  was adsorbed by CaO for the first 30 minutes as maximum purity of  $\text{H}_2$  of 88.7%  $\text{H}_2$  can be obtained for 12.5%Ni-CG-AN but after the adsorption period  $\text{H}_2$  purity and  $\text{CH}_4$  conversion decreases to 81.5%  $\text{H}_2$ , 71.3%  $\text{H}_2$  at equilibrium and 76.5% of  $\text{CH}_4$  conversion (see Figures 5.23 and 5.24). This is a result of the shift of forward reaction according to Le Chatelier's principle shown in Eq. (5.1).  $\text{CH}_4$  conversion of 79.4% (Figure 5.24) is found, which is in consistent to that obtained for 12.5%Ni reported by Chanburanasiri [24]. Note that 70-75% of  $\text{H}_2$  is obtained for conventional SMR process as shown in Figure A.6 and reported by ref. [66]. For first 45 minutes of 12.5%Ni-CN-AN, adsorption period is observed the maximum purity of  $\text{H}_2$  of 92.7%  $\text{H}_2$  is obtained (Figure 5.23b) and 80% of  $\text{CH}_4$  conversion (Figure 5.24). It is noted that CaO- $\text{Ca}_{12}\text{Al}_{14}\text{O}_{33}$  CG-AN can adsorb  $\text{CO}_2$  more than CN-AN sorbent for high-temperature  $\text{CO}_2$  sorption tests; however, when

CG-AN was combined with Ni-based catalyst and used as one-body catalytic sorbent material, 12.5%Ni-CG-AN shows no impact on CO<sub>2</sub> sorption compared with 12.5%Ni-CN-AN. This might be due to surface area after impregnation of Ni on modified sorbent of 12.5%Ni-CN-AN is higher than that of 12.5%Ni-CG-AN as structure of CN-AN is denser than CG-AN. In addition, pore diameter of 12.5%Ni-CN-AN is larger than that of 12.5%Ni-CG-AN so that it could enhance the accessibility of CO<sub>2</sub> molecules to diffuse into the pore easily, the results was confirmed by BET shown in Table 5.7.



**Figure 5.23:** Gas product composition (dry basis) of 12.5%Ni-CG-AN (a) and 12.5%Ni-CN-AN (b) for sorption enhanced steam methane reforming Condition: at atmospheric pressure, reaction temperature of 600°C, S/C of 3 and total flow rate 60ml/min.



**Figure 5.24:** CH<sub>4</sub> conversion of 12.5%Ni-CG-AN and 12.5%Ni-CN-AN for sorption enhanced steam methane reforming Condition: at atmospheric pressure, reaction temperature of 600°C, S/C of 3 and total flow rate 60mL/min.

Figure 5.25 (a and b) shows morphology of 12.5%Ni-CG-AN and 12.5%Ni-CN-AN before and after SESMR tests. The results reveal that particles of 12.5%Ni-CN-AN became larger after SESMR when compared with 12.5%Ni-CG-AN. This result shows that 12.5%Ni-CN-AN suffered sintering effect greater than 12.5%Ni-CG-AN.

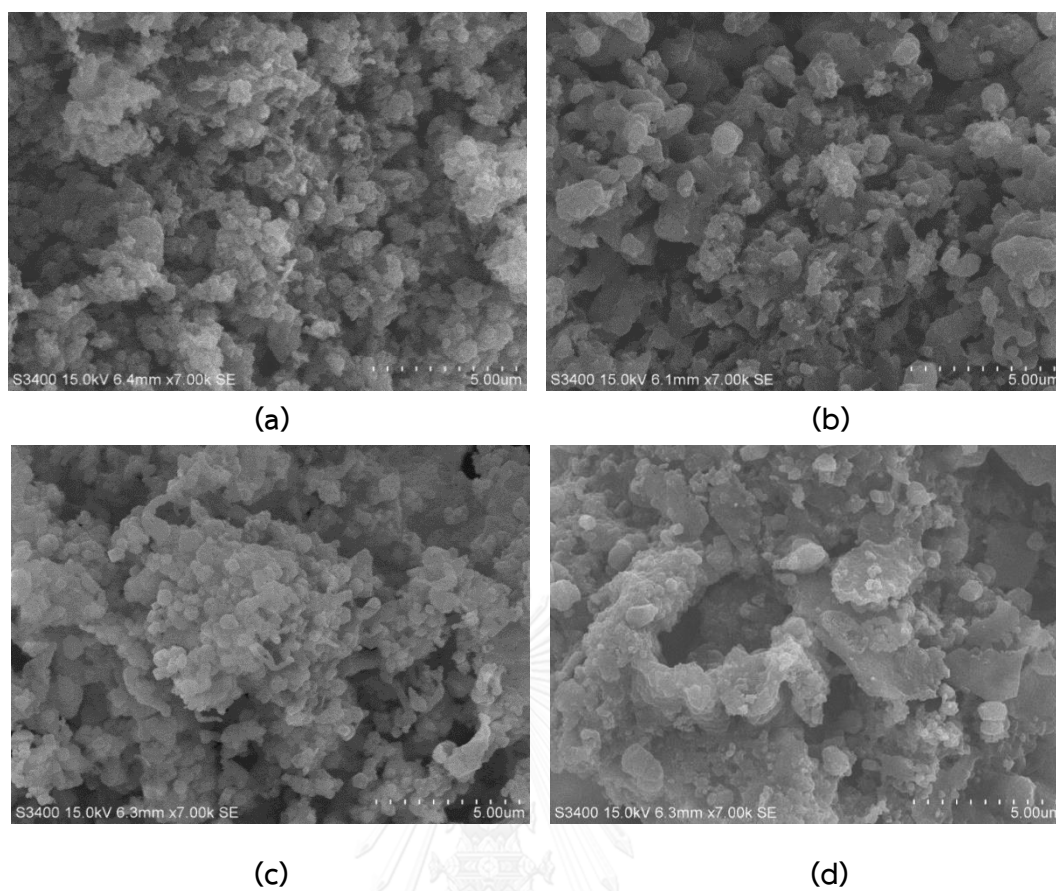


**Figure 5.25:** Morphology of 12.5%Ni-CG-AN and 12.5%Ni-CN-AN for sorption enhanced steam methane reforming Condition: at atmospheric pressure, reaction temperature of 600°C, S/C of 3 and total flow rate 60ml/min. a) fresh of 12.5%Ni-CG-AN b) 12.5%Ni-CG-AN after test of SESMR c) fresh of 12.5%Ni-CN-AN d) 12.5%Ni-CN-AN after test of SESMR.

### 5.2.2 The use of surfactant-modified CaO-based alumina as sorbent material

Figure 5.26 shows the use of 12.5%Ni-CG-AN-CTAB 3mM and 12.5%Ni-CN-AN-CTAB 3mM as catalytic sorbent for SESMR. The results show that by using 12.5%Ni-CG-AN-CTAB 3mM as catalytic sorbent, CO<sub>2</sub> was adsorbed by CaO on hybrid multifunction catalyst for 30 minutes, where the maximum purity of H<sub>2</sub> is 91.2% H<sub>2</sub> and 83% of CH<sub>4</sub> conversion (Figure 5.26a and figure 5.27). After the adsorption period, H<sub>2</sub> purity and CH<sub>4</sub> conversion decreases to 76.8 %H<sub>2</sub> at and 75.5% of CH<sub>4</sub> conversion equilibrium. For 12.5%Ni-CN-AN-CTAB, the result shows that H<sub>2</sub> purity gradually decreases from 88.7% to 74% at equilibrium and also CH<sub>4</sub> conversion reduces from 82.2% to 70.4%. These results indicate that 12.5%Ni-CG-AN-CTAB 3mM has better impact on SESMR than 12.5%Ni-CN-AN-CTAB 3mM.

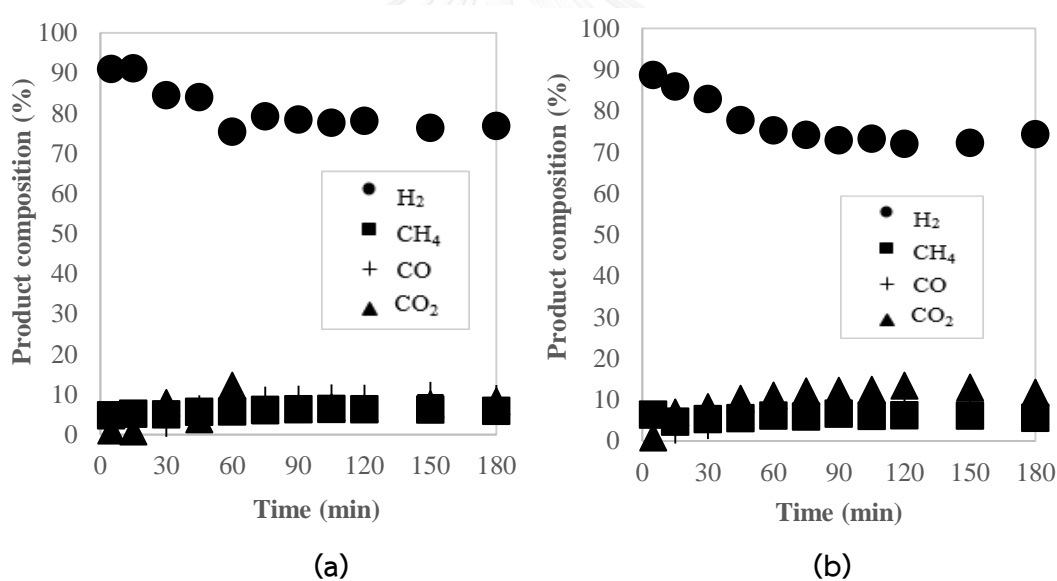


**Figure 5.26:** Gas product composition (dry basis) of (a) 12.5%Ni-CG-AN-CTAB 3mM and (b) 12.5%Ni-CN-AN-CTAB 3mM for sorption enhanced steam methane reforming Condition: at atmospheric pressure, reaction temperature of 600°C, S/C of 3 and total flow rate 60ml/min.

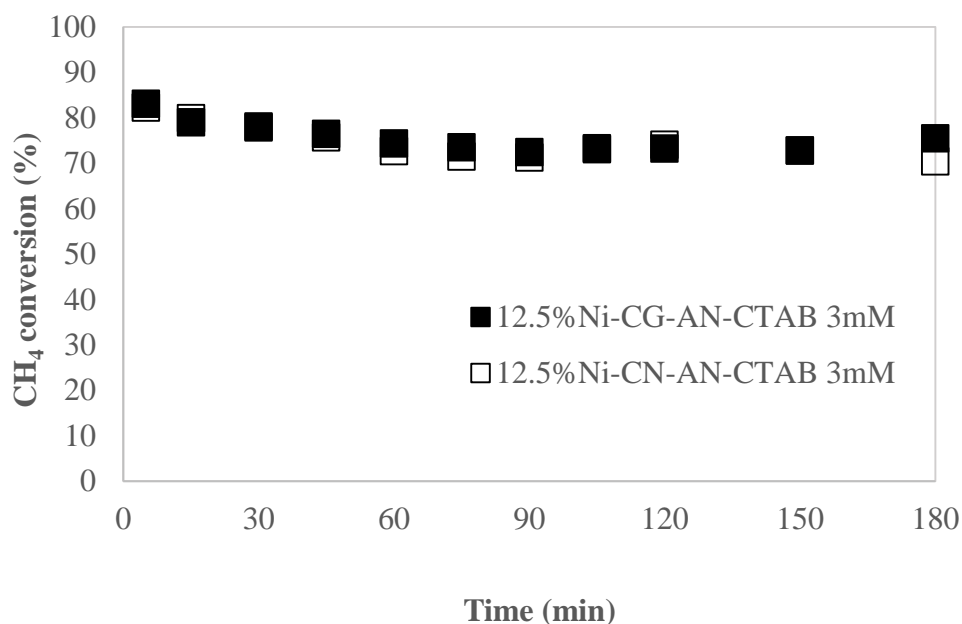


**Figure 5.27:** CH<sub>4</sub> conversion of 12.5%Ni-CG-AN-CTAB 3mM and 12.5%Ni-CN-AN-CTAB 3mM for sorption enhanced steam methane reforming Condition: at atmospheric pressure, reaction temperature of 600°C, S/C of 3 and total flow rate 60ml/min.

Figure 5.28 shows morphology of 12.5%Ni-CG-AN-CTAB 3mM and 12.5%Ni-CN-AN-CTAB 3mM for both as fresh material and after tested in SESMR (Figure 5.28a and 5.28b). The result reveals that particles of the material are more aggregated due to the formation of CaCO<sub>3</sub>. 12.5%Ni-CG-AN-CTAB 3mM shows morphology of particle smaller than 12.5%Ni-CN-AN-CTAB 3mM as shown in Figure 5.28d. Note that higher H<sub>2</sub> production found with 12.5%Ni-CG-AN-CTAB 3mM might be due to higher %Ni on surface of sorbent as the results from SEM-EDX reveal 5.62% of Ni on 12.5%Ni-CN-AN-CTAB 3mM and 7% of Ni on 12.5%Ni-CG-AN-CTAB 3mM. Pore diameter of both sorbent was observed in table 5.6. 12.5%Ni-CN-AN-CTAB 3mM showed pore diameter of multifunctional catalyst more than 12.5%Ni-CG-AN-CTAB 3mM 6 nm. Although surface area of 12.5%Ni-CN-AN-CTAB 3mM presented higher than 12.5%Ni-CG-AN-CTAB 3mM, it might be nickel metal clatching on modified sorbent but it cannot improve adsorption period.



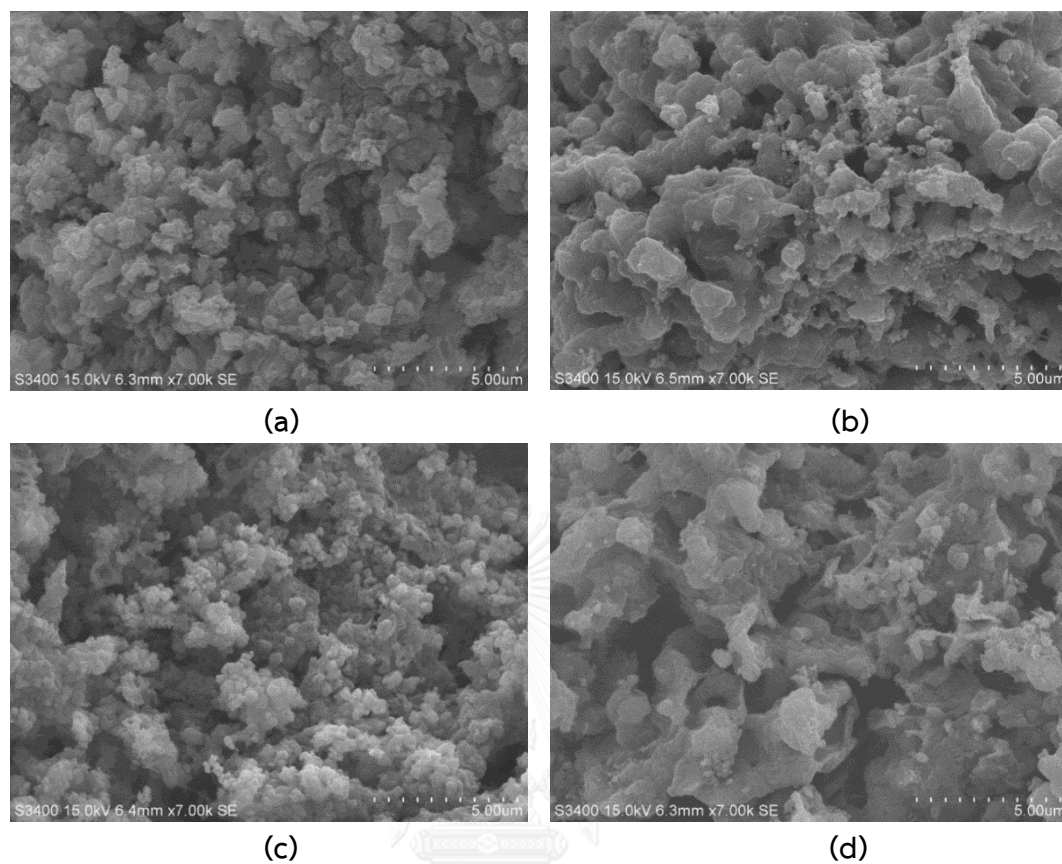
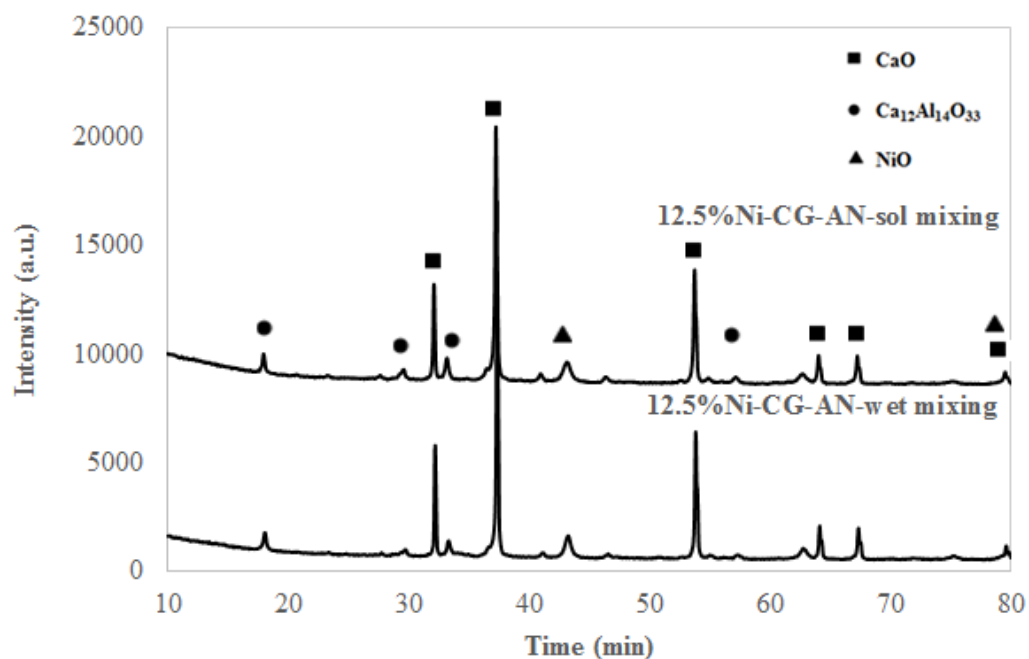


**Figure 5.28:** Morphology of 12.5%Ni-CN-AN-CTAB 3mM for sorption enhanced steam methane reforming Condition: at atmospheric pressure, reaction temperature of 600°C, S/C of 3 and total flow rate 60ml/min. a) fresh of 12.5%Ni-CG-AN-CTAB 3mM b) 12.5%Ni-CG-AN-CTAB 3m after test of SESMR c) fresh of 12.5%Ni-CN-AN-CTAB 3mM d) 12.5%Ni-CN-AN-CTAB 3m after test of SESMR

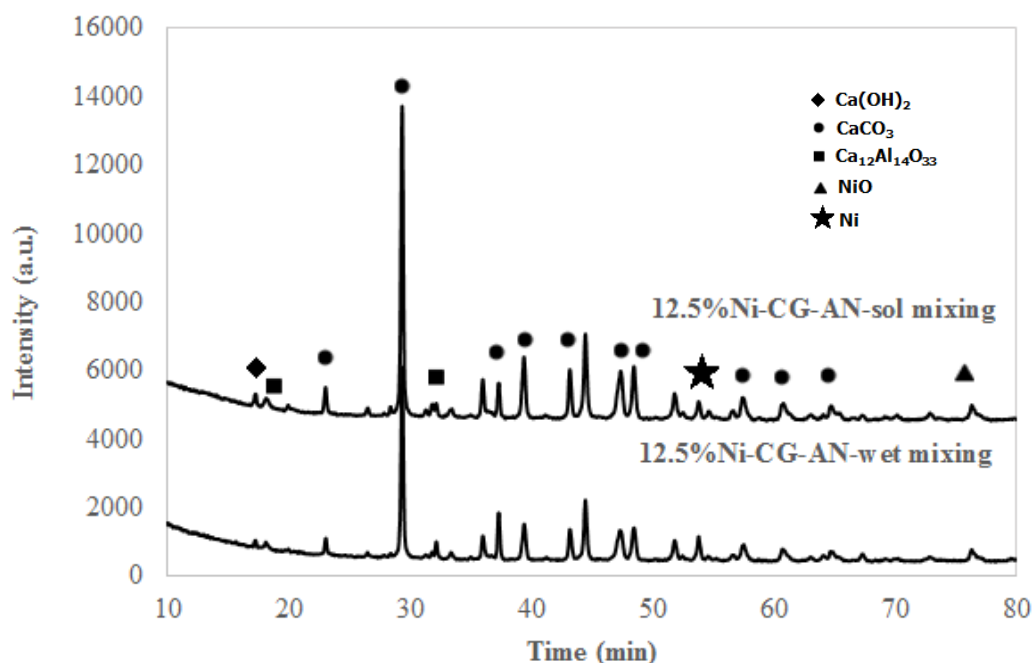
### 5.2.3 The effect of synthesis method for catalytic sorbent material

From the above results, catalytic sorbent materials prepared by wet mixing method shows fairly improvement of hydrogen production from SESMR. As a consequence, sol mixing was selected for comparison with wet-mixing method.

Figure 5.29 shows XRD pattern of hybrid catalytic sorbent materials prepared from sol mixing and wet mixing methods. The main peaks representing CaO-Ca<sub>12</sub>Al<sub>14</sub>O<sub>33</sub> are observed similar to those found in Figure 5.23a, therefore it could be conclude that different method has no effect on phase of CaO and Ca<sub>12</sub>Al<sub>14</sub>O<sub>33</sub>. XRD was used identified CaCO<sub>3</sub>, Ca(OH)<sub>2</sub>, Ni as increased substrate on multifunction catalyst after SESMR test in figure 5.30b. This XRD characterization was observed same to Figure 5.29b.



(a)

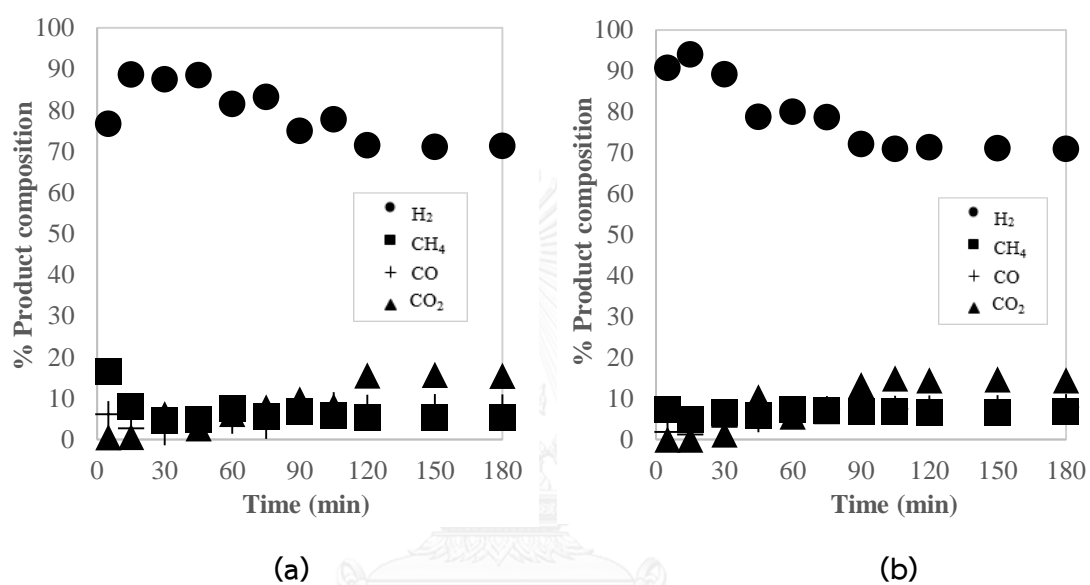


(b)

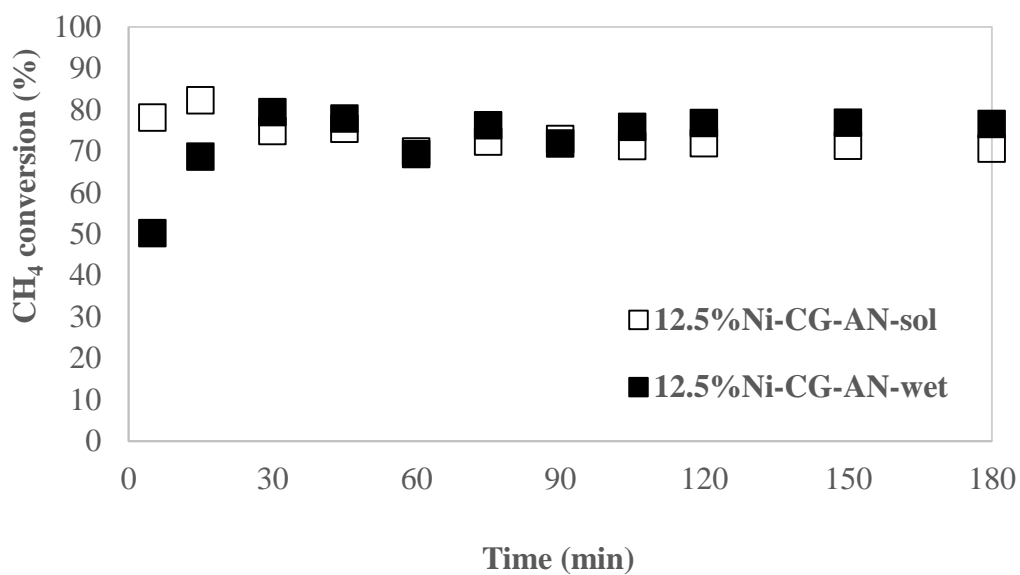
**Figure 5.29:** XRD of fourth hybrid multifunctional catalyst fresh (a) and after SESMR test (b). (12.5%Ni-12.5%Ni-CG-AN-wet mixing and 12.5%Ni-CG-AN-sol mixing)

Figure 5.30 presents product composition obtained from SESMR using catalytic sorbents prepared by sol mixing and wet mixing methods. The results show adsorption period of 30 minutes with the maximum  $H_2$  purity of 94 % and 82.3% of  $CH_4$  conversion in Figure 5.31. At equilibrium,  $H_2$  purity and  $CH_4$  conversion decreases to 71.3% and 70.64%, respectively. An improvement of  $H_2$  purity observed with the sorbent prepared by sol mixing method might be because in sol mixing calcium d-gluconic acid was transformed to calcium oxide by calcination at  $900^\circ C$  then, CaO was added into solution. At this state, CaO reacted with  $H_2O$  and became  $Ca(OH)_2$ . Because of the volume increase from CaO to  $Ca(OH)_2$  and the expansion of particle caused by the exothermic hydration of CaO, the aggregates crack and swell and the regular hexagonal crystalloids of  $Ca(OH)_2$  are generated. Sol-mixing method ensures uniform distribution of Ca/Al equal which enhances the  $CO_2$  sorption ability of the synthesized  $CaO-Ca_{12}Al_{14}O_{33}$  [67].

The result in adsorption period shows H<sub>2</sub> purity is higher than 94%, which is highest %H<sub>2</sub> observed in this study. It is noted that although H<sub>2</sub> production with the use of with 12.5%Ni-CG-AN prepared by sol mixing technique offers higher purity than that prepared by wet mixing; however, sol mixing method requires higher energy consumption than wet mixing technique as the material needs to be calcined twice.



**Figure 5.30:** Gas product composition (dry basis) of 12.5%Ni-CG-AN at different synthesis method including wet mixing (a) and sol mixing (b) for sorption enhanced steam methane reforming Condition: at atmospheric pressure, reaction temperature of 600°C, S/C of 3 and total flow rate 60ml/min.



**Figure 5.31:** CH<sub>4</sub> conversion of 12.5%Ni-CG-AN wet mixing and 12.5%Ni-CG-AN sol mixing for sorption enhanced steam methane reforming Condition: at atmospheric pressure, reaction temperature of 600°C, S/C of 3 and total flow rate 60ml/min.

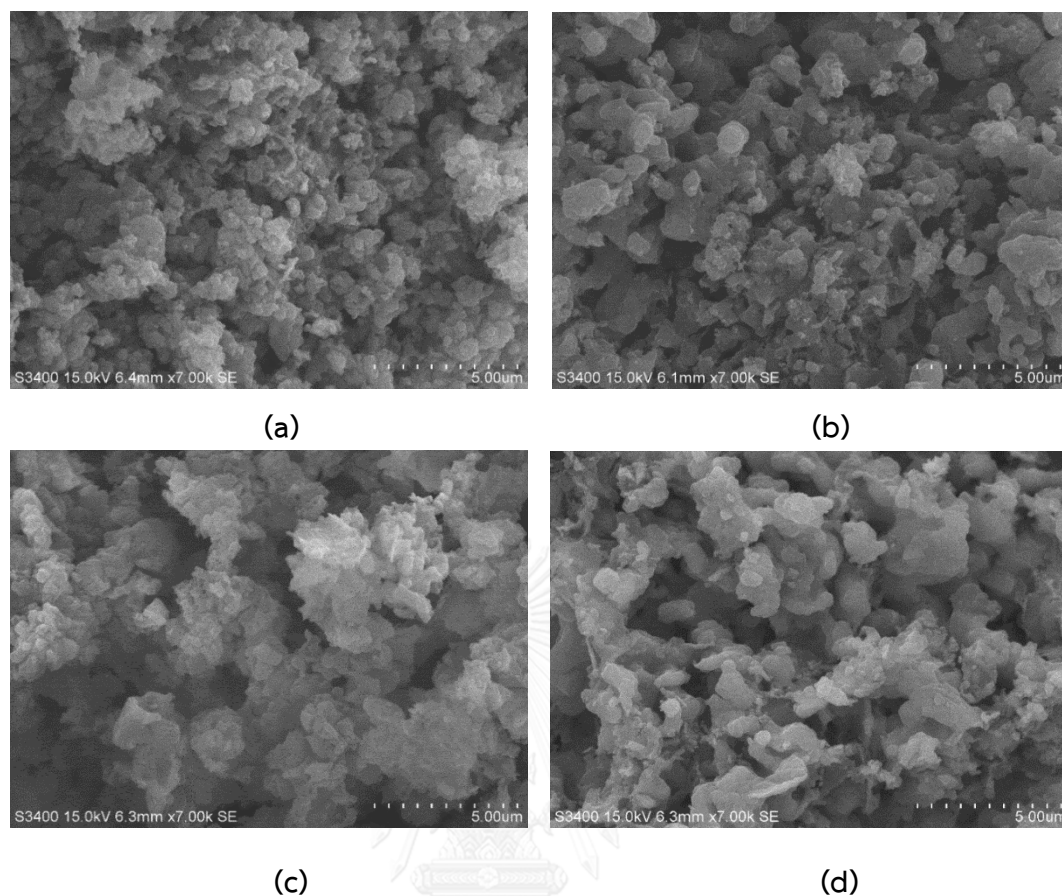


**Figure 5.32:** morphology of 12.5%Ni-CG-AN wet mixing and 12.5%Ni-CG-AN sol mixing for sorption enhanced steam methane reforming Condition: at atmospheric pressure, reaction temperature of 600°C, S/C of 3 and total flow rate 60ml/min. a) fresh of 12.5%Ni-CG-AN wet mixing b) 12.5%Ni-CG-AN wet mixing after test of SESMR c) fresh of 12.5%Ni-CG-AN sol-mixing d) 12.5%Ni-CG-AN sol mixing after test of SESMR.

Table 5.6 summarizes textural properties of sorbents and hybrid multifunctional catalysts. High surface area is observed with CG-AN sol-mixing and CG-AN-CTAB 3 mM wet-mixing and the area reduces when the sorbents were impregnated by 12.5%Nickel due to Ni molecules might block pore of the sorbent. In contrast, CG-AN, CN-AN, and CN-AN-CTAB 3 mM synthesized by wet mixing show an increase of surface area when the sorbent was impregnated by 12.5%Ni. The adhesion of Ni

molecules on support might be occurred on surface area, So surface area of above three sorbent are increased when impregnated by Ni.

**Table 5.6:** Summary textural properties results of sorbents and hybrid multifunctional catalysts when Nickel was impregnated on sorbents.

Sample	Surface area (m <sup>2</sup> /g)	Pore volume (cm <sup>3</sup> /g)	Pore diameter (nm)	Ni content (%)
CG-AN sol-mixing	15.98	0.0326	7.71	-
12.5%Ni-CG-AN sol-mixing	11.80	0.0344	11.53	9.93
CG-AN	11.27	0.0100	6.79	-
12.5%Ni-CG-AN wet-mixing	12.38	0.0227	9.87	9.43
CG-AN-CTAB 3mM	14.12	0.0162	4.587	-
12.5%Ni-CG-AN-CTAB 3mM	13.26	0.0368	10.54	7.90
CN-AN	7.31	0.0134	8.76	-
12.5%Ni-CN-AN wet-mixing	13.79	0.0371	10.74	10.66
CN-AN-CTAB 3mM	6.26	0.0106	10.76	-
12.5%Ni-CN-AN-CTAB 3mM	16.92	0.0516	16.80	7.23

Table 5.7 summarizes the results of using different catalytic sorbent materials for sorption-enhanced steam methane reforming (SESMR). The hybrid material 12.5%Ni-CG-AN sol mixing and 12.5%Ni-CN-AN wet mixing provide shorter adsorption time but high hydrogen purity when compared with other sorbents. With the consideration of H<sub>2</sub> purity and CH<sub>4</sub> conversion, 12.5%Ni-CG-AN-CTAB 3 mM shows the

best performance for SESMR process as H<sub>2</sub> purity and CH<sub>4</sub> conversion are higher than other sorbents for longer period of time. When comparison hydrogen purity and CH<sub>4</sub> conversion with conventional catalyst (Figures A6-A7), Our results reveal that modified-catalytic sorbent can improve H<sub>2</sub> production over conventional catalyst of SR process.

**Table 5.7:** Summary results of all hybrid multifunctional catalysts for sorption-enhanced steam methane reforming (SESMR). Condition: 2 g. of catalyst at atmospheric pressure, reaction temperature of 600°C, S/C of 3 and total flow rate 60ml/min.

Sample	Time of adsorption (min)	Maximum H <sub>2</sub> purity (%)	H <sub>2</sub> equilibrium at 180 min (%)	CH <sub>4</sub> conversion (%)
12.5%Ni/Al <sub>2</sub> O <sub>3</sub> conventional catalyst	-	72.25	70	80
12.5%Ni-CG-AN sol-mixing	30	94	71.3	82.3
12.5%Ni-CG-AN wet-mixing	45	88.7	71.3	79.4
12.5%Ni-CG-AN-CTAB 3mM wet-mixing	45	91.2	76.8	83
12.5%Ni-CN-AN wet-mixing	30	92.7	74.5	80
12.5%Ni-CN-AN-CTAB 3mM wet-mixing	45	88.7	74.3	82.2



## CHAPTER VI

### CONCLUSION AND RECOMMENDATION

#### 6.1 Conclusion

This work is tempted to improve properties of catalytic sorbent material used to produce hydrogen via sorption enhanced steam methane reforming (SESMR). CO<sub>2</sub> sorption capacity and stability of the synthetic sorbents were examined for high-temperature CO<sub>2</sub> sorption and for SESMR, the works are summarized as follows:

1. Technique to examine CO<sub>2</sub> sorption capacity has an effect on examination of sorption performances. Two set-up experiments, TGA and fixed-bed reactor were used to test CO<sub>2</sub> sorption ability of CaO. The results showed that using TGA provides higher CO<sub>2</sub> sorption capacity than using fixed-bed reactor due to the effect of external mass transfer.

2. Sorption temperature is found to have effect on sorption capacity: increasing temperature from 600 to 800°C leads to a decrease of sorption capacity due to exothermic reaction of carbonation reaction.

3. Different calcium precursors provide different polymorphs of synthetic CaO and also the ability to adsorb CO<sub>2</sub>. Calcium d-gluconic acid (CG) offers higher CO<sub>2</sub> sorption capacity than calcium nitrate (CN) in mixed CO<sub>2</sub>/N<sub>2</sub> system (15%v/v CO<sub>2</sub>) at 600°C due to it possesses higher surface area.

4. Improvement of CaO-based sorbent was investigated by adding surfactants: cetyltrimethyl ammonium bromide (CTAB) or sodium dodecyl sulfate (SDS) during the synthesis step. The results show that by adding surfactant at its CMC value, CG-AN-CTAB provides a slight higher sorption capacity when compared with that without adding surfactant. This result is due to higher surface area is obtained when CTAB is

added. In contrast, comparative sorption capacity is observed with the addition of SDS surfactant, CG-AN-SDS.

5. Effect of CTAB concentration on properties of synthetic CaO-based alumina sorbents, CG-AN and CN-AN was investigated. The experimental results show 3 mM of CTAB can improve capacity of both sorbents as this concentration could provide suitable number of micelle leads to a proper textural properties and morphology.

6. Stability of CG-AN-CTAB 3mM and CN-AN-CTAB 3mM was studied continually from CO<sub>2</sub> sorption capacity for 10 cycles. CG-AN-CTAB 3mM shows CO<sub>2</sub> sorption capacity higher than CN-AN-CTAB 3mM for all cycles. Sorption capacity of CN-AN-CTAB 3mM decreases 30.9% from cycle 1 to 10 while CO<sub>2</sub> sorption capacity of CG-AN-CTAB 3mM reduced 36.8% from cycle 1 to 10.

7. The improved CaO-based alumina sorbents were further incorporated with NiO to use as catalytic sorbent material for sorption enhanced steam methane reforming (SESMR). Incorporating 12.5% of NiO with CG-AN-CTAB 3mM by wet-mixing provides the best performance of which 91.2% H<sub>2</sub> and 83% CH<sub>4</sub> conversion.

## 6.2 Recommendation

1. Addition of surfactants during synthesis step of CaO can lead to an improvement of sorbent properties toward high CO<sub>2</sub> sorption capacity. However, pH of solution, temperature of the synthesis and order of adding surfactant into solution could also affect on properties of sorbent. This is interesting for the future studies in order to further improve properties of sorbents.

2. Selective calcium precursor has an effect to properties of sorbent because our results have been shown that obvious different properties of sorbent is observed with the use of different precursors.

3. Reduction amount of nickel on modified sorption is interesting because in this thesis, CO<sub>2</sub> sorption period in SESMR shows short time of adsorption due to NiO may block pore of the modified sorbent, leading to lower sorption capacity of CO<sub>2</sub>.

## REFERENCES

- [1] Smitkova, M., Janiček, F., and Riccardi, J. Life cycle analysis of processes for hydrogen production. International Journal of Hydrogen Energy 36 (2011): 7844-7851.
- [2] Cooper, H.W. Fuel Cells, the Hydrogen Economy and You. CEP (Chemical Engineering Progress) (2007).
- [3] Trygve, R.E.F.H.P.J.S.V.Ø.U. Hydrogen production and storage R&D priorities and gaps. International Energy Agency. 33 (2006).
- [4] Liu, J.A. Kinetics, catalysis and mechanism of methane steam reforming WORCESTER POLYTECHNIC INSTITUTE Massachusetts, United States, 2006.
- [5] Maluf, S.S., and Assaf, E.M. Ni catalysts with Mo promoter for methane steam reforming. Fuel 88 (2009): 1547-1553.
- [6] Kim, H.-W., Kang, K.-M., Kwak, H.-Y., and Kim, J.H. Preparation of supported Ni catalysts on various metal oxides with core/shell structures and their tests for the steam reforming of methane. Chemical Engineering Journal 168 (2011): 775-783.
- [7] Essaki, K., Muramatsu, T., and Kato, M. Effect of equilibrium shift by using lithium silicate pellets in methane steam reforming. International Journal of Hydrogen Energy 33 (2008): 4555-4559.
- [8] Obradović, A., Likozar, B., and Levec, J. Catalytic surface development of novel nickel plate catalyst with combined thermally annealed platinum and alumina coatings for steam methane reforming. International Journal of Hydrogen Energy 38 (2013): 1419-1429.
- [9] Lertwittayanon, K., et al. Effect of CaO–ZrO<sub>2</sub> addition to Ni supported on  $\gamma$ -Al<sub>2</sub>O<sub>3</sub> by sequential impregnation in steam methane reforming. International Journal of Hydrogen Energy 35 (2010): 12277-12285.
- [10] Zhu, X., Wei, Y., Wang, H., and Li, K. Ce–Fe oxygen carriers for chemical-looping steam methane reforming. International Journal of Hydrogen Energy 38 (2013): 4492-4501.

- [11] Izquierdo, U., et al. Hydrogen production from methane and natural gas steam reforming in conventional and microreactor reaction systems. International Journal of Hydrogen Energy 37 (2012): 7026-7033.
- [12] Bej, B., Pradhan, N.C., and Neogi, S. Production of hydrogen by steam reforming of methane over alumina supported nano-NiO/SiO<sub>2</sub> catalyst. Catalysis Today 207 (2013): 28-35.
- [13] Huang, T.-J., and Chen, H.-M. Hydrogen production via steam reforming of methanol over Cu/(Ce,Gd)O<sub>2-x</sub> catalysts. International Journal of Hydrogen Energy 35 (2010): 6218-6226.
- [14] Pérez-Hernández, R., Gutiérrez-Martínez, A., Palacios, J., Vega-Hernández, M., and Rodríguez-Lugo, V. Hydrogen production by oxidative steam reforming of methanol over Ni/CeO<sub>2</sub>-ZrO<sub>2</sub> catalysts. International Journal of Hydrogen Energy 36 (2011): 6601-6608.
- [15] López, P., et al. Hydrogen production from oxidative steam reforming of methanol: Effect of the Cu and Ni impregnation on ZrO<sub>2</sub> and their molecular simulation studies. International Journal of Hydrogen Energy 37 (2012): 9018-9027.
- [16] Vizcaino, A., Carrero, A., and Calles, J. Hydrogen production by ethanol steam reforming over Cu-Ni supported catalysts. International Journal of Hydrogen Energy 32 (2007): 1450-1461.
- [17] Zhang, B., Tang, X., Li, Y., Xu, Y., and Shen, W. Hydrogen production from steam reforming of ethanol and glycerol over ceria-supported metal catalysts. International Journal of Hydrogen Energy 32 (2007): 2367-2373.
- [18] Biswas, P., and Kunzru, D. Steam reforming of ethanol for production of hydrogen over Ni/CeO<sub>2</sub>-ZrO<sub>2</sub> catalyst: Effect of support and metal loading. International Journal of Hydrogen Energy 32 (2007): 969-980.
- [19] Ni, M., Leung, D.Y.C., Leung, M.K.H., and Sumathy, K. An overview of hydrogen production from biomass. Fuel Processing Technology 87 (2006): 461-472.
- [20] Florin, N.H., and Harris, A.T. Enhanced hydrogen production from biomass with in situ carbon dioxide capture using calcium oxide sorbents. Chemical Engineering Science 63 (2008): 287-316.

- [21] Bičáková, O., and Straka, P. Production of hydrogen from renewable resources and its effectiveness. International Journal of Hydrogen Energy 37 (2012): 11563-11578.
- [22] Xie, M., Zhou, Z., Qi, Y., Cheng, Z., and Yuan, W. Sorption-enhanced steam methane reforming by in situ CO<sub>2</sub> capture on a CaO–Ca<sub>9</sub>Al<sub>6</sub>O<sub>18</sub> sorbent. Chemical Engineering Journal 207–208 (2012): 142-150.
- [23] Lima da Silva, A., and Müller, I.L. Hydrogen production by sorption enhanced steam reforming of oxygenated hydrocarbons (ethanol, glycerol, n-butanol and methanol): Thermodynamic modelling. International Journal of Hydrogen Energy 36 (2011): 2057-2075.
- [24] Chanburanasiri, N., Ribeiro, Ana M., Rodrigues, Alirio E., Arpornwichanop, A., Laosiripojana, N., Praserttham, P., Assabumrungrat, S. Hydrogen Production via Sorption Enhanced Steam Methane Reforming Process Using Ni/CaO Multifunctional Catalyst. Industrial & Engineering Chemistry Research 50 (2011): 13662-13671.
- [25] Bertoni, M.I.e. Cage Structure Materials for n-type Transparent Conducting Oxides. Northwestern University, Evanston, IL, United State, 2007.
- [26] Huang, Z.-s.L.N.-s.C.a.Y.-y. Effect of Preparation Temperature on Cyclic CO<sub>2</sub> Capture and Multiple Carbonation–Calcination Cycles for a New Ca-Based CO<sub>2</sub> Sorbent. Ind. Eng. Chem. Res. 45 (2006): 1911-1917.
- [27] Carlota O. Rangel-Yagui, A.P.-J., and Leoberto Costa Tavares Micellar solubilization of drugs. J Pharm Pharmaceut Sci (2005): 147-163.
- [28] Al-Koofee, M.E.M.D.A.F. Effect of Temperature Changes on Critical Micelle Concentration for Tween Series Surfactant. Global Journal of Science Frontier Research Chemistry 13 (2013).
- [29] Barelli, L., Bidini, G., Gallorini, F., and Servili, S. Hydrogen production through sorption-enhanced steam methane reforming and membrane technology: A review. Energy 33 (2008): 554-570.
- [30] Wang, X., Wang, N., and Wang, L. Hydrogen production by sorption enhanced steam reforming of propane: A thermodynamic investigation. International Journal of Hydrogen Energy 36 (2011): 466-472.

- [31] Rydén, M., and Ramos, P. H<sub>2</sub> production with CO<sub>2</sub> capture by sorption enhanced chemical-looping reforming using NiO as oxygen carrier and CaO as CO<sub>2</sub> sorbent. Fuel Processing Technology 96 (2012): 27-36.
- [32] Song, C., Overview of Hydrogen Production Options for Hydrogen Energy Development, Fuel-Cell Fuel Processing and Mitigation of CO<sub>2</sub> Emission. In Proc. 20th International Pittsburgh Coal Conference, Pittsburgh, PA, USA, 2003.
- [33] Trygve, R.E.F.H.P.J.S.V.Ø.U. HYDROGEN PRODUCTION AND STORAGE R&D PRIORITIES AND GAPS; INTERNATIONAL ENERGY AGENCY: Paris, France., 2006; p 33.
- [34] Mortola, V.B., Damyanova, S., Zanchet, D., and Bueno, J.M.C. Surface and structural features of Pt/CeO<sub>2</sub>-La<sub>2</sub>O<sub>3</sub>-Al<sub>2</sub>O<sub>3</sub> catalysts for partial oxidation and steam reforming of methane. Applied Catalysis B: Environmental 107 (2011): 221-236.
- [35] Rocha, K.O., et al. Catalytic partial oxidation and steam reforming of methane on La<sub>2</sub>O<sub>3</sub>-Al<sub>2</sub>O<sub>3</sub> supported Pt catalysts as observed by X-ray absorption spectroscopy. Applied Catalysis A: General 431-432 (2012): 79-87.
- [36] de Souza, V.P., Costa, D., dos Santos, D., Sato, A.G., and Bueno, J.M.C. Pt-promoted  $\alpha$ -Al<sub>2</sub>O<sub>3</sub>-supported Ni catalysts: Effect of preparation conditions on oxidation and catalytic properties for hydrogen production by steam reforming of methane. International Journal of Hydrogen Energy 37 (2012): 9985-9993.
- [37] Roy, P.S., Park, N.-K., and Kim, K. Metal foam-supported Pd-Rh catalyst for steam methane reforming and its application to SOFC fuel processing. International Journal of Hydrogen Energy 39 (2014): 4299-4310.
- [38] Feio, L.S.F., et al. The effect of ceria content on the properties of Pd/CeO<sub>2</sub>/Al<sub>2</sub>O<sub>3</sub> catalysts for steam reforming of methane. Applied Catalysis A: General 316 (2007): 107-116.
- [39] Zeppieri, M., Villa, P.L., Verdone, N., Scarsella, M., and De Filippis, P. Kinetic of methane steam reforming reaction over nickel- and rhodium-based catalysts. Applied Catalysis A: General 387 (2010): 147-154.
- [40] Duarte, R.B., Nachtegaal, M., Bueno, J.M.C., and van Bokhoven, J.A. Understanding the effect of Sm<sub>2</sub>O<sub>3</sub> and CeO<sub>2</sub> promoters on the structure and activity of Rh/Al<sub>2</sub>O<sub>3</sub> catalysts in methane steam reforming. Journal of Catalysis 296 (2012): 86-98.

- [41] Wang, Y., et al. Highly active and stable Rh/MgOAl<sub>2</sub>O<sub>3</sub> catalysts for methane steam reforming. Catalysis Today 98 (2004): 575-581.
- [42] Zhai, X., Ding, S., Liu, Z., Jin, Y., and Cheng, Y. Catalytic performance of Ni catalysts for steam reforming of methane at high space velocity. International Journal of Hydrogen Energy 36 (2011): 482-489.
- [43] de Abreu, A.J., Lucrédio, A.F., and Assaf, E.M. Ni catalyst on mixed support of CeO<sub>2</sub>-ZrO<sub>2</sub> and Al<sub>2</sub>O<sub>3</sub>: Effect of composition of CeO<sub>2</sub>-ZrO<sub>2</sub> solid solution on the methane steam reforming reaction. Fuel Processing Technology 102 (2012): 140-145.
- [44] Roh, H.-S., Jun, K.-W., and Park, S.-E. Methane-reforming reactions over Ni/Ce-ZrO<sub>2</sub>/Al<sub>2</sub>O<sub>3</sub> catalysts. Applied Catalysis A: General 251 (2003): 275-283.
- [45] Salhi, N., Boulahouache, A., Petit, C., Kiennemann, A., and Rabia, C. Steam reforming of methane to syngas over NiAl<sub>2</sub>O<sub>4</sub> spinel catalysts. International Journal of Hydrogen Energy 36 (2011): 11433-11439.
- [46] Martavaltzi, C.S., and Lemonidou, A.A. Hydrogen production via sorption enhanced reforming of methane: Development of a novel hybrid material—reforming catalyst and CO<sub>2</sub> sorbent. Chemical Engineering Science 65 (2010): 4134-4140.
- [47] Martavaltzi, C.S., and Lemonidou, A.A. Development of new CaO based sorbent materials for CO<sub>2</sub> removal at high temperature. Microporous and Mesoporous Materials 110 (2008): 119-127.
- [48] Witoon, T. Characterization of calcium oxide derived from waste eggshell and its application as CO<sub>2</sub> sorbent. Ceramics International 37 (2011): 3291-3298.
- [49] Li, Y., et al. Effect of rice husk ash addition on CO<sub>2</sub> capture behavior of calcium-based sorbent during calcium looping cycle. Fuel Processing Technology 90 (2009): 825-834.
- [50] C.E. Quincoces, S.D., A.M. Alvarez, M.G. Gonzalez Effect of addition of CaO on Ni/Al<sub>2</sub>O<sub>3</sub> catalysts over CO<sub>2</sub> reforming of methane. Materials Letters 50 (2001): 21-27.
- [51] Chen, H., et al. Enhancement of reactivity in surfactant-modified sorbent for CO<sub>2</sub> capture in pressurized carbonation. Fuel Processing Technology 92 (2011): 493-499.

- [52] Akgornpeak, A., Witoon, T., Mungcharoen, T., and Limtrakul, J. Development of synthetic CaO sorbents via CTAB-assisted sol-gel method for CO<sub>2</sub> capture at high temperature. Chemical Engineering Journal 237 (2014): 189-198.
- [53] Luo, C., Zheng, Y., Ding, N., Wu, Q.L., and Zheng, C.G. SGCS-made ultrafine CaO/Al<sub>2</sub>O<sub>3</sub> sorbent for cyclic CO<sub>2</sub> capture. Chinese Chemical Letters 22 (2011): 615-618.
- [54] Huang, C.-H., Chang, K.-P., Yu, C.-T., Chiang, P.-C., and Wang, C.-F. Development of high-temperature CO<sub>2</sub> sorbents made of CaO-based mesoporous silica. Chemical Engineering Journal 161 (2010): 129-135.
- [55] Wenqiang Liu, N.L., Bofeng, G.W., and Dinizdacosta., J. Calcium Precursors for the Production of CaO Sorbents for Multicycle CO<sub>2</sub> Capture. Environ. Sci. Technol 44 (2010): 841-847.
- [56] Zhou, Z., Qi, Y., Xie, M., Cheng, Z., and Yuan, W. Synthesis of CaO-based sorbents through incorporation of alumina/aluminate and their CO<sub>2</sub> capture performance. Chemical Engineering Science 74 (2012): 172-180.
- [57] Dennis, J.S., and Pacciani, R. The rate and extent of uptake of CO<sub>2</sub> by a synthetic, CaO-containing sorbent. Chemical Engineering Science 64 (2009): 2147-2157.
- [58] Kim, J.-N., Ko, C.H., and Yi, K.B. Sorption enhanced hydrogen production using one-body CaO-Ca<sub>12</sub>Al<sub>14</sub>O<sub>33</sub>-Ni composite as catalytic absorbent. International Journal of Hydrogen Energy 38 (2013): 6072-6078.
- [59] Park, J., and Yi, K.B. Effects of preparation method on cyclic stability and CO<sub>2</sub> absorption capacity of synthetic CaO-MgO absorbent for sorption-enhanced hydrogen production. International Journal of Hydrogen Energy 37 (2012): 95-102.
- [60] W.N.R. Wan Isahak, M.I., J. Mohd Jahim, J. Salimon and M.A. Yarmo Transesterification of Palm Oil Usinf Nano-Calcium Oxide as a Solid Base Catalyst. World Applied Sciences (2010): 17-22.
- [61] El-Sheikh, S.M., El-Sherbiny, S., Barhoum, A., and Deng, Y. Effects of cationic surfactant during the precipitation of calcium carbonate nano-particles on their size, morphology, and other characteristics. Colloids and Surfaces A: Physicochemical and Engineering Aspects 422 (2013): 44-49.



- [62] Gürses, A., Karaca, S., Aksakal, F., and Açikyildiz, M. Monomer and micellar adsorptions of CTAB onto the clay/water interface. Desalination 264 (2010): 165-172.
- [63] Inoue, M., and Hirasawa, I. The relationship between crystal morphology and XRD peak intensity on CaSO<sub>4</sub>·2H<sub>2</sub>O. Journal of Crystal Growth 380 (2013): 169-175.
- [64] Danov, K.D., Basheva, E.S., Kralchevsky, P.A., Ananthapadmanabhan, K.P., and Lips, A. The metastable states of foam films containing electrically charged micelles or particles: Experiment and quantitative interpretation. Advances in Colloid and Interface Science 168 (2011): 50-70.
- [65] Moisés R. Cesário Braúlio S. Barros, Y.Z., Claire Courson,, and Dulce M. A. Melo, a.A.K. CO<sub>2</sub> Sorption Enhanced Steam Reforming of Methane Using Ni/CaO-Ca<sub>12</sub>Al<sub>14</sub>O<sub>33</sub> Catalysts. Adv. Chem. Lett 1 (2014).
- [66] Lipman, T., An overview of hydrogen production and storage systems with renewable hydrogen case studies. In office of energy Efficiency and renewable energy fuel cell technology program, 2011.
- [67] Lemonidou, C.S.M.a.A.A. Parametric Study of the CaO-Ca<sub>12</sub>Al<sub>14</sub>O<sub>33</sub> Synthesis with Respect to High CO<sub>2</sub> Sorption Capacity and Stability on Multicycle Operation Ind. Eng. Chem. Res 47 (2008): 9537–9543.



APPENDIX

จุฬาลงกรณ์มหาวิทยาลัย  
CHULALONGKORN UNIVERSITY

## APPENDIX A

### CHARACTERIZATION OF SORBENT AND CATALYSTS

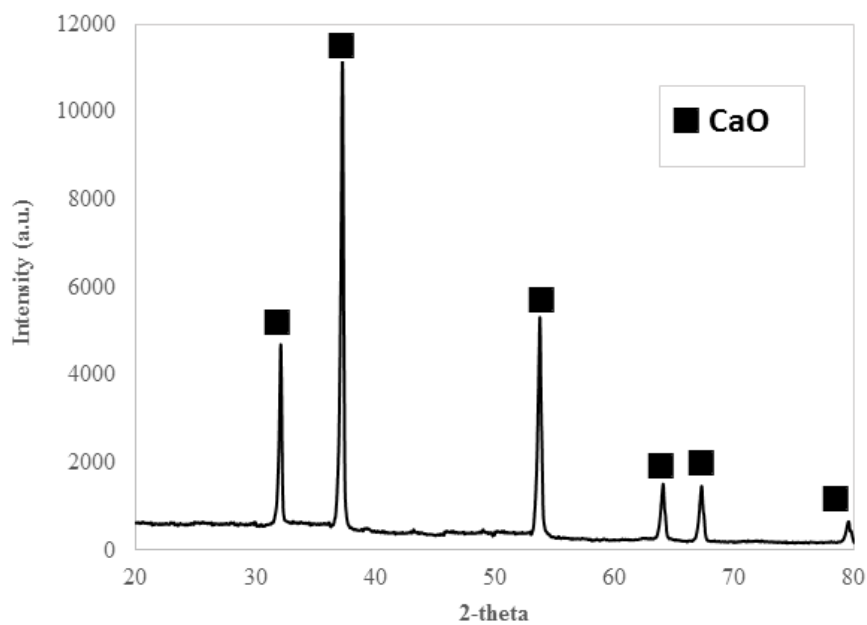


Figure A.1: XRD pattern of commercial calcium oxide

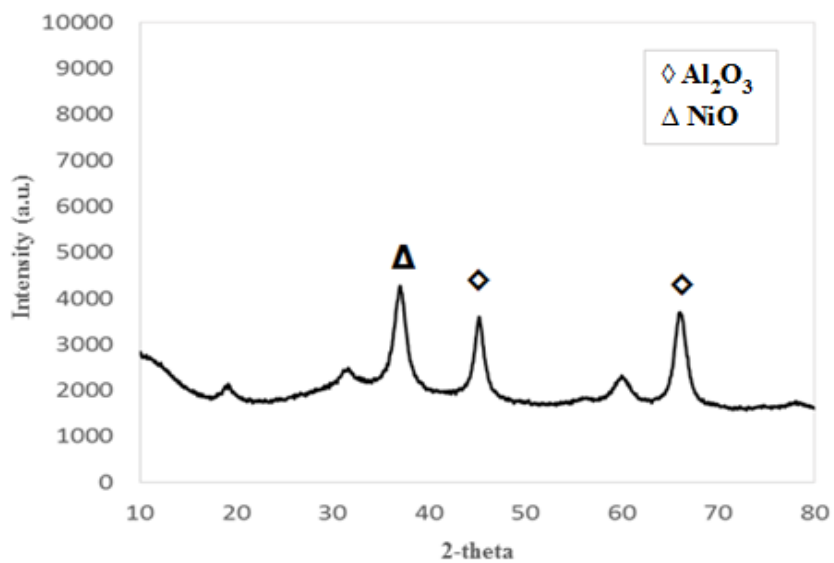
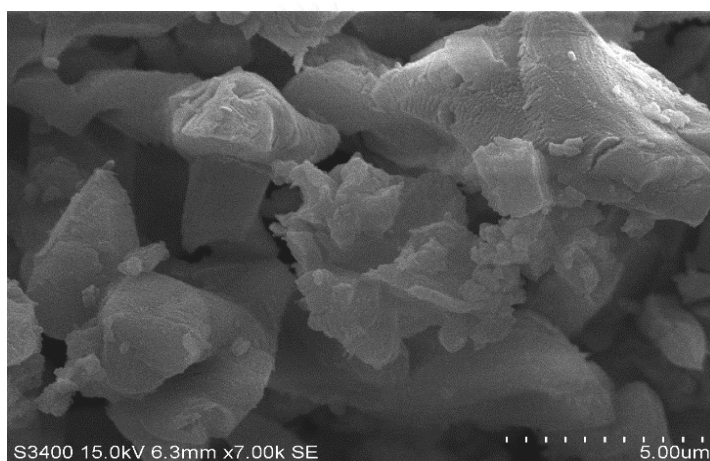
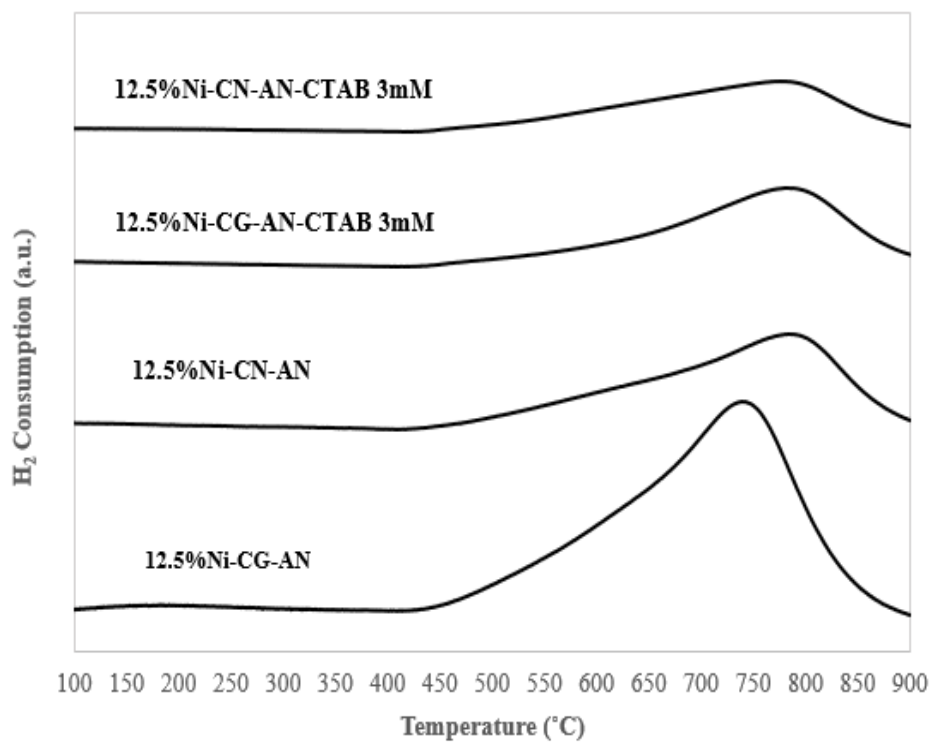


Figure A.2: XRD of 12.5%Ni/Al<sub>2</sub>O<sub>3</sub> conventional catalyst.

**Table A.1:** BET surface area, pore volume and pore diameter of CaO and Ni/Al<sub>2</sub>O<sub>3</sub>.

Sample	Surface area (m <sup>2</sup> /g)	Pore volume (cm <sup>3</sup> /g)	Pore diameter (nm)	%Ni dispersion
CaO commercial	6.9506	0.007633	23.9809	-
12.5%Ni/Al <sub>2</sub> O <sub>3</sub>	68.2	0.204	8.526	11.84

**Figure A.3:** Morphology of Calcium oxide**Figure A.4:** Morphology of 12.5%Ni/Al<sub>2</sub>O<sub>3</sub>



**Figure A.5:** H<sub>2</sub>-TPR of fourth hybrid multifunctional catalyst. (12.5%Ni-CN-AN, 12.5%Ni-CG-AN, 12.5%Ni-CN-AN-CTAB 3mM and 12.5%Ni-CG-AN-CTAB 3mM)  
Condition: 10%v/v of H<sub>2</sub> in N<sub>2</sub>, total flow rate 50ml/min.

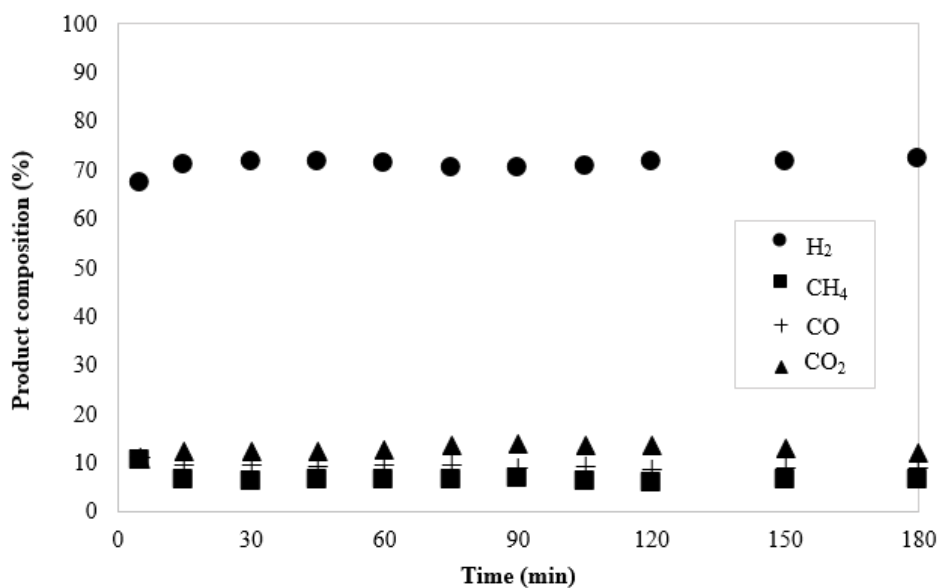


**Figure A.6:** Gas product composition (dry basis) of 2 g. of 12.5%Ni/Al<sub>2</sub>O<sub>3</sub> Condition: atmospheric pressure at 600°C, S/C =3 and total flow 60 mL/min.

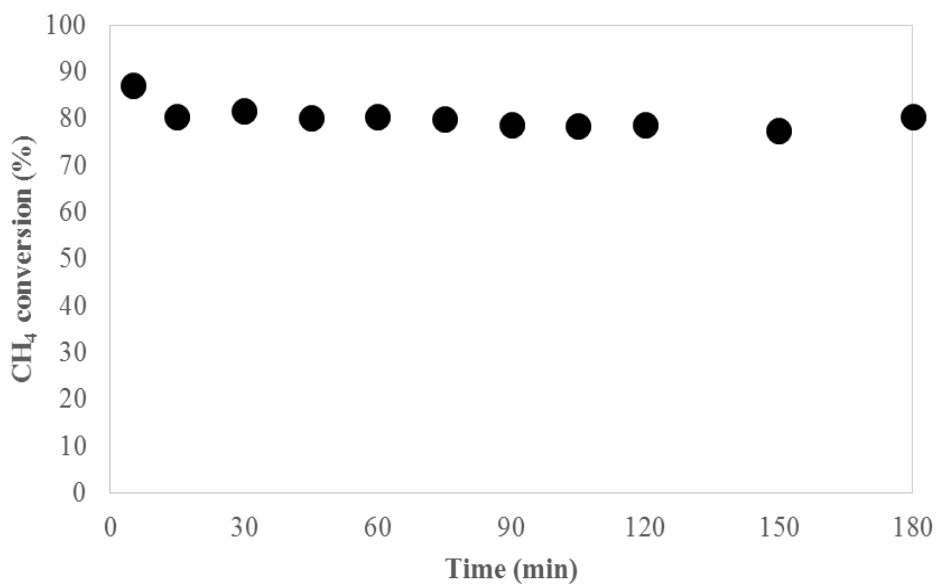


**Figure A.7:** CH<sub>4</sub> conversion of 2 g. of 12.5%Ni/Al<sub>2</sub>O<sub>3</sub> Condition: atmospheric pressure at 600°C, S/C =3 and total flow 60 mL/min.

## APPENDIX B

### CALCULATION OF ADSORPTION CAPACITY AND SORPTION-ENHANCED STEAM METHANE REFORMING

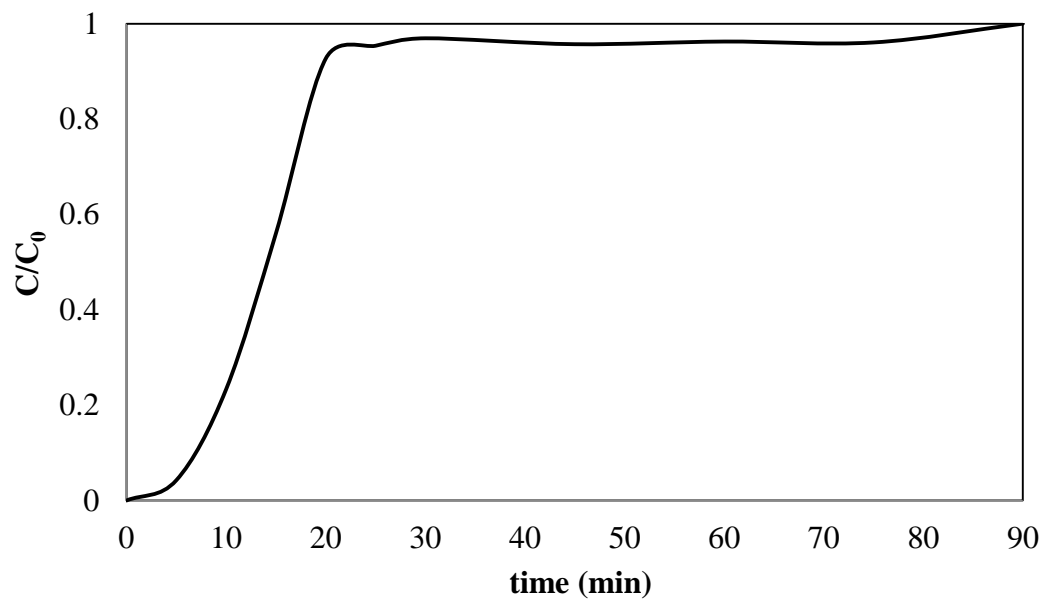


**Figure B.1:** Breakthrough curves of CO<sub>2</sub> sorption by 1g of Calcium Oxide Operating conditions: atmospheric pressure, 600°C, and 15%v/v CO<sub>2</sub> (balanced N<sub>2</sub>).

#### B.1 Adsorption capacity of adsorbent

$W_{\text{sat}}$  = amount of CO<sub>2</sub> (g) derived by amount of adsorbent (g)

$$= \frac{F_A \times \text{above graph area}}{\text{amount of adsorbent}} \quad \dots \text{(B.1)}$$

1. Find rate of feed ( $F_A$ )

$$F_A = u_0 c_0 M$$

Where  $F_A = \text{rate of feed } \left(\frac{\text{g}}{\text{min}}\right)$   
 $u_0 = \text{velocity of feed } \left(\frac{\text{g}}{\text{min}}\right)$   
 $c_0 = \text{concentration of feed } \left(\frac{\text{g}}{\text{mol}}\right)$

Therefore;

$$F_A = 60 \left(\frac{\text{cm}^3}{\text{min}}\right) \times (1.079 \times 10^{-5}) \left(\frac{\text{mol}}{\text{cm}^3}\right) \times 44 \left(\frac{\text{g}}{\text{mol}}\right)$$

$$= 0.0284 \frac{\text{g}}{\text{min}}$$

2. Find above graph area

$$\begin{aligned} \text{Above graph area} &= \int_0^{120} \left(1 - \frac{c}{c_0}\right) dt \\ &= 16.05 \text{ min} \end{aligned}$$

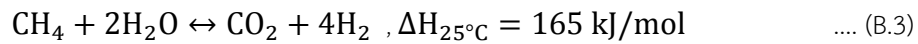
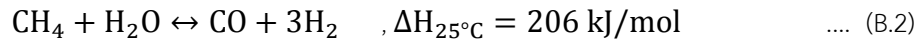
Substitute 1-2 into equation B.1

$$\begin{aligned} W_{sat} &= \frac{0.0284 \left(\frac{\text{g}}{\text{min}}\right) \times 16.05(\text{min})}{1.0003 (\text{g})} \\ &= 0.456 \frac{\text{gCO}_2}{\text{g sorbent}} \end{aligned}$$

Therefore, 1 g of CaO can adsorb 0.456 g of CO<sub>2</sub> at 600°C, atmospheric pressure and 15%v/v CO<sub>2</sub> (balanced N<sub>2</sub>).



## B.2 H<sub>2</sub> composition and CH<sub>4</sub> conversion



For the study, the experiment were performed using excess steam at  $S/C = 3$  followed by stoichiometry

$$\begin{aligned} S/C &= \frac{Y_{\text{H}_2\text{O},in}}{Y_{\text{CH}_4,in}} \\ &= \frac{3 \text{ mole}}{1 \text{ mole}} \\ &= 3 \end{aligned} \quad \dots \text{ (B.5)}$$

$$\% \text{H}_2 \text{ product composition} = \frac{\text{mol H}_2}{\text{mol of all product}} \quad \dots \text{ (B.6)}$$

$$\% \text{CH}_4 \text{ conversion} = \frac{F_{\text{CH}_4,in} - F_{\text{CH}_4,out}}{F_{\text{CH}_4,in}} \times 100 \quad \dots \text{ (B.7)}$$

## APPENDIX C

### CALIBRATION CURVE

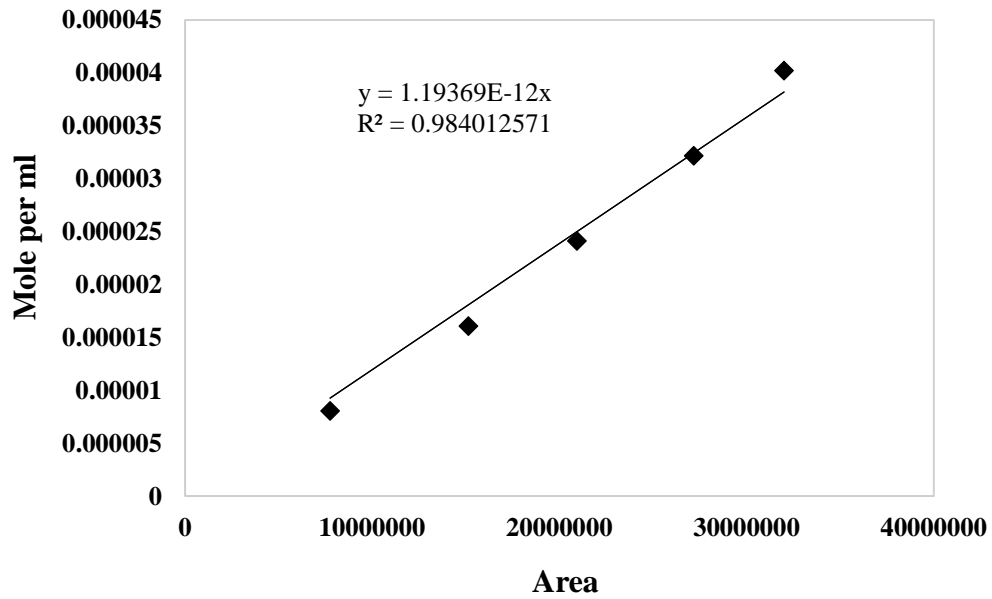


Figure C.1: Calibration curve of H<sub>2</sub>

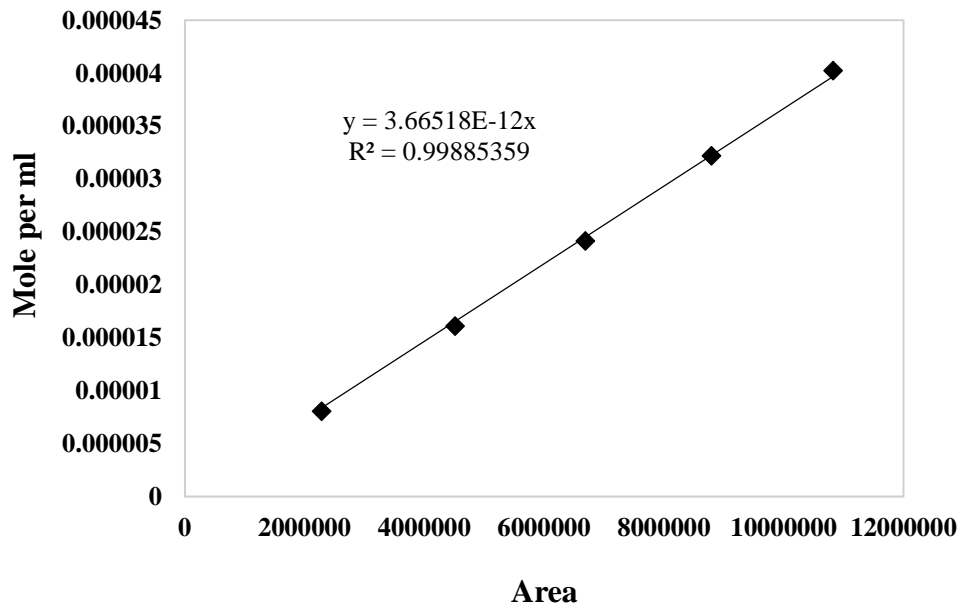


Figure C.2: Calibration curve of CH<sub>4</sub>

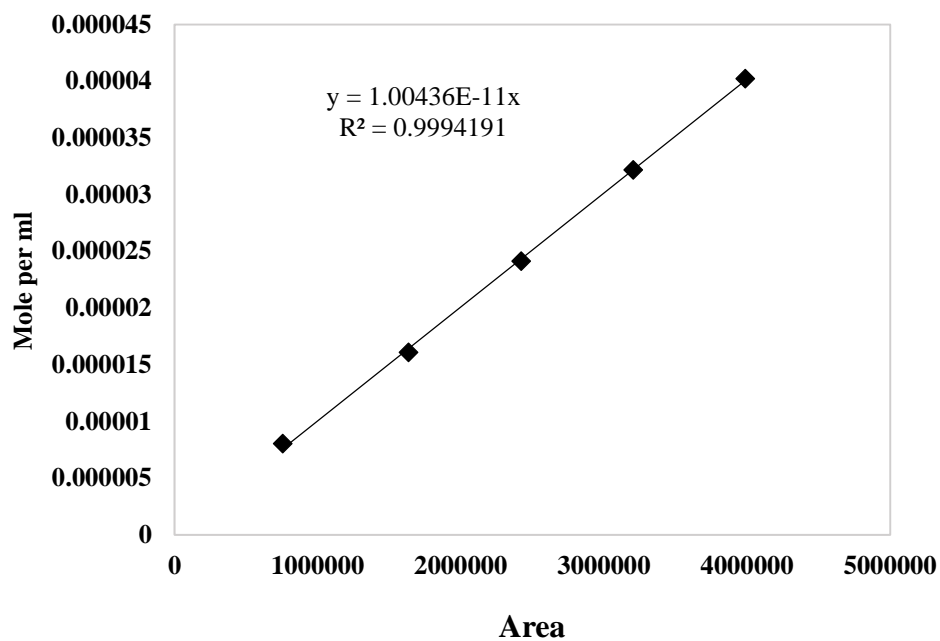
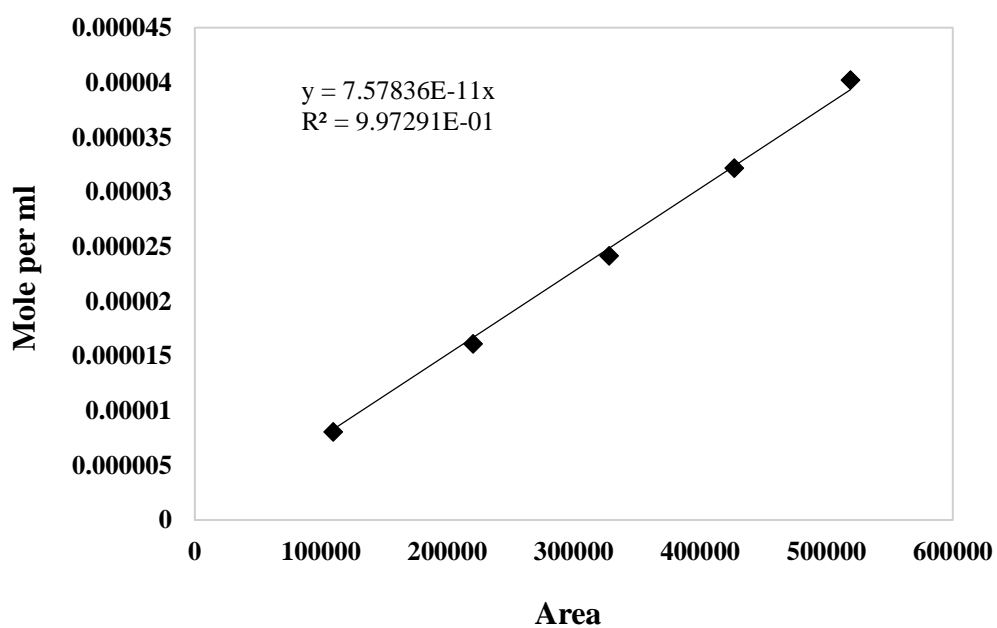


Figure C.3: Calibration curve of CO

Figure C.4: Calibration curve of CO<sub>2</sub>

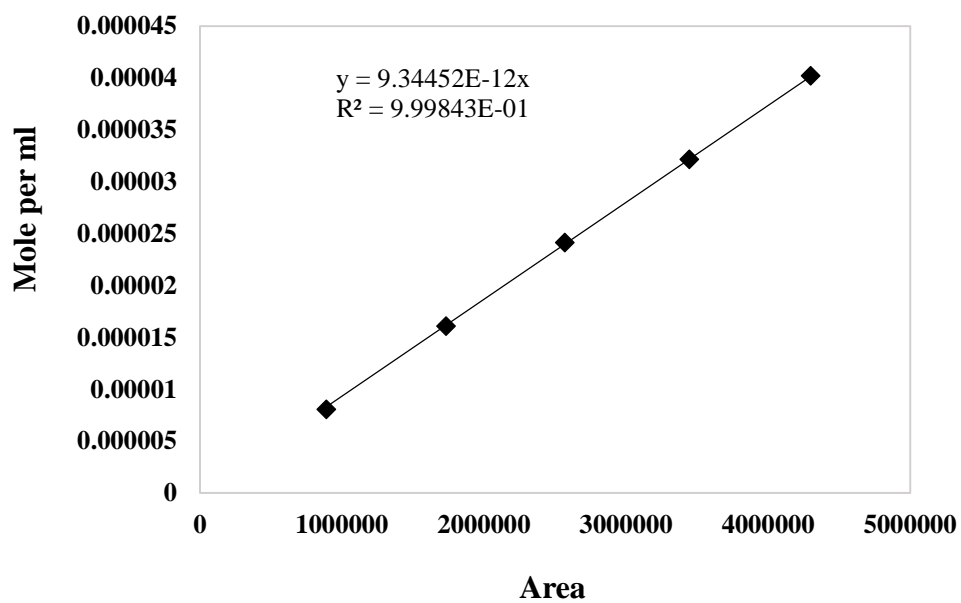


Figure C.5: Calibration curve of N<sub>2</sub>



## VITA

Miss Piya Pecharaumporn was born in Uttaradit province, Thailand, on October 12, 1989. She finished high school from Uttaradit Daruni School, Uttaradit, Thailand, 2007. She received her Bachelor's Degree of Chemical Engineering, Silpakorn University, Thailand, 2011. She has been studying Master's Degree of Chemical Engineering, Chulalongkorn University, Thailand, 2015.

